Synthesis, Characterization and Applications of Antimicrobial Materials

Faisal Suleiman Khalil Mustafa

Submitted to the
Institute of Graduate Studies and Research
in partial fulfillment of the requirements for the degree of

Doctor of Philosophy
in
Chemistry

Eastern Mediterranean University
July 2021
Gazimağusa, North Cyprus

Approval of the Institute of Graduate Studies and Research

Prof. Dr. Ali Hakan Ulusoy
Director

I certify that this thesis satisfies all the requirements as a thesis for the degree of Doctor of Philosophy in Chemistry.

Prof. Dr. İzzet Sakallı
Chair, Department of Chemistry

We certify that we have read this thesis and that in our opinion it is fully adequate in scope and quality as a thesis for the degree of Doctor of Philosophy in Chemistry.

Assoc. Prof. Dr. Mümtaz Güran
Co-Supervisor

Prof. Dr. Mustafa Gazi
Supervisor

Examining Committee

1. Prof. Dr. Ayfer Kalkan Burat
2. Prof. Dr. Mustafa Gazi
3. Prof. Dr. Bahire Filiz Şenkal
4. Prof. Dr. Elvan Yılmaz
5. Asst. Prof. Dr. Mehmet İlktaç

ABSTRACT

Three distinct materials were synthesised, characterized, and tested as antibacterial agents in this thesis. The ability of the synthesised materials to decontaminate polluted water was also studied.

Firstly (in chapter 1), a novel compound ({[1,3-bis(2,4,5-trichlorophenoxy) propan-2-yl] oxy}-3-(2,4,5-trichlorophenoxy) hexan-2-ol) (TPTH) was synthesized and characterized. Biological evaluation of the compound was investigated by performing an antimicrobial activity and cytotoxic assays. The compound displayed good antimicrobial activity with minimum inhibition concentration detected as 0.02µg/mL, 0.08µg/mL and 0.15µg/mL against Methicillin Sensitive *Staphylococcus Aureus* (MSSA), Methicillin Resistant *Staphylococcus Aureus* (MRSA) and *Escherichia coli* (*E. coli*) respectively. Additionally, a well diffusion assay demonstrated that the zone of inhibition of *S. aureus,* MRSA and *E. coli* was 24 mm, 22 mm and 18 mm respectively. MTT assay results revealed that, at a range of effective anti-microbial concentrations, TPTH is non-toxic against stem cells.

Secondly (in chapter 2), ethylenediamine-epichlorohydrin-trichlorophenol (EET) crosslinked polymer was synthesized and characterized. EET exhibited substantial antibacterial activity with inhibition zones of 38 and 64 mm against *E. coli* and *S. Aureus* bacteria. Therefore, it was applied to treat methyl orange (MO) and rhodamine B (RB) dyes containing synthetic aqueous solutions under varying operation parameters. Notably, 10 and 15 mg of EET removed 98.72 % of MO at pH 8 and 92.45% of RB at pH 3. The EET demonstrated a fast adsorption rate and the adsorption

data fit well with the pseudo-second-order for both dyes, suggesting chemisorption. Also, considering the correlation coefficient values, the experimental dataset fit suitably with the Temkin equation for RB and Langmuir equation for MO.

Lastly (in chapter 3), novel Li doped $Zn_{0.5}Ni_{0.5}Fe_2O_4$ (Li/ZNF) photosensitive catalyst was prepared to degrade toxic antiseptic 2,4,5-trichlorophenol (TCP) and inhibit bacteria. Characterization of Li/ZNF nanoparticles revealed it possesses a bandgap of 2.89 eV, exhibited a total pore volume of 0.298 cm^3/g with a crystallite size and percent crystallinity of 16.9 nm and 76.8% respectively. Degradation of TCP (50 ppm) with 10 mg Li/ZNF under optimized conditions (pH 3, 4 mM H_2O_2 and 353 nm UV- light) reached 80% after 6 h with a degradation rate constant of 0.0019 min^{-1}. The efficiency of reusable Li/ZNF composite to degrade 50 ppm TCP decreased by 14% after the fifth cycle. According to the antibacterial tests; 15 and 25 mg of Li/ZNF were sufficient to completely inhibit both *S. aureus* and *E. coli* bacteria under UV and dark (without UV light) conditions, respectively. The photocatalytic mechanism was established based on the active radical quenching tests which revealed the contribution of $^{\bullet}OH$ and $^{\bullet}O_2^-$ radicals.

Keywords: Trichlorophenol; epichlorohydrin; antimicrobial; antiseptic; non-toxic; dye adsorption; polymer; thermodynamic; ternary photocatalyst; degradation; Li-doped Zn-Ni ferrites.

ÖZ

Bu tezde üç farklı materyal sentezlenmiş, karakterize edilmiş ve antibakteriyel ajan olarak test edilmiştir. Sentezlenen malzemelerin kirli suyu dekontamine edebilme özeliği de incelenmiştir.

İlk olarak (1. bölümde), yeni bir madde ({[1,3-bis(2,4,5-triklorofenoksi) propan-2-il]oksi}-3-(2,4,5-triklorofenoksi) heksan-2-ol) (TPTH), sentezlendi ve karakterize edildi. Maddenin biyolojik değerlendirmesi, antimikrobiyal aktivite ve sitotoksik testler yapılarak araştırıldı. Metisiline Duyarlı *Staphylococcus Aureus* (MSSA), Metisiline Dirençli *Staphylococcus Aureus* (MRSA) ve *Escherichia coli*'ye (*E. coli*) karşı iyi antimikrobiyal aktivite sergileyen bileşiğin, sırası ile minimum inhibisyon konsantrasyonları 0.02µg/mL, 0.08µg/mL ve 0.15µg/mL olarak bulunmuştur. Ek olarak, kuyu difüzyon analizi, *S. aureus*, MRSA ve *E. coli*'nin inhibisyon bölgesinin sırasıyla 24 mm, 22 mm ve 18 mm olduğunu göstermiştir. MTT analizi, bir dizi etkili anti-mikrobiyal konsantrasyonda TPTH'nin kök hücrelere karşı toksik olmadığını ortaya koydu.

İkinci olarak (2. bölümde), etilendiamin-epiklorohidrin-triklorofenol (EET) çapraz bağlı polimer sentezlendi ve karakterize edildi. EET, *E. coli* ve *S. Aureus* bakterilerine karşı 38 ve 64 mm'lik inhibisyon bölgeleri ile önemli antibakteriyel aktivite sergiledi. Bu nedenle, sentetik sulu çözeltiler içeren metil oranj (MO) ve rodamin B (RB) boyalarının değişen çalışma parametreleri altında incelenmesi uygun bulunmuştur. Özellikle, 10 ve 15 mg EET, pH 8'de MO'nun %98.72'sini ve pH 3'te RB'nin %92.45'ini emmiştir. EET, hızlı bir adsorpsiyon grafiği göstermiş ve adsorpsiyon

verileri, her iki boya için yalancı ikinci derece kinetiğine uyduğu ve bu da ortamda kimyasal absorpsiyon gerşekleştiğini göstermektedir. Ayrıca, korelasyon katsayısı değerleri dikkate alındığında, deneysel veri seti, RB için Temkin denklemine ve MO için Langmuir denklemine uymaktadır.

Son olarak (3. bölümde), toksik antiseptik 2,4,5-triklorofenol'ü (TCP) parçalamak ve bakterileri inhibe etmek için yeni Li katkılı $Zn_{0.5}Ni_{0.5}Fe_2O_4$ (Li/ZNF) ışığa duyarlı katalizör hazırlandı. Li/ZNF nanoparçacıklarının karakterizasyonu, katalizörün 2.89 eV'lik bir bant aralığına sahip olduğunu, kristalit boyutu ve yüzde kristallik sırasıyla 16.9 nm ve %76.8 olduğu, 0.298 cm^3/g toplam gözenek hacmi sergilediğini ortaya çıkardı. Optimize edilmiş koşullar altında (pH 3, 4 mM H_2O_2 ve 353 nm UV ışığı) 10 mg Li/ZNF ile TCP'nin (50 ppm) bozunması, 0,0019 dk^{-1} bozunma oranı sabiti ile 6 saatın sonunda %80'e ulaştı. Yeniden kullanılabilir Li/ZNF kompozitinin 50 ppm TCP'yi azaltma verimliliği, beşinci döngüden sonra %14 azaldı. Antibakteriyel testlere göre; 15 ve 25 mg Li/ZNF, sırasıyla UV ve karanlık (UV ışığı olmadan) koşullar altında hem S. aureus hem de *E. coli* bakterilerini tamamen inhibe etmek için yeterli bulunmuştur. Fotokatalitik mekanizma, $^{\bullet}OH$ ve $^{\bullet}O_2^-$ radikallerinin katkısını ortaya koyan aktif radikal söndürme testleriyle incelenmiştir.

Anahtar Kelimeler: Triklorofenol; epiklorohidrin; antimikrobiyal; antiseptik; toksik olmayan; boya adsorpsiyonu; polimer; termodinamik; üçlü fotokatalizör; bozulma; Li katkılı Zn-Ni ferritleri.

DEDICATION

I would like to dedicate this thesis to my father's soul who was supporting me from the first day of this Ph.D. journey, waiting to see this day and congrats me with a lot of proudness and brighten eyes, using his pointer finger to point at me and saying this is my son. Now, I would say; be proud of me where ever you be right now. May your soul rest in peace my dear father. Moreover, I want to thanks my mother and my family (brothers and sisters) for their supporting and loving until this day.

ACKNOWLEDGMENT

First and foremost, praise be to Allah, the most merciful, and peace be upon his messenger. I'd like to express my gratitude to Prof. Dr. Mustafa Gazi, my supervisor, and Assoc. Prof. Dr. Mümtaz Güran, my co-supervisor, for their advice, support, and supervision. I'd also like to thank Assoc. Prof. Dr. Akeem Oladipo for creating a pleasant working environment. No words can adequately express my sincere gratitude for his efforts throughout the last two years of my PhD. I am fortunate to have the opportunity to work with him; he has aided me in developing my academic personality, career, and research methodology. I wish him good health and happiness. I am also grateful to my committee members: Prof. Dr. Elvan Yilmaz, Assoc. Prof. Dr. Mehmet İlktaç, Prof. Dr. Bahire Filiz Şenkal, and Asst. Prof. Dr. Ayfer Kalkan Burat for their time and sincere efforts.

Special thanks to my friends, who have aided me in several ways. Particularly Arwa, Selma, Cahit, Ayo, Pelin, Selin, Meltem, Basma, Khawla, Abdullah, Mamoon, Namık, and many others; for their encouragement and assistance through my studies.

TABLE OF CONTENTS

LIST OF TABLES

LIST OF FIGURES

Chapter 1

INTRODUCTION

The goal of this PhD project is to develop antimicrobial materials capable of decontaminating hazardous antiseptic compounds such as 2,4,5-trichlorophenol (TCP) and other contaminants in water. As a result, a number of procedures were used to synthesize three different materials. The antibacterial and water decontamination efficacy of the synthesized compounds were determined.

This thesis is divided into three parts. **Part I** describes and discusses the synthesis of a novel compound ({[1,3-bis(2,4,5-trichlorophenoxy) propan-2-yl] oxy}-3-(2,4,5-trichlorophenoxy) hexan-2-ol) (TPTH) by condensation reaction between (TCP) and epichlorohydrin (ECH) then characterized by different techniques. Biological evaluation of the new compound was investigated by performing an antimicrobial activity and cytotoxic assays. Thermal instability of the starting compound (TCP) was improved and analyzed by thermogravimetric analysis.

Part II focuses on the synthesis of ethylene diamine-epichlorohydrin-trichlorophenol (EET) cross-linked polymer via a condensation polymerization technique. The EET was characterized, its antimicrobial efficiency was investigated and then used to adsorb methyl orange (MO) and rhodamine B (RB) dyes from water under varying operation parameters.

Part III describes the synthesis of Li/$Zn_{0.5}Ni_{0.5}Fe_2O_4$ (Li/ZNF) via co-precipitation

and doping methods. Li/ZNF was characterized and its antibacterial activity was examined under dark and UV-light individually via time-kill assay.

1.1 Antimicrobial materials

Recently, the number of infectious diseases caused by microorganisms increased tremendously. Therefore, pathogens are very interesting nowadays because of their ability to be modified and transformed into resistant pathogens against antimicrobial materials [1]. Materials that possess antimicrobial activity have been investigated for biomedical use to decrease the bacterial infection that are found in hospitals [2]. These materials have the ability to inhibit or kill the microbes, however, some of them have a poor inhibition activity against resistant microbes. In addition, they face difficulties to work in dynamic environment [3]. Due to these reasons some antimicrobial materials have been modified from natural or synthetic sources including polymers (modified chitosan, heparin with calcium, polyacrylamides and polyacrylates with tertiary or quaternary amine groups), quaternary ammonium molecules and metal oxide compounds of organic and inorganic antimicrobial nanoparticles respectively [1].

1.1.1 Antimicrobial small molecules

In general compounds with nitrogen, chlorine, fluorine, sulfide and phosphorus act as antimicrobial agent such as streptomycins, sulphonamides, and penicillins [4]. Penicillin inhibits the cross linking activity in bacteria wall and prevents the formation of new cell wall that leads to death [5]. A similar mechanism is shown by penicillin derivatives such as cephalosporins, monobactams, and carbapenems [6]. In contrast,

quinolone kills bacteria by targeting DNA-topoisomerase complexes of microorganisms [7].

1.1.1.1 Epichlorohydrin

Epichlorohydrin (ECH) (Figure 1) is an organic compound with a chlorine atom, classified as a chiral molecule with epoxy ring and racemic mixture. It is evenly soluble in water and soluble in polar organic solvents. Furthermore, it is an extremely reactive electrophilic compound and was synthesized from glycerol [8]. Usually used during the production of epoxy resins as a cross-linker with natural polymers.

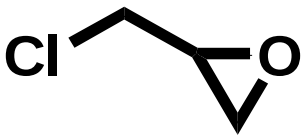

Figure 1: Structure of Epichlorohydrin (ECH)

1.1.1.2 Ethylenediamine

Ethylenediamine (EDA) (Figure 2) was synthesized in different ways like reacting ethanolamine with ammonia and catalyst, or by aminolysis of ethylene dichloride with ammonia. It has wide applications such as chelating agent, surfactant, fungicide and insecticide [9]. Moreover, EDA and ethylenediamine tetraacetic acid (EDTA) were used as cross-linker in the membrane and graphene oxide to increase the stability of the membrane in aqueous solutions and chitosan to adsorb heavy metals respectively; [10,11]. Furthermore, EDA was used in the backbone of the polymers such as poly(dimethylamine-co-ethylenediamine-co-epichlorohydrin) to remove copper ions from wastewater [12].

Figure 2: Structure of Ethylenediamine (EDA)

1.1.2 Antimicrobial polymers

Many different applications of polymers have been reported that include antimicrobial activity [13]. Research articles revealed that, chitosan is a natural polymer with amine groups that follows two different mechanisms to kill bacteria. Firstly, it forms a positive charge on nitrogen which interacts with negative charge of bacteria cell wall and prevents the transport of materials into the bacterial cell [14]. Secondly, chitosan inhibits the synthesis of bacterial RNA via binding with the DNA of bacteria [15]. On the other hand, polyhexamethylene biguanide is a synthetic antimicrobial polymer that kills various microorganisms. It functions by disrupting bacterial cell wall which leads to death [16]. 2-[(4-Fluorophenyl)amino]-2-oxoethyl-2-methylacrylate is another synthetic polymer that is synthesized via free-radical copolymerization and due to the high amount of fluorine content, this polymer has the ability to inhibit microbial growth [17]. Lastly, ethyl and butyl acrylates were modified via copolymerization using triclosan which has three chlorine atoms in one moiety. Therefore the antimicrobial activity of these acrylate polymers is increased with higher amount of triclosan groups [18]. These polymers function by inhibiting the enoylacyl carrier protein reductase and deactivating fatty acid synthesis [19].

1.1.3 Antibacterial of nanoparticles

1.1.3.1 Spinel ferrite magnetic

Spinel ferrite magnetic nanoparticles are very interesting nowadays due to their wide applications in nanoscience. Photocatalytic application is widely used to treat the

environment due to outstanding features such as super magnetic properties, photochemical stability, electrical properties, narrow bandgap, inexpensive and catalytic applications [20,21]. The structure of the spinel ferrite nanoparticles is MFe_2O_4, where M is a metal cation. Here, oxygen can form two different cubic shapes, tetrahedral and octahedral crystallographic sites (Figure 3) with metal and iron ions respectively [22].

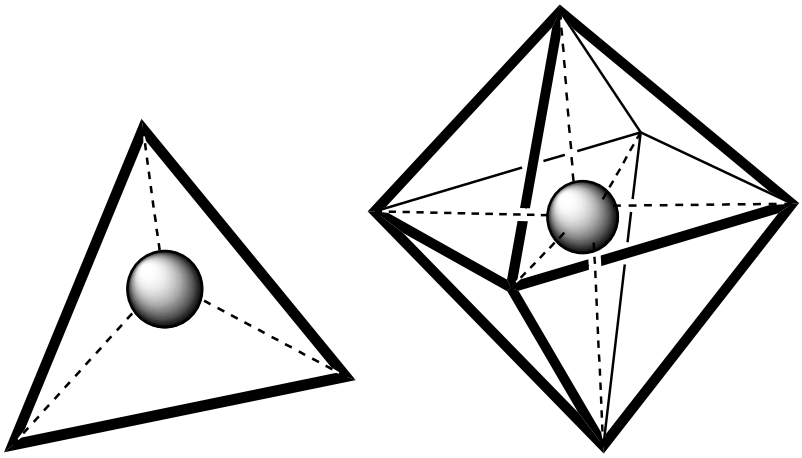

Figure 3: Tetrahedral and octahedral crystallographic sites

These nanoparticles are very attractive in biomedical applications due to magnetic resonance imaging. This feature give them ability to be controlled via magnetic field [23]. Moreover, doped ferrites nanoparticles are used as antimicrobial materials for water purification because of their ability to affect dynamic bacteria growth by some metal ions such as Cu, Zn, and Ag combined with nanoparticles. A simple way can be applied to filter these nanoparticles by magnetic field after purification process [24]. The main mechanism of metal oxide nanoparticles to kill bacteria is to damage the cell membrane of bacteria by electrostatic interaction [25].

1.2 Environmental pollutants

Pollutants in the environment have direct or indirect effects on living species such as humans, animals, plants, and microorganisms. Carcinogens, such as chlorophenol chemicals, are among the contaminants that have a direct influence on organisms. Dyes and pathogens, on the other hand, are contaminants that can affect living organism in both direct and indirect ways. Dyes at low concentrations in water can prevent sunlight to reach the aquatic environment which inhibits the photosynthesis of marine algae [26]. Additionally, they can be carcinogenic for organisms when the concentration increases beyond the acceptable range. Pathogens have an indirect effect on the environment because they have accessibility to potable water resources. Besides this property, they cause sickness if they invade the body of the living organisms.

1.2.1 Chlorophenol compounds

The spread of irresistible infections is generally preventable by the utilization of effective antiseptic agents. However, many antiseptic compounds have high toxicity which limits their usage. As a result, while synthesis of a new antiseptic material is critical, developing an effective and non-toxic antiseptic agent remains a significant challenge.

Chlorophenol compounds (organochlorine compounds) are weak acids that were used as antiseptic agents in the past. Studies conducted in the 1990s showed that chlorophenol compounds such as o,m,p-chlorophenols, dichlorophenols, trichlorophenols, tetrachlorophenols and pentachlorophenol have a devastating antimicrobial activity against a range of microorganisms mainly by altering the K^+/ Na^+ ratio of the bacterial cell [27–31]. These compounds are released into the environment as a product of chemical and pharmaceutical industries or through the

degradation of pesticides such as chlorinated cyclohexanes and chlorobenzenes [32,33].

2,4,5-Trichlorophenol (TCP) is one of the strongest antiseptics; it was investigated further and shown to have high killing and inhibitory effect on the growth of bacteria [28]. However, despite the effective killing of microorganisms, it's application is very limited due to its high carcinogenicity and listed by the Environmental Protection Agency (EPA) as one of 31 high priority pollutants [28,30,34]. It was produced by hydrolysis of 1,2,4,5-tetrachlorobenzene (TCB) in the presence of sodium hydroxide and methanol [35,36]. Additionally, it was used to prepare polychlorinated dibenzo-p-dioxins (PCDDs) via different mechanisms [37].

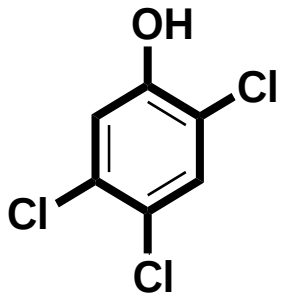

Figure 4: Structure of 2,4,5-trichlorophenol

1.2.2 Dyes

The most common sources of coloured wastewater, which causes major environmental concerns, are the paper, leather, and textile industries [38]. Generally, in different industries; around 10000 positive and negative type of dyes are available and used. The majority of these dyes are dumped into the environment following the production process and then transported into water sources [26,39–43]. Methyl orange (MO) is an anionic azo dye (has one azo linkage (-N=N-) in its structure), which generates two

distinct structures, each with its own colour (red and yellow), and has been utilized in printing shops, pharmaceutical, food, and textile sectors due to resonance [44,45]. Studies showed that it is water-soluble, resistant to biodegradation, carcinogenic and chemically stable [46,47]. While Rhodamine B (RB) a cationic dye usually appears in two different forms as salt and lactone [48]. Because of its fluorescence, it has been utilized as a tracking agent in the pharmaceutical industry, as well as in paper printing and textiles [49,50]. A tiny amount of these dyes in water is affecting the aquatic environment not just because of the toxicity, also the ability to inhibit light penetration [26,41,42]. When humans or animals are exposed to fatal doses of dyes, they can develop dermatitis, cancer, pulmonary infection, and even death [43,51,52].

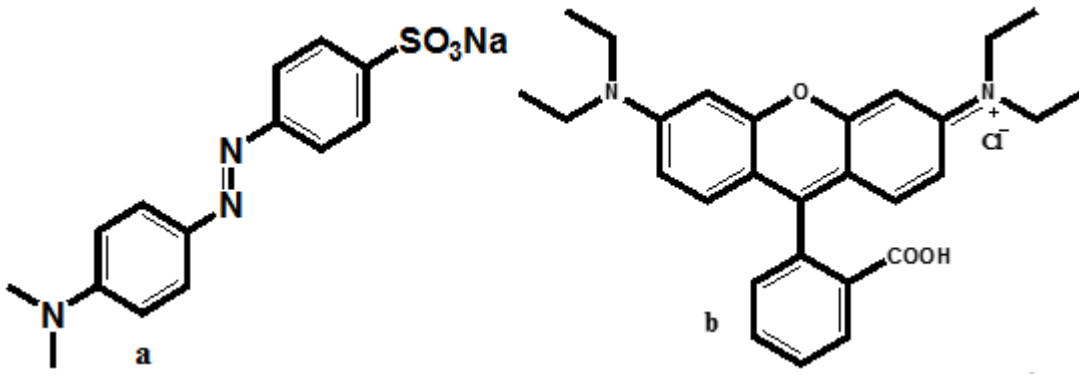

Figure 5: Structure of a) Methyl orange and b) Rhodamine B

1.2.3 Pathogens

Water borne diseases caused by pathogenic bacteria are one of the global health concerns in the 21st century and these pathogenic bacteria can be transmitted via different liquid sources. Besides, many water sources such as pools, lakes and rivers may get infected with saprophytic or pathogenic bacteria which can lead to various environmental, industry or health-related problems. Moreover, the presence of pathogens in water is a serious problem limiting the accessibility to potable water

resources. For instance, the use of untreated water from open sources such as rivers, streams and dams can cause severe water-borne infections [53].

Pathogenic bacteria can be categorized into Gram-positive and Gram-negative species. Particularly. Methicillin Sensitive *Staphylococcus Aureus* (MSSA) and Methicillin Resistant *Staphylococcus Aureus* MRSA are Gram-positive bacteria which are developed from *Staphylococcus Aureus* and very difficult to treat [54]. MSSA produces Panton-Valentine leucocidin, this material is toxic and can destroy white blood cells [55]. MRSA was found to be resistant to β-lactam antibiotics such as penicillin, amoxicillin, oxacillin, methicillin and cephalosporin [56]. *Escherichia coli* (E. *coli*) is a Gram-negative bacteria found in intestine and has killed more than two million humans per year through both intraintestinal and extraintestinal diseases [57].

1.3 Treatment of contaminated water

The goal of water treatment is to increase the quality of the water. The methods used to treat contaminated water are determined by the quality of the water supply, the source of the water, the kind of pollutant, and the intended use of the treated water.

One of the most effective methods to remove pollutants from solutions is adsorption, besides the non-selectivity feature; it is inexpensive nature and easy to use [58]. using polymers as an adsorbent to remove dyes from wastewater has become favorable because of their eco-friendly nature, renewability and reported superior performance [59]. Chitosan is one of the most common natural polymer that has been used to extract dyes from wastewater due to its non-toxicity, biological and chemical properties. Munagapati et al. utilized chitosan beads to remove MO from aqueous solution by bonding hydroxyl group from the dye with protonated amino groups on chitosan with

an uptake capacity of 73 mg/g [60]. Alginate beads were used to extract 0.08 mg/g of RB dye from the solution by Kaushal and Tiwari [61]. Ethylenediamine-epichlorohydrin cross-linked polymer was used to remove nitrite ion (11.7 mmol/g) after preparing it via condensation polymerization method [62], and also the same polymer was used to remove reactive brilliant red dye from wastewater and demonstrated high removal efficiency which was ascribed to its hydrophilic and hydrophobic groups [63]. Poly(dimethylamine-co-ethylenediamine-co-epichlorohydrin) was used to remove copper ions from wastewater as a chelating agent [12].

1.3.1 Water contaminated by bacteria

Water contaminated by bacteria can be treated in different ways using either chlorination, ozonation, ultraviolet radiation (UV), catalysts or antimicrobial compounds and polymers. Some of these methods consume time, need high cost and might produce harmful products. Although the chlorination method is the simplest and considered effective method, but chlorine can react with organic compounds in water and form trichloromethane which is carcinogenic and mutagenic [64]. In contrast, many drugs have been used as antimicrobial for both Gram-positive and Gram-negative bacteria species such as penicillin and amoxicillin, they can inhibit the transpeptidase that stimulates the last step in the cell wall biosynthesis of bacteria [65-70]. Also, some polymers can inhibit or kill bacteria, polymers with hydrophobic (chlorine, fluorine) and cationic groups (quaternary nitrogen functional group) and) such as chitosan, chitosan derivatives, poly lysine. These polymeric materials have reportedly exhibited antibacterial activities by disrupting the cell wall membrane of the bacteria via charge or by the reaction with the protein in the membrane [71–73]. Also, various catalysts have been studied and reported to demonstrate effective

antibacterial activities such as Ag/MgO, Cu/TiO2, and ZnO under dark and light-activated conditions [74–76].

1.3.2 Water contaminated by TCP

Carcinogenic compounds like TCP can exist in water and accumulate in the lipid layer of organisms even though it is slightly soluble [31]. Due to the carcinogenicity of TCP, various technics have been applied to remove it from environment including liquid-liquid extraction from wastewater by using hydrophobic ionic liquids [77]. Also, the adsorption technique was used to remove it via montmorillonites material modified with an organic surfactant, this material demonstrated a maximum adsorption capacity of 368 mg/g at pH 4 [34]. Zheng et al. used chitosan to adsorb chlorophenol compound with an uptake capacity of 0.22 mmol/Kg at pH 6.2 [78]. In addition, advanced oxidation processes like photocatalysis can degrade chlorophenol compounds to a permissible concentration [79]; TiO_2 was used to degrade TCP from 50 µM to 4 µM within five hours under UV-light [80].

1.3.3 Water contaminated by dyes

Water contaminated by dyes have been treated via different techniques and varying degrees of success have been achieved [81–83]. Ifebajo et al used 50 mg of $CoO{-}CuFe_2O_4$ to degrade 20 ppm of eriochrome black T (EBT) under sunlight within 90 min and achieved 99.4% degradation [84]. Mandal and Natarajan synthesized $ZnO/Zn_xFe_{3-x}O_4$ viand used to adsorb (75%) acid blue 113 and (37%) orange II within 6 h [85]. Other methods have been used to treat dye-contaminated water such as reverse osmosis, photolysis, ion exchange, precipitation, electro-photocatalysis, biological treatment, chemical oxidation, and adsorption [86,87]. Some nanoparticles reported as photocatalytic degradation such as $ZnFe_2O_4$. $ZnFe_2O_4$ was used to degrade acid orange II [88]. On the other hand, spinel ferrite nanoparticles were used as an

adsorbent to remove pollutants. Among these nanoparticles, Fe_3O_4 modified with L-arginine was used to remove 66.66 mg/g of reactive blue 19 from wastewater suggested that the reactive blue 19 bound with the protonated amine groups of the coted surface of Fe_3O_4 [89]. $NiFe_2O_4$ was used to adsorb 138.5 mg/g of methylene blue and other heavy metals because of 3D interconnected porous structure [90].

Chapter 2

ANTIMICROBIAL COMPOUND AND TOXICITY TEST

2.1 Introduction

Dissemination of infectious diseases such as bacteria is mostly preventable by using effective antiseptic agents in healthcare systems like hospitals and the environment. However, they have limited applications due to their potential toxicity. To improve this feature, scientists face many challenges.

Chlorophenol compounds were used as antiseptic agents in the past. Studies conducted in 1990s revealed their destructive antimicrobial activity against multiple microorganisms mainly by altering the Na^+/K^+ ratio of the bacterial cell [27,28]. Examples include o,m,p-chlorophenols, dichlorophenols, 2,4,5-trichlorophenols (TCP), tetrachlorophenols and pentachlorophenols [29–31]. One of the strongest antiseptics is TCP, which was shown to have high inhibitory effect on the growth of bacteria. Despite the effective killing of microorganisms, the applications TCP are very limited, because of its high toxicity [28,30].

Epichlorohydrin (ECH), is an organochlorine compound with an epoxy ring and exists as a chiral molecule with a racemic mixture. It is soluble in polar organic solvents and sparingly soluble in water. Furthermore, it is synthesized from glycerol and usually used as a reactant in production of epoxy resins such as ECH with Bisphenol-S and A, and as a cross-linker for polymeric compounds [8,91–95].

Here, we describe the synthesis of a novel compound, {[1,3-bis(2,4,5-trichlorophenoxy) propan-2-yl] oxy}-3-(2,4,5-trichlorophenoxy) hexan-2-ol (TPTH). TCP was modified by using ECH in the presence of a triethylamine (TEA) as a base. Following the chemical characterization of the compound by analytical and spectral analysis, we performed assays to evaluate the antimicrobial activity and cytotoxicity of the novel compound.

2.2 Methodology

2.2.1 Materials

TCP, ECH and diethyl ether (Sigma-Aldrich), triethylamine (TEA), Mueller Hinton Broth (MHB) and dimethyl Sulfoxide (DMSO) (Merck), MacConkey agar (MCA) (Himedia), Mannitol salt agar (MSA) (Neogen). Standard strains of *Escherichia coli* (*E. coli*, ATCC 25922), *Staphylococcus aureus* (*S. aureus*, ATCC 29213) and Methicillin-resistant *Staphylococcus aureus* (MRSA, NCTC 12493) were used in Broth Microdilution test; Wharton's Jelly- Mesenchymal Stem Cells (WJ-MSCs) and human Platelet Lysate (hPL) were obtained from cell therapy center (University of Jordan), α-MEM media (Gibco, cat#22561-021), Penicillin-Streptomycin (Gibco,cat#15140-122), L-glutamine (Gibco, cat#25030-024), MTT [3-[4,5-dimethyl-2-thiazolyl]-2,5-diphenyl-2H-tetrazolium bromide] (Bioworld, cat#42000092) were used in toxicity test.

2.2.2 Instruments

{[1,3-bis(2,4,5-trichlorophenoxy) propan-2-yl] oxy}-3-(2,4,5-trichlorophenoxy) hexan-2-ol (TPTH) was characterized by ^{1}H and ^{13}C NMR (Nuclear magnetic resonance spectroscopy): BRUKER, modal A197/32/EG, Type: Ascend, long hold time S.N: Z123221/1003, Germany (Jordan University). Mass spectroscopy (MS): Bruker APEX-IV (7 Tesla), syringe pump with a flow rate of 120 µl/min, Germany

(Jordan University). Scanning electron microscope (SEM): FEITM.VERSA 3D, USA (Jordan University). Fourier Transform Infrared Spectroscopy (FTIR) (PerkinElmer, UK) (Eastern Mediterranean University). Ultraviolet–visible spectroscopy (UV–vis) (T90þ, PG Instruments Ltd, UK) (Eastern Mediterranean University). Thermo gravimetric analysis (TGA) (HITACHI, STA7300, Japan) (Eastern Mediterranean University). Tissue Culture Incubator (Memmert, Schwabach, Germany), Glomax plate reader (Promega, Madison, WI, USA) (Jordan University).

2.2.3 Methods

2.2.3.1 Synthesis of TPTH

In a 50 mL round bottom flask, 2.50 mol of TCP was dissolved with 1.00 mol of ECH, with a mole ratio of 2.5:1. Then, 1 mL of TEA was added as a base and the mixture was stirred at 250 rpm for 5 h at 85°C. The product was formed; the base and the unreacted liquids were removed by a vacuum oven at 50°C overnight. To purify the compound, re-precipitation was performed by using diethyl ether as a solvent and water as precipitating agent, this process was repeated three times. A red solid product (TPTH, Figure 6) was collected and dried at 40°C overnight (percentage yield 88%) [96].

2.2.3.2 Antimicrobial activity assays

2.2.3.2.1 Determination of minimum inhibitory concentrations (MICs)

Broth Micro dilution assay was performed using 1 x 10^{-2} g TPTH in 1 x 10^{-3} L DMSO as stock concentration to find MIC value. Afterwards *S. aureus* and MRSA were spread in MSA, 0.4% oxacillin supplemented MSA individually, and *E. coli* in MCA, the agars were incubated at 37°C overnight. MHB was used to prepare stock solutions of different bacteria individually and adjusted by McFarland standard (0.5 McFarland

= 1.0 x 10^9 CFU/mL). Finally, 1.0x10^7 CFU/mL of each bacteria solution was prepared from the stock solutions.

96-well U- bottom micro-dilution plates were filled by 5 x 10^{-5} L of MHB individually (first well didn't include) . 1 x 10^{-4} L of TPTH solution (1 x 10^{-2} g/mL) was added into the first well and followed by serial dilutions as follow, 5 x 10^{-5} L of the stock solution (first well) was transferred to second well after mixing the solution in the second well another 5 x 10^{-5} L was transferred to the third well and so on. Finally, 5 x 10^{-5} L of a bacteria solution (100 x10^5 CFU/mL) was added individually to each well except negative control wells (last two wells) to observe a contamination of media or compound solutions, the last step was repeated for each bacteria species. In the end, micro-plates were incubated at 37°C for 24 h under aerobic conditions. The MIC values were calculated according to the last well without bacteria growth.

2.2.3.2.2 Determination of inhibition zones by agar well diffusion method

Agar well diffusion assay was performed by using standard strains of *E. coli*, *S. aureus,* and MRSA to test the antimicrobial diffusion activity of the TPTH. The inoculation of each bacteria strain with a concentration of 100 x 10^5 CFU/mL was done by using sterile swabs. After the bacteria were inoculated into the MHA, two different holes were made by using a circular sterile cutter with a 6.00 mm diameter. Afterwards, 5 x 10^{-5} L of TPTH stock solution (1 x 10^{-2} g/mL) and 5% DMSO (as a control) were added into the holes individually for *E. coli, S. aureus,* and MRSA. Then, the agar plates were incubated at 37°C for 24 h under aerobic conditions. The zone of inhibition was measured in diameters [97].

2.2.4 Toxicity assay

WJ-MSCs were cultured as an attached monolayer and maintained in α-MEM media supplemented with 5% of hPL, 1% Penicillin-Streptomycin, and 2 x 10^{-3}M L-glutamine. Cells were incubated in a 5% carbon dioxide Tissue Culture Incubator for 24 h at 37°C.

Cytotoxicity of TPTH was determined by MTT assay. WJ-MSCs were seeded into 96-well plates (2×10^3 cells/well) and allowed to attach for 24 h, then treated with different concentrations of TPTH compound (0.05 - 100) µg/mL and one left as a control. 96-well plates were incubated at 37°C for 72 h in a 5% Carbon dioxide incubator. After incubation, the old medium was replaced with 0.1 mL fresh medium and 0.015 mL of MTT (5 mg/mL) was added to each well individually and the plates were incubated for three hours at 37°C. Then, the process was stopped by adding 0.05 mL DMSO for each well and lift for 10 min, this process repeated four times and the average was calculated. Optical density (O.D.) was measured at 570 nm using a Glomax plate reader and percent viability was calculated as follow:

$$\%Viability = \frac{O.D._{(sample)}}{O.D._{(control)}} x100\% \quad (1)$$

2.3 Results and discussion

2.3.1 Reaction and synthesis mechanism of TPTH

{[1,3-bis(2,4,5-trichlorophenoxy) propan-2-yl] oxy}-3-(2,4,5-trichlorophenoxy) hexan-2-ol (TPTH) was synthesized by condensation reaction and characterized. The chemical equation and synthesis mechanism are shown in Figures 6 and 7.

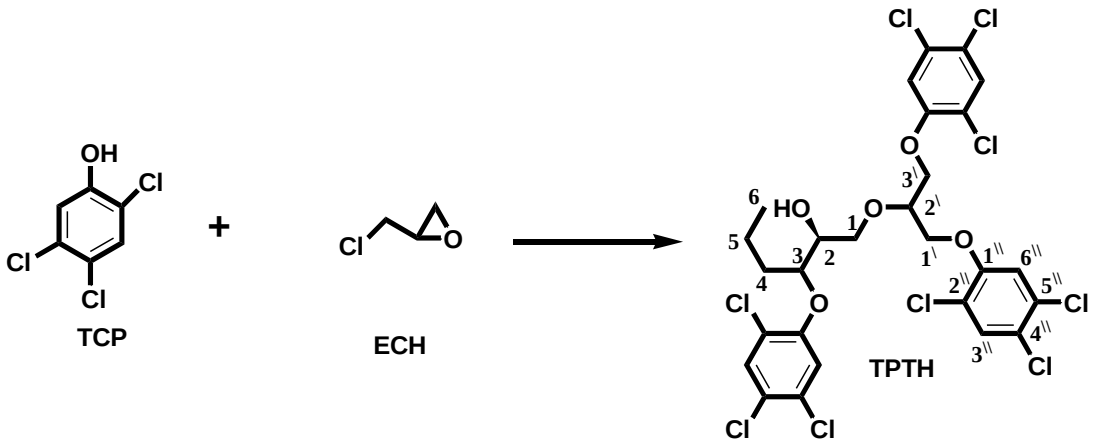

Figure 6: Chemical reaction for TPTH

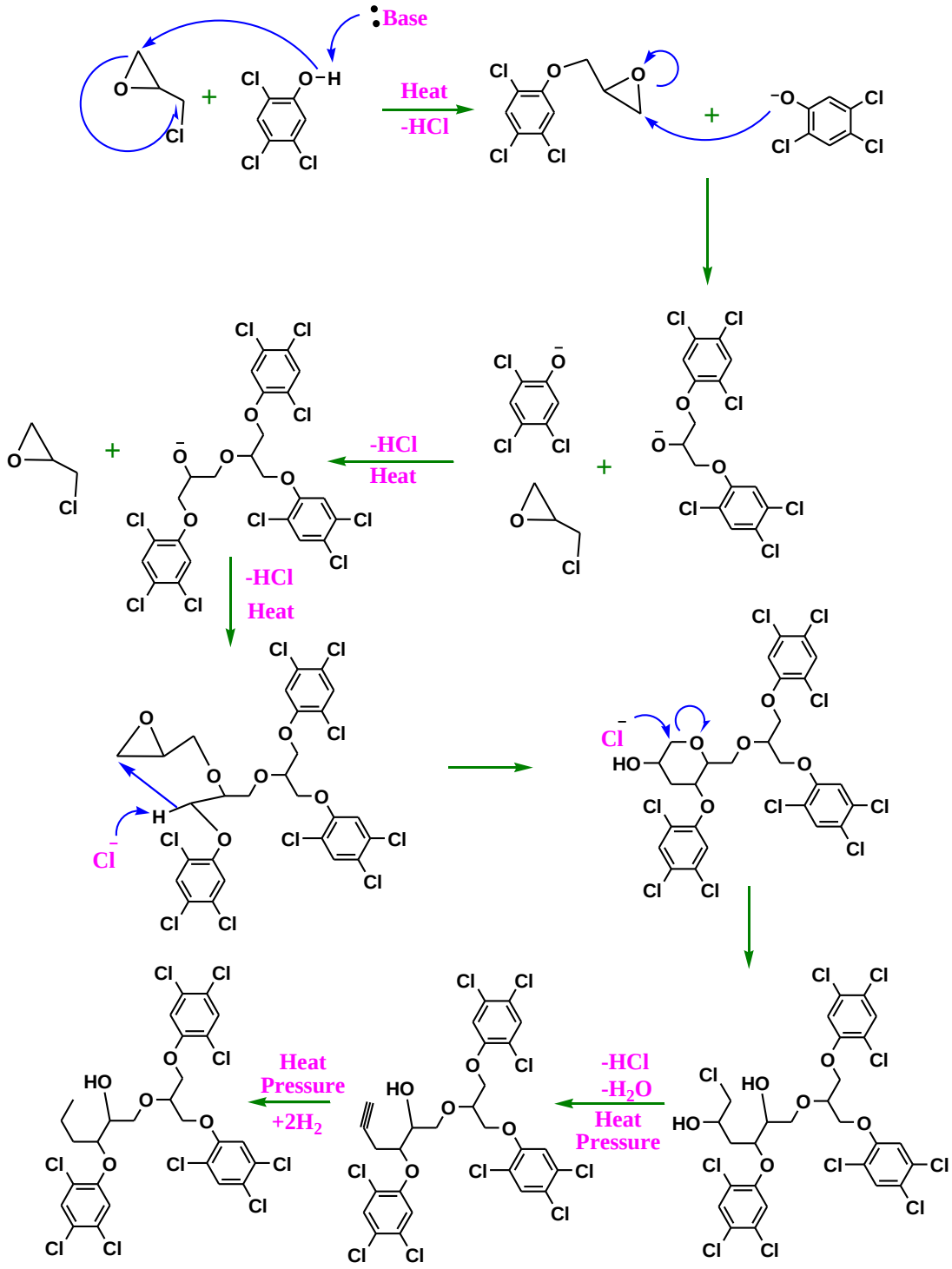

Figure 7: Suggested mechanism to prepare TPTH

2.3.2 Fourier-transform infrared spectroscopy (FT-IR)

FT-IR of TPTH was analyzed to compare TPTH with ECH and TCP as shown in Figure 8. The main peak of interest was for the hydroxyl group. It appeared at 3438.5

cm^{-1} in TCP spectra (Figure 8a), however, it disappeared in TPTH peaks (Figure 8b) because of the reaction with ECH [98]. Peaks of C=C in the chlorophenol ring appeared between 1600-1450 cm^{-1} (Figure 8a), these peaks overlapped in (Figure 8b) because of three chlorophenoxyl rings in TPTH [99]. A new C-H and O-H peaks formed in TPTH and appeared at 3000 and 3093 cm^{-1} respectively. Peaks at 925 and 721 cm^{-1} correlate with (C-O-C) epoxy and (C-Cl) in ECH spectra (Figure 8c) [100]. These peaks disappeared in the novel compound (TPTH) see (Figure 8b) due to the reaction. A new C-O-C ether between ECH and TCP was appeared at 1029 cm^{-1} in Figure 8b [101].

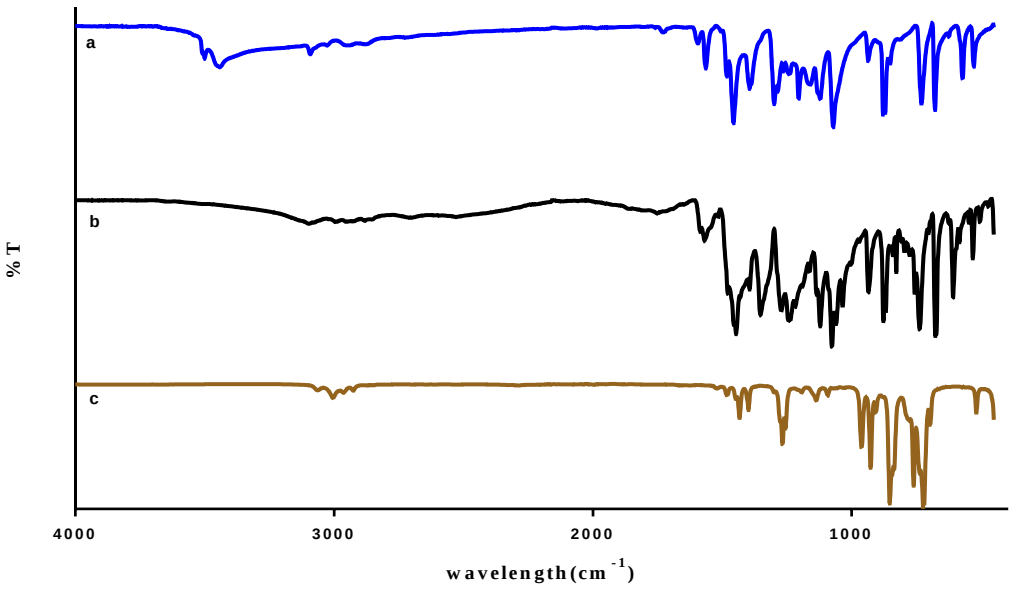

Figure 8: Fourier-transform infrared spectroscopy (FTIR) of a) TCP, b) TPTH and c) ECH.

2.3.3 Ultraviolet-visible spectroscopy (UV-vis)

UV-vis spectroscopy of TPTH was analyzed and compared with TCP as shown in (Figure 9). TCP possesses an absorption range between 312 to 200 nm (Figure 9a) [98]. In comparison with TPTH, notably, the absorption of TPTH (Figure 9b) was

increased and started from 392 nm. This increasing was happened due to the resonance of double bonds (Π bonds) of three benzene rings inside the structure of the novel compound (Figure 6).

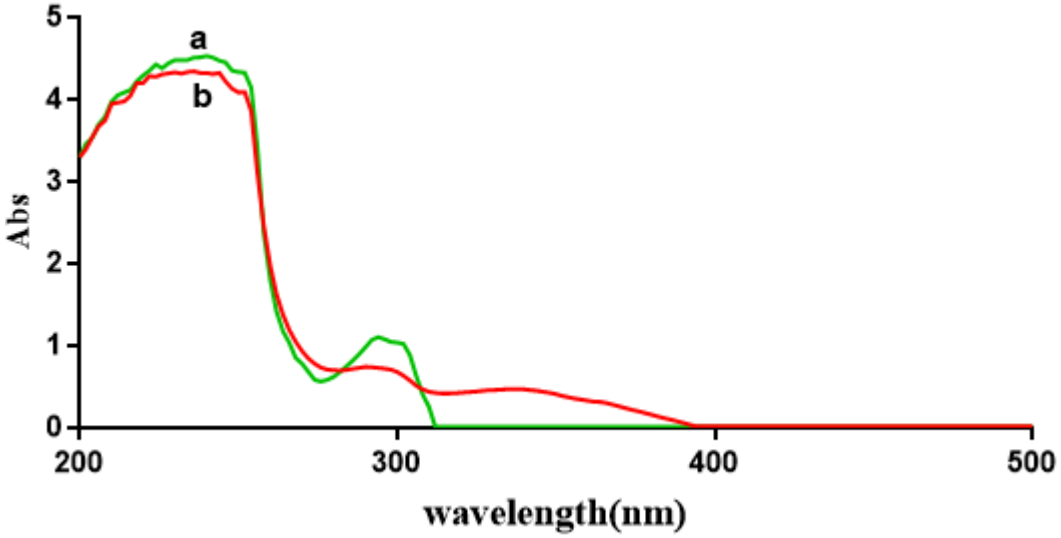

Figure 9: Ultraviolet-visible spectroscopy (UV-vis) of a) TCP and b) TPTH

2.3.4 Thermogravimetric analysis (TGA)

The thermal properties of TCP and TPTH were analyzed by TGA (Figure 10). According to the TGA profiles, around 1.5% and 0.16% weight loss of TCP and TPTH respectively occurred when the temperature increased to 100°C. After this temperature, the weight loss sharply increased to 100% at 210°C of TCP. Decreasing in weight % was due to the decomposition of TCP structure and the production of gases such as hydrogen chloride gas, chlorine gas, carbon monoxide and carbon dioxide [102]. In contrast, the novel compound (TPTH) has a high molecular weight (747 g/mol) with nine C-Cl bonds, an ether structure and three chlorophenol moieties (resonance, Π-bonds) which lead to a more stable structure [103]. The notable mass loss was noticed beyond 250°C and remained stable beyond 370°C demonstrating that. TPTH is thermally stable when compared with the precursor material.

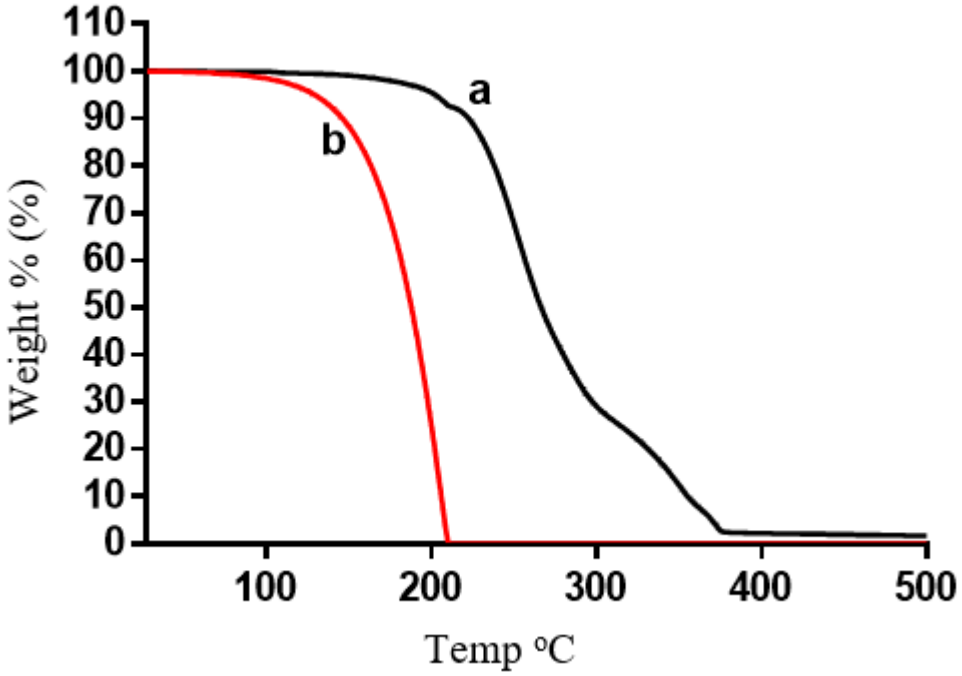

Figure 10: TGA analysis of a) TPTH and b) TCP

2.3.5 Scanning electron microscope (SEM) and transmission electron microscopy (TEM)

SEM and TEM were used to analyze the surface morphology of the novel compound (TPTH). TPTH possesses a visible crystal surface morphology as shown in Figure 11a. For TEM analysis, 7.47 x 10^{-2} g of TPTH was dissolved in acetonitrile solvent and placed on a microscopic glass slide, then left for two days under vacuum to dry. Figure 11b illustrates spherical micelles with narrow size distribution (0.337 to 0.590 µm diameter) and low aggregation of TPTH. From this result, TPTH can be dissolved completely without forming a high aggregation. The same observation was noted by Mosharraf and Nystrom when they studied the effect of particle size and shape [104].

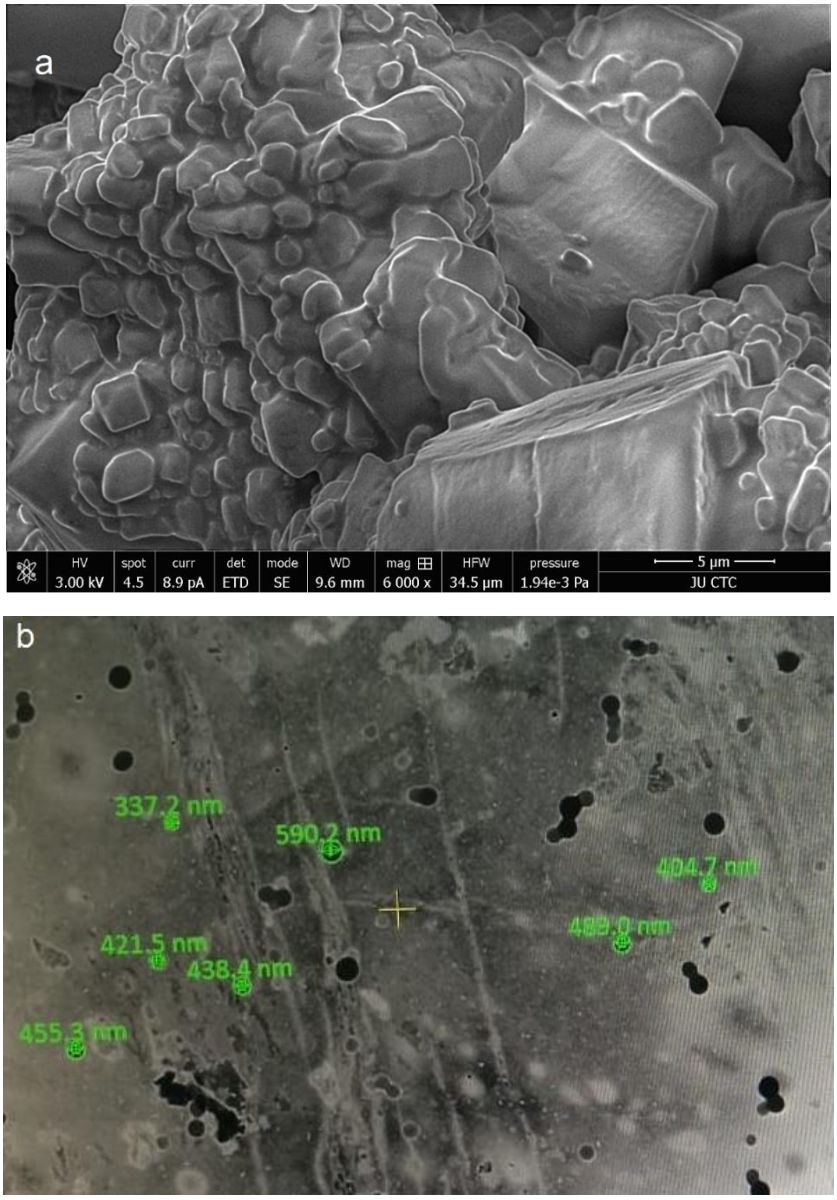

Figure 11: a) Scanning Electron Microscope (SEM micrograph,6000x) and b) Transmission Electron Microscopy (TEM micrograph, 8000x) of the TPTH

2.3.6 Molecular ions mass spectroscopy (MS)

The ion spectrum of TPTH and its fragments were studied by MS in negative ion mode. Figure 12 shows the molecular peak of the TPTH molecule at 747 m/z with 20.4 percent intensity and followed by an ion which appeared at 749 m/z with 15.3% referring to TPTH with chlorine isotope, this molecular weight suitable with 5O, 9 Cl, 23 H, and 27 C. The highest abundance molecular ion peak referred to two

trichlorophenoxy ions at 392 m/z. Finally, one ion of trichlorophenoxy appeared at 196 m/z with 12.0% intensity [105].

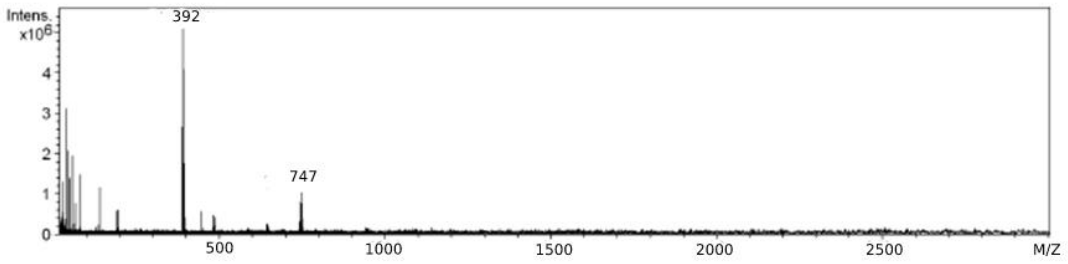

Figure 12: Mass spectroscopy (MS) of TPTH in negative ion mode with mass/charge (M/Z)

2.3.7 Nuclear magnetic resonance spectroscopy (^{1}H-NMR and ^{13}C-NMR)

TPTH ($C_{27}H_{23}O_5Cl_9$) characterized by using ^{13}C-NMR and ^{1}H-NMR (Figure 13 and Table 1). From ^{13}C-NMR notably, seven different types of carbon signal were observed as follows: Precisely, presence of nine chlorinated olefinic carbons (δ 118.6 ppm, 121.3 ppm, 153.4 ppm), six methines (δ 115.9 ppm, 131.0 ppm), three oxygenated olefinic carbons of the benzene rings (δ 158.8 ppm), three oxygenated methines (δ 40.0 ppm, 63.8 ppm, 68.9 ppm), three oxygenated methylenes (δ 46.14 ppm, 53.0 ppm, 53.0 ppm), two methylenes (δ 59.13 ppm, 71.7 ppm), and one methyl (δ 11.9 ppm) are tabulated in Table 1. ^{1}H-NMR shows different types of protons (Figure 13a) that are tabulated in Table 1. The main peak of interest was for singlet hydrogen, three different peaks appeared at δH 4.4, 6.9, and 7.7 for hydrogen of hydroxyl group and two hydrogens of trichlorophenoxy rings respectively. Notably, the hydrogen of the hydroxyl group became broadened due to hydrogen bonding.

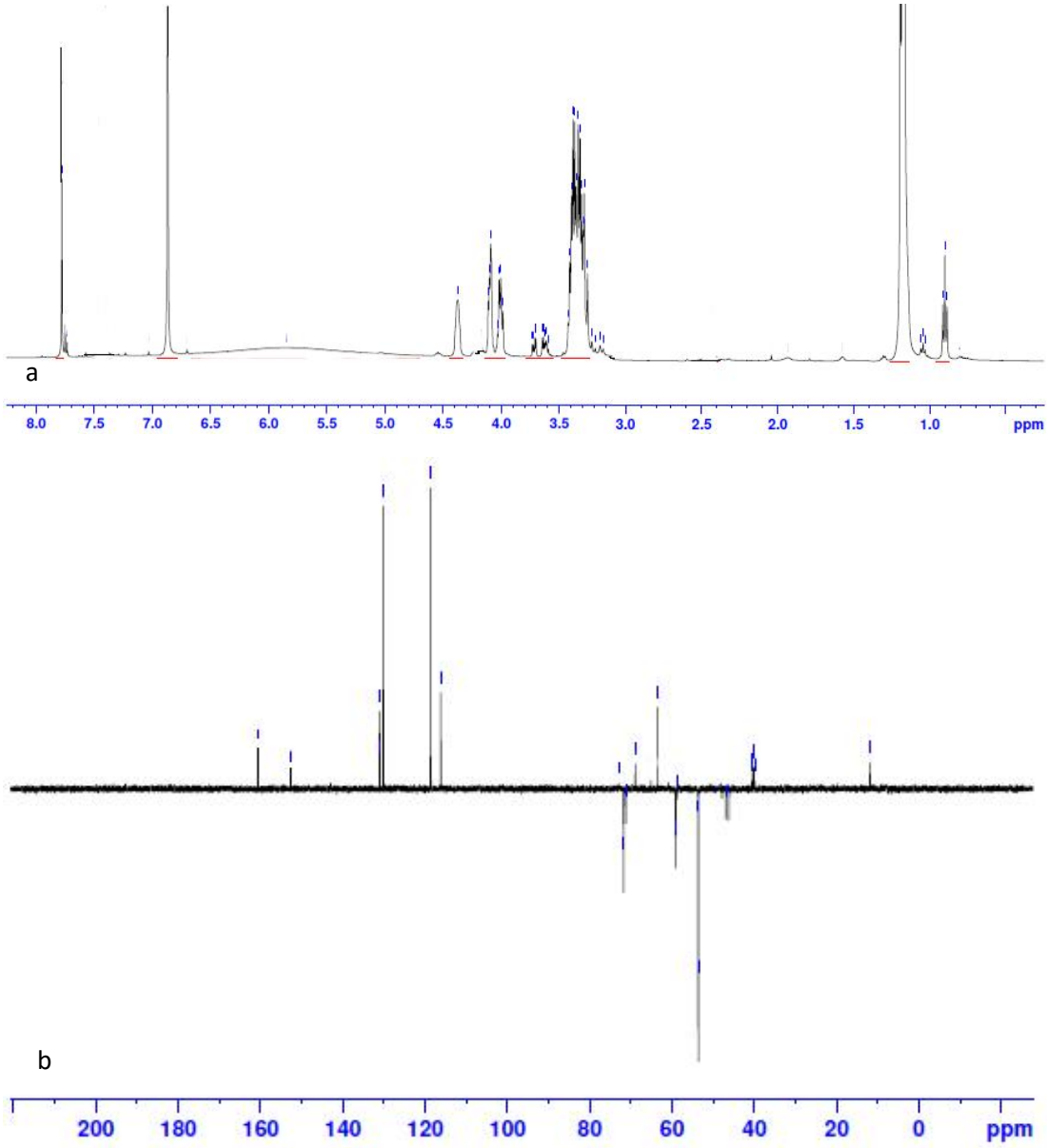

Figure 13: a) ^{1}H-NMR and b) ^{13}C-NMR of TPTH

Table 1: ^{1}H and ^{13}C (deuterated water) spectral data of TPTH (δ in ppm, J in Hz).

Code*	δ_C	δ_H (J in Hz)
1	46.14	4.1 (2H, d, J =5.35)
2	68.9	3.4 (1H, m), 4.4 (1H, s)
3	40.0	4.01 (1H, m)
4	71.7	1.02 (2H, m)
5	59.13	1.16 (2H, m)
6	11.9	0.9 (3H, t, J =6.7)
1\	53.0	3.7 (2H, d, J =6.25)
2\	63.8	3.4 (1H, quintet, J =6.25)
3\	53.0	3.7 (2H, d, J =6.25)
1\\	158.8	-
2\\	118.6	-
3\\	131.0	7.7 (1H, s)
4\\	121.3	-
5\\	153.4	-
6\\	115.9	6.9 (1H,s)

*Code represents indicated element in Figure 5.

2.3.8 Antimicrobial activity assays

Broth Micro dilution assay was used to determine the minimum inhibition concentration (MIC) of TPTH. 0.02 and 0.08 μg/mL were the minimum concentrations that inhibited the growth of *S. aureus* and MRSA bacteria respectively. In contrast, *E. coli* bacterial needed 0.15 μg/mL to disrupt the growth. The performance of TPTH is compared with reported triclosan (TCS) and benzalkonium chloride. MIC value of TPTH is three times better than TCS (0.5 μg/mL) in the presence of *E. coli* [106]. On the other hand, with *S. aureus*, TPTH is ten and twenty times effective than TCS (0.1 μg/mL) and benzalkonium chloride (0.5 μg/mL) respectively [107].

On the other hand, a well diffusion assay was used to determine the antimicrobial activity of TPTH with bacteria that were mentioned before by measuring the zones of the inhibition. Figure 14 shows the results of this inhibition with 18, 24, and 22 mm inhibition zone with *E. coli*, *S. aureus*, and MRSA bacteria respectively. TPTH possesses hydroxyl group and chlorine atoms which responsible for the antimicrobial activities of this novel compound. Based on prior studies and the functional groups in the TPTH, it can be deduced that chlorine atoms can oxidize the bacterial cell and destroy the enzymes within the cell wall by interacting with the bacterial lipids, resulting in death [108,109]. From these results, TPTH is considered a potential antimicrobial compound.

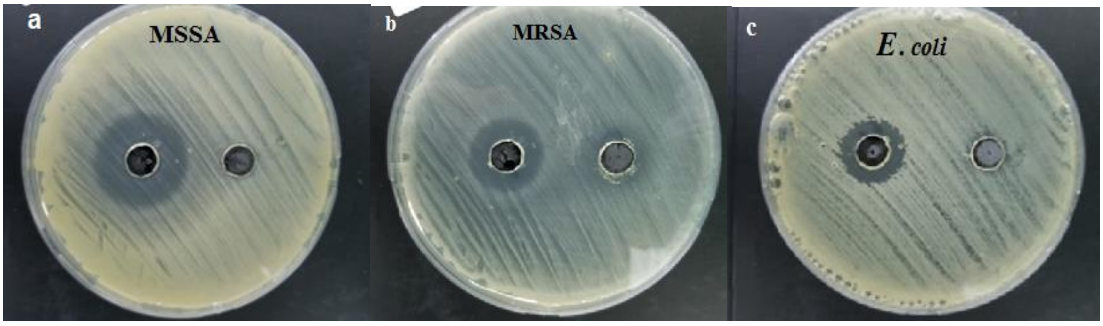

Figure 14: Well diffusion assay for TPTH (10 mg/mL and 50 µL) against; (a) *S. aureus* on MSA (24.00 mm), (b) MRSA on MSA (22.00 mm) and (c) *E. coli* on MHA (18.00 mm). Holes diameter: 6.00 mm. DMSO was used as a control (50 µL). Incubation time was 24 h at 37°C

2.3.9 Toxicity assay

Stem cells were used to determine the toxicity effect of TPTH by calculating the percent viability. Herein, different concentrations of TPTH (0.05 – 100 µg) were mixed with a fixed concentration of stem cells individually. To calculate percent viability of stem cells, one solution of these cells was left as control then plotted Vs Log (conc. µg) as shown in Figure 15.

The effect of TPTH concentration is illustrated in Figure 15. As TPTH solution concentration increased from 0.05-10 µg/mL, the percent viability stabilized at 97%. Beyond 10 µg/mL, when the concentration of TPTH is increased to 50 and 100 µg/mL the percent viability decreases sharply to 20%. This might be due to the dechlorination process which consumed the oxygen that is necessary for cells to stay alive. A similar result was observed by KARNS et al. with 0.1 mM of TCP [110]. However, TCP has been established as a toxic compound for humans by causing apoptosis, oxidative stress, and endoplasmic reticulum stress [111]. Also, the toxicity result of this novel compound was compared with benzalkonium chloride and noticed that at 10 µg/mL of benzalkonium chloride, % viability decreased to 20% [112]. Thus, from the MTT

assay, the result suggests that TPTH concentration can be used until 10 µg/mL (which is within MIC values of TPTH obtained in this study) without harm for human cells.

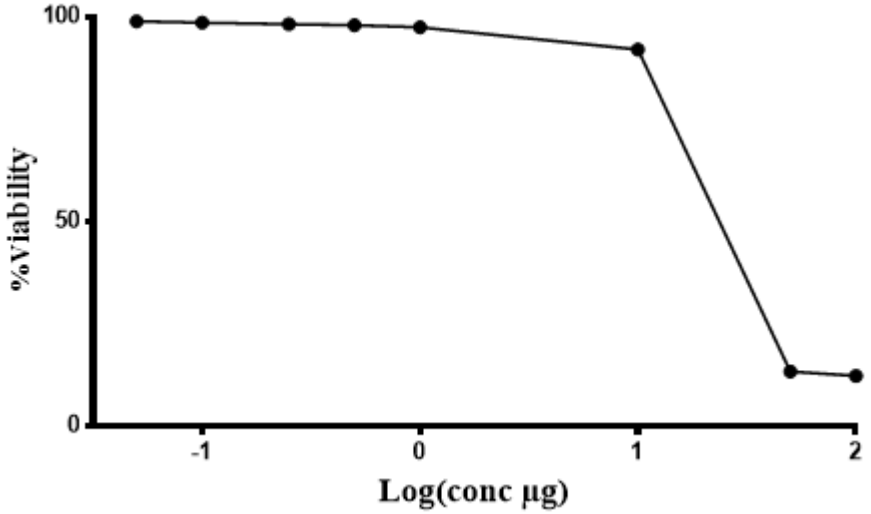

Figure 15: %Variability of Stem Cells Vs Log (conc. in mg) of TPTH. (Concentration of TPTH solutions were 0.05 to 100 µg, the concentration of stem cells was $2x10^3$ cells/well, the incubation time was 72 h at 37°C with 5% CO_2. Concentration of MTT solution was 5 mg/mL and incubation time was 3 h at 37°C. The concentration of DMSO to inhibit the reaction was 50 mL well and the duration was 10 min)

2.4 Conclusion

Herein, {[1,3-bis(2,4,5-trichlorophenoxy) propan-2-yl] oxy}-3-(2,4,5-trichlorophenoxy) hexan-2-ol (TPTH) was synthesized and characterized. TPTH is thermally stable; the results demonstrate that less than 1% of TPTH was degraded within the first 160°C, but around 98% degradation was observed at 370°C. The performance of TPTH for the inhibition of different bacteria was investigated for the killing of both Gram-positive (*S. aureus* and MRSA) and Gram-negative (*E. coli*). 0.02, 0.08, and 0.15 µg/mL of TPTH; and 18, 22, and 24 mm were the minimum inhibition concentrations and inhibition zones against *E. coli*, MRSA, and *S. aureus* respectively. Furthermore, MTT assay (toxicity test) showed 97% viability of stem

cells until 10 µg/mL of TPTH concentration after 72 h, this range includes MIC values of three different bacteria. Results herein show that TPTH is an alternative antimicrobial material with low toxicity and sufficient thermal stability that can be used for humans, animals, and the environment without risks or concerns.

Chapter 3

ANTIBACTERIAL POLYMER AND DYE REMOVAL

3.1 Introduction

Water pollution emanating from textiles, paper and leather tanning industries is an increasing environmental problem [38]. Globally, ~10 x 10^3 dyes are available and used in different industries; the majority of these dyes remaines in the water after the manufacturing processes and mix into water sources [26,39-43]. Azo dyes like methyl orange (MO) is anionic and is often used in textiles, food industries, pharmaceutical and printing shops [45]. Reports reveal that it is a carcinogenic, water-soluble, chemically stable and resistant to biodegradation [46,47]. While rhodamine B (RB) a cationic dye is a fluorescent-based xanthine dye, usually used as a tracking molecule in pharmaceutical industries, paper printing and textile [49,50]. Reports show that it is carcinogenic and neurotoxic. It causes respiratory and gastrointestinal tract irritation, and reproductive toxicity in both humans and animals [113]. The presence of a tiny amount of these dyes in water is unfavourable for the aquatic environment due to their toxicity and ability to inhibit light penetration [26,41,42]. Exposure to a concentrated dosage of the dyes is lethal and can trigger different diseases including cancer, lungs infection and dermatitis [43,52].

Adsorption technique is widely used to remove dyes from solutions due to its simplicity, the non-selectivity and inexpensive nature [58]. The use of polymers as an adsorbent to extract dyes from wastewater has become favorable due to their eco-

friendly nature (most of them), renewability and reported superior performance [59]. Among these polymers, chitosan has commonly been applied due to its non-toxic nature, biological and chemical properties. Munagapati et al. employed chitosan beads to extract 73 mg/g of MO from aqueous solution and suggested that the MO bound with the hydroxyl and protonated amino groups on the surface of chitosan [60]. Kaushal and Tiwari [61] applied alginate beads to remove 0.08 mg/g of RB dye from the aqueous solution. Ethylenediamine-epichlorohydrin cross-linked polymer was prepared by condensation polymerization effectively adsorbed 11.7 mmol/g of nitrite ions [62], and also demonstrated high removal efficiency reactive brilliant red dye from wastewater which was ascribed to its hydrophilic and hydrophobic groups [63]. Poly(dimethylamine-co-ethylenediamine-co-epichlorohydrin) was used as a chelating agent for copper ions from wastewater [12]. It is worthy to mention that polymeric adsorbents have consistently demonstrated high performance in water treatment considering these numerous reports [60–63].

Note that the presence of pathogens in water is another serious problem limiting the accessibility to potable water resources. Even though the majority of the polymeric adsorbents have demonstrated sufficient adsorptive capability, very few possess antimicrobial activities. Like chitosan, chlorophenol compounds (like 2,4,5-trichlorophenol, TCP) have been applied as antiseptic agents due to their devastating antimicrobial activity [27]. However, they have limited application because of their potential toxicity [30].

To design a polymeric material with sufficient adsorption efficiency and substantial antimicrobial activity, ethylenediamine-epichlorohydrin-trichlorophenol (EET) cross-linked polymer was prepared via a condensation polymerization technique. The

physicochemical characters of the as-prepared EET were investigated and its adsorptive behaviour in the presence of methyl orange and rhodamine B dyes was established under varying conditions (pH, initial concentration, EET dosage and temperature). Furthermore, thermodynamics, Langmuir, Temkin and Freundlich adsorption isotherms, and adsorption kinetics of EET polymer were calculated. In the addition, the inhibition growth of EET polymer was observed against *E. coli* and *S. Aureus* bacteria. Also, the reusability tests of EET cross-linked polymer were studied over five repeated reuse cycles.

3.2 Methodology

3.2.1 Materials

Methyl orange (MO, 327.33 g/mol) (BDH). Rhodamine B (RB, 479.02 g/mol), TCP, chloroform, ECH, hydrochloric acid, EDA, ethanol and sodium chloride (Sigma-Aldrich). *Escherichia coli* (*E. coli*, ATCC 25922), and *Staphylococcus aureus* (S. aureus, ATCC 29213). Muller Hinton Agar (MHA), acetone and TEA (Merck). Bacteria and MHA were used in the disk diffusion assay.

3.2.2 Instruments

Ethylenediamine-epichlorohydrin-trichlorophenol cross-linked polymer (EET) was characterized by TGA (HITACHI, STA7300, Japan) and DSC (204 F1: NETZSCH, Germany) (Jordan University), elemental analysis (EuroEA3000, UK) (Jordan University), Scanning electron microscope (SEM): FEITM.VERSA 3D, USA (Jordan University). Infrared absorption spectra (FTIR) (PerkinElmer, UK) (Jordan University). MO and RB were analyzed by UV-vis spectroscopy (T90+ Ultraviolet-visible spectrophotometer PG Instruments Ltd, UK) (Eastern Mediterranean University).

3.2.3 Methods

3.2.3.1 Synthesis of cross-linked polymer (EET)

15.2 mmol of TCP was mixed with 235 and 50 µL of ECH and EDA respectively in a 50 mL round bottom flask, with 2:4:1 mol ratio. To allow this reaction to occur, 1 mL of TEA was added to the mixture (as a base) and was stirred for 5 h at 250 rpm and 85°C. The cross-linked polymer was formed and precipitated by itself; TEA and unreacted liquids were evaporated at 50°C by a vacuum oven overnight. Then chloroform was used to remove unreacted compounds by washing. The products (Figure 16) was filtered then washed more than once by water and last with acetone. Finally, EET was dried at 40°C overnight (percentage yield 76.2%).

3.2.3.2 Adsorption experiments

100 mL beakers with 25 mL dye solutions (MO and RB) were used to perform all adsorption trials at 200 rpm. Different adsorption parameters were investigated such as adsorption dosage (10, 15 and 20 mg), initial concentration (10 - 100 mg/L), pH (2 – 9), effect of temperature (30, 40 and 50°C) and reaction time (0 – 24 h). The pH of the solutions was adjusted by 1 x 10^{-1} mol. L^{-1} of HCl and 1 x 10^{-1} mol. L^{-1} NaOH. The average of duplicate trials was reported for each parameter. After adsorption, the solution was filtered by filter paper, and the filtrate analyzed for residual RB and MO concentrations by UV-vis spectroscopy at λ_{max} 354 and 464 nm, respectively.

Linear equations were used to determine the concentrations of RB and MO absorbed with $R^2 \geq 0.999$ for both dyes. The uptake capacity at any time (q_t) or equilibrium (q_e) (mg/g) and removal (%) of the polymer were calculated by the following equations: [114]

$$q_t = \frac{(C_i - C_t)V}{m} \quad (2)$$

$$q_e = \frac{(C_i - C_e)V}{m} \quad (3)$$

$$\%\,\mathrm{Re}\,moval = \frac{(C_i - C_e)}{C_i} x100\% \quad (4)$$

where m is the mass of the adsorbent in (g), C_i and C_t (mg/L) is the initial concentration of dye and the concentration of dye solution at any time respectively, V is the volume of the solution in (L). The intake capacity at equilibrium, q_e (mg/g).

To understand the adsorption mechanism, the zero-point charge (pH_{zpc}) of EET was studied using a drift method as follows: initial pH (2 – 9) was adjusted by NaOH or HCl. 10 mg of adsorbent was added individually for each pH and agitated at room temperature for 24 h then pH final was measured for each solution and plotted vs initial pH (Figure 16), zero-point charge of EET determined as 6.5 [115]. The absorption results were examined with three different isotherm linear models (Langmuir, Temkin and Freundlich) which have been described in detail elsewhere [116]. Furthermore, the thermodynamic behaviour was examined at different temperatures (30, 40 and 50°C) considering the following equations [117]:

$$K_c = \frac{q_e}{C_e} \quad (5)$$

$$\ln(K_c) = \left(\frac{\Delta S^o}{R}\right) + \left(\frac{\Delta H^o}{nRT}\right) \quad (6)$$

$$\Delta G^o = \Delta H^o - T\Delta S^o \quad (7)$$

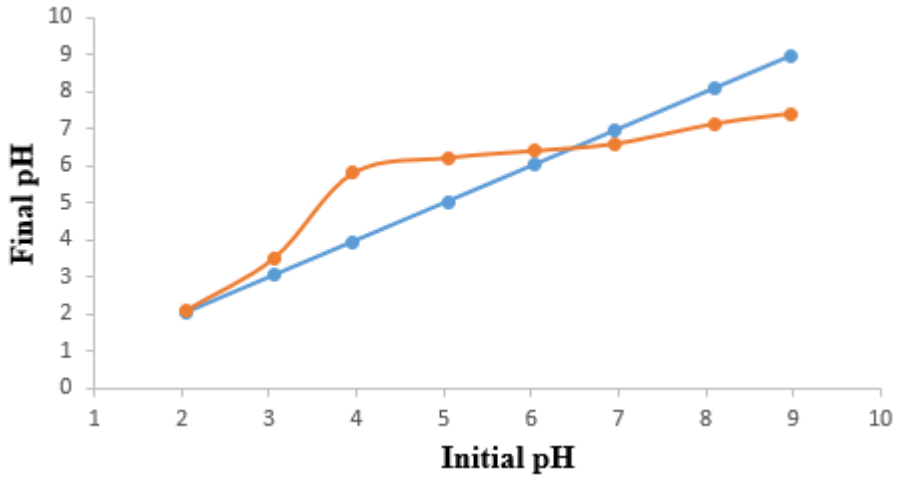

Figure 16: Zero-point charge of EET cross linked polymer blue and orange are initial and final pH respectively

3.2.3.3 Desorption and regeneration of cross-linked polymer

The desorption process of MO and RB dyes were performed using 0.01 g of cross-linked polymer-loaded with RB and MO dyes individually in 25 mL of ethanol and 25 mL of 1 x 10^{-1} mol. L^{-1} HCl, respectively. The EET-loaded dyes were horizontally shaken for 24 h at 200 rpm and room temperature. Then the solutions were filtered and the residual RB and MO concentrations were analyzed at λ_{max} (354 and 286 nm) respectively. Afterwards, distilled water was used to wash the cross-linked polymer and dried at 40°C, then reuse cycles were successfully obtained under optimum conditions.

3.2.3.4 Disc diffusion assay

Standard strains of *E. coli* and *S. aureus* were used to test the antibacterial activity of EET cross-linked polymer by disc diffusion. The inoculation of each bacteria strain with a 1 x 10^{7} CFU/mL concentration was done by using sterile swabs. After the bacteria were inoculated into the MHA, the empty discs and EET cross-linked polymer discs were transferred on the agar plates for *S. aureus* and *E. coli* bacteria. Then, the

agar plates were incubated at 37°C for 24 h under aerobic conditions. The zone of inhibition was measured in diameters.

3.3 Results and discussion

3.3.1 Characterization of EET cross-linked polymer

EET cross-linked polymer was synthesized by condensation polymerization and characterized by different methods, the chemical equation of this reaction shown in Figure 17.

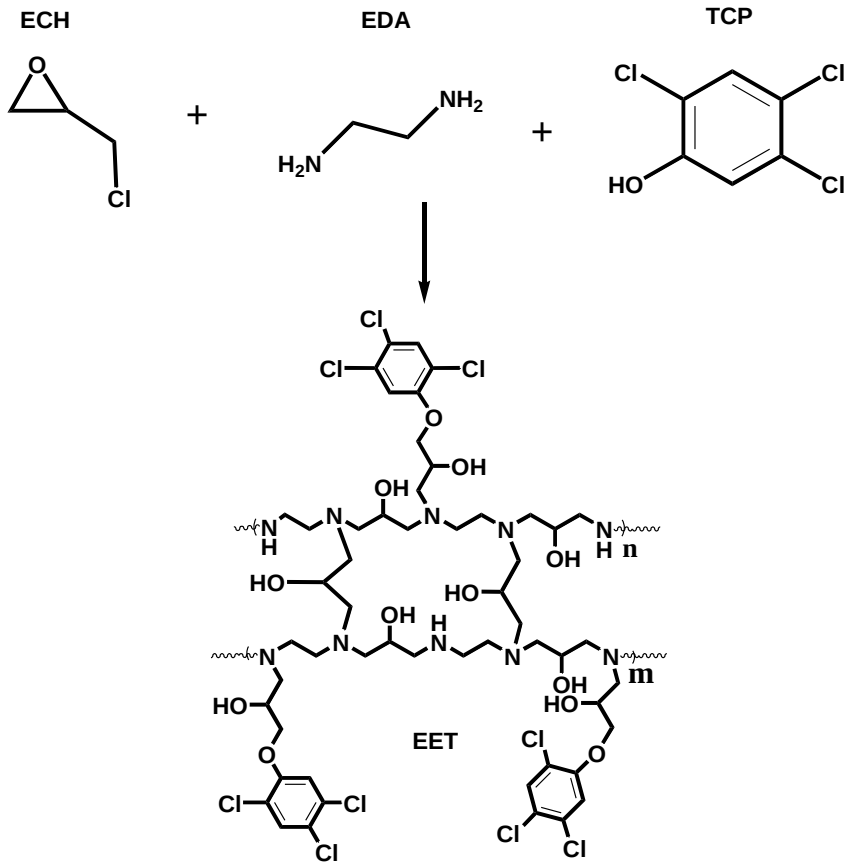

Figure 17: Chemical reaction of EDA, ECH and TCP to form EET cross-linked polymer

3.3.1.1 Thermogravimetric analysis and differential scanning calorimetry

The thermal properties of the EET were analyzed by TGA and DSC. Figure 18 shows the results of a) TGA and b) DSC of the polymer. Figure 18b shows an endothermic

peak for the EET. Glass transition (T_g) appeared at -24.7°C when the polymer changed from solid-state to a rubbery state. Peaks between 20 and 200°C referred to as a change in the polymer states (from rubbery state to liquid state), this change is accompanied by a change in density (when the density changes, the mass will change). The main peak of decomposition appeared between 273 to 400°C. This result was supported by TGA (Figure 18a). Around 1% weight loss of polymer occurred when the temperature increased to 195°C. Beyond 200°C, the weight loss gradually increased to 83% at 400°C and stabilized at 86%. The decrease in mass% most probable was due to not only the degradation of the backbone (N-C, C-C) bonds in the polymer but also, from the branches (trichlorophenol, C-C, C-O and C-H bonds). The decomposition of chlorophenol moieties will form gases such as CO, CO_2, Cl_2, and HCl [102]. It can be concluded from these results that the compound is thermally stable.

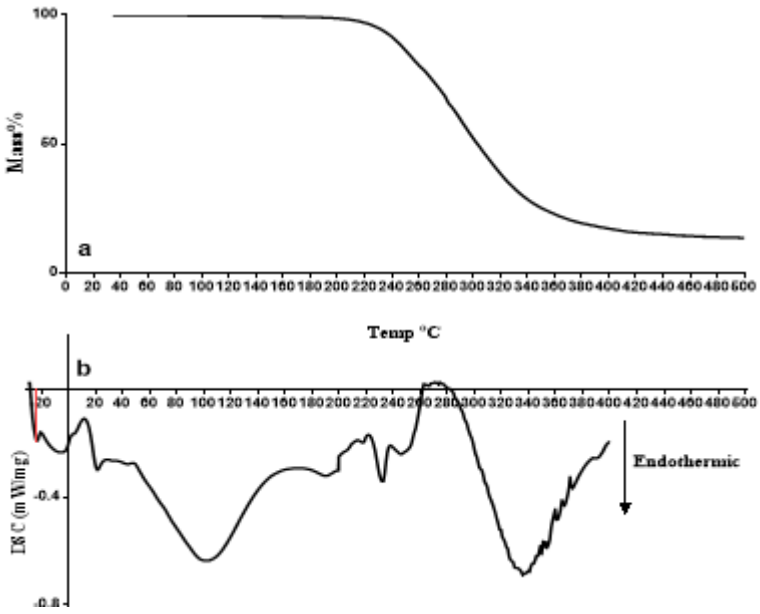

Figure 18: a) TGA and b) DSC of the EET cross-linked polymer

3.3.1.2 Fourier-transform infrared spectroscopy (FT-IR)

Fourier Transform Infra-Red (FT-IR) was utilized to compare EET with EDA and ECH molecules as shown in Figure 19. Peaks at 2860 and 2926 cm^{-1} correlated with C-H bonds in EDA Figure 19a, these peaks overlapped and shifted to 2829 and 2948 cm^{-1} in the cross-linked polymer Figure 19b. The intensity of amine groups (N-H) which appeared at 1591 cm^{-1} (Figure 19a) decreased in Figure 19b due to the reaction with ECH in the back bone of the polymer, branched with TCP and cross-linked. A primary amine left in the product and appeared at 1600 cm^{-1} (Figure 19b).

In the EET, new C−N peaks between EDA and ECH appeared at 1289 and 1249 cm^{-1}. The band at 3294 cm^{-1} (Figure 18b) referred to N-H and O-H groups [118]. Epoxy group(C-O-C) and C-Cl bond in ECH appeared at 925 and 721 cm^{-1} Figure 19c [100]. These peaks disappeared in the EET cross-linked polymer (Figure 19b), due to the reaction. A new ether group (C-O-C) appeared at 1029 cm^{-1} in Figure 19b as a branch between ECH and TCP [101]. Figure 20 shows the FT-IR spectrum of cross-linked polymer (EET) before (Figure 20b) and after adsorption of MO (Figure 20c) and RB (Figure 20a) dyes. From Figure 20c, the peak at 1600 cm^{-1} referred to amine (N-H) group disappeared after adsorption of MO dye, also (S=O) from the dye appeared at 1122 cm^{-1} [119]. Peaks between 1000 –1100 cm^{-1} changed because of the interaction between the EET and MO dye molecules. On the other hand, the peaks around 1350 cm^{-1} in Figure 20a became wider due to the chemical interaction between nitrogen in the EET and oxygen in the carboxylate ion in RB dye molecules.

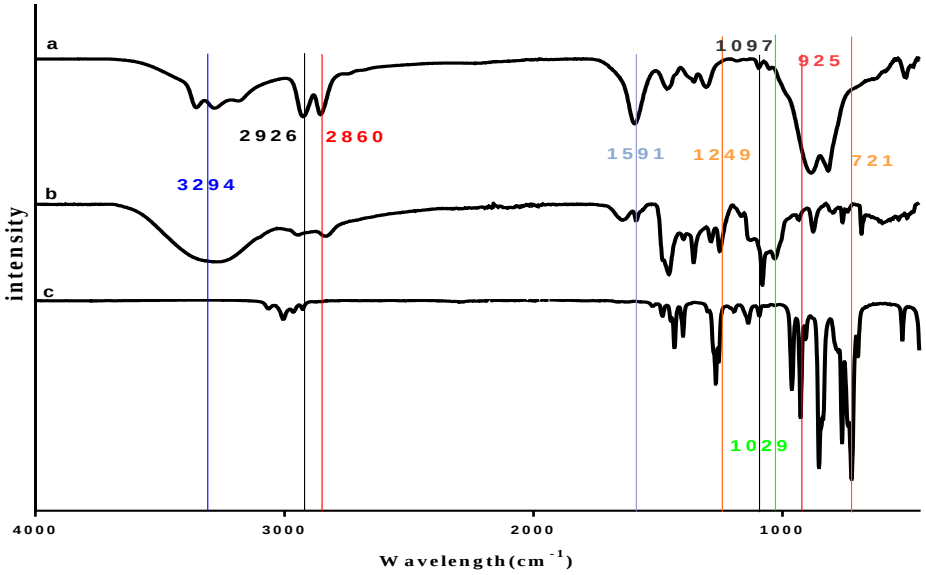

Figure 19: FT-IR of a) EDA, b) EET cross-linked polymer and c) ECH

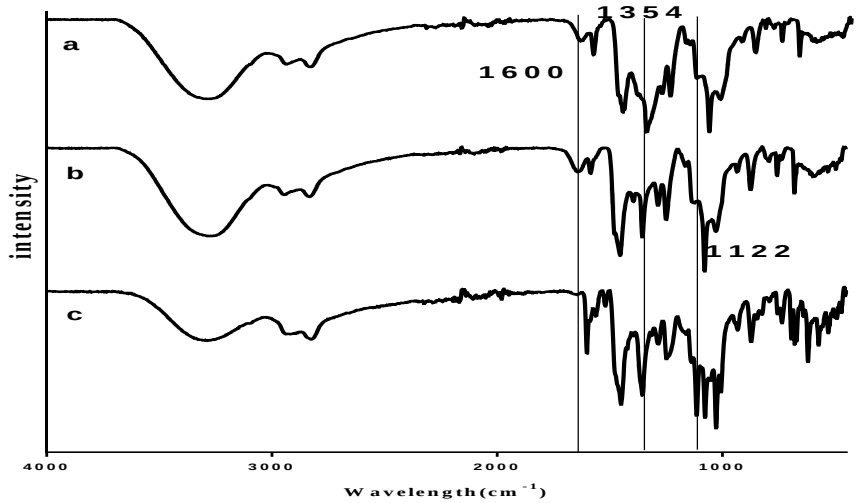

Figure 20: FT-IR of a) polymer adsorbed RB dye, b) polymer before adsorption and c) polymer adsorbed MO dye

3.3.1.3 Determination of the polymer composition

The polymer formations were examined by elemental analysis. The amount of TCP that has been reacted can be specified via the percentage of chlorine in the cross-linked polymer. Table 2 shows 8.18% of chlorine in the EET which is 2.18 x 10^{-3} mol of TCP reacted with ECH as a branch on the backbone of the polymer. Also, 4.99% of nitrogen

was found which indicated that all the amount of EDA had reacted with ECH in the polymer.

Table 2: Elemental analysis of the EET cross-linked polymer.

Sample	%C	%Cl	%N	%H
EET	35	8.18	4.99	44.33

3.3.1.4 Scanning Electron Microscope (SEM)

The surface morphologies of EET before and after adsorption of RB and MO were examined by SEM and shown in Figure 21a-c. The EET exhibited a rough surface with visible pores of an average diameter of 2.86 µm (Figure 21a) before adsorption. After the adsorption process of MO dye (Figure 21b) and RB dye (Figure 21c), the surface morphologies of EET showed that the majority of the pores were filled by the adsorbed dyes. Comparatively, the surface morphology of EET containing MO dye exhibited a less roughened topology than that of EET containing RB dye molecules. Noticeably, EET-RB exhibited a little rough surface with some unoccupied pores which might be attributed to the fact that RB is bulkier (479.02 g/mol) than MO dye (327.33 g/mol). The observation is consistent with the Freundlich isotherm results which suggested physisorption may contribute to RB adsorption.

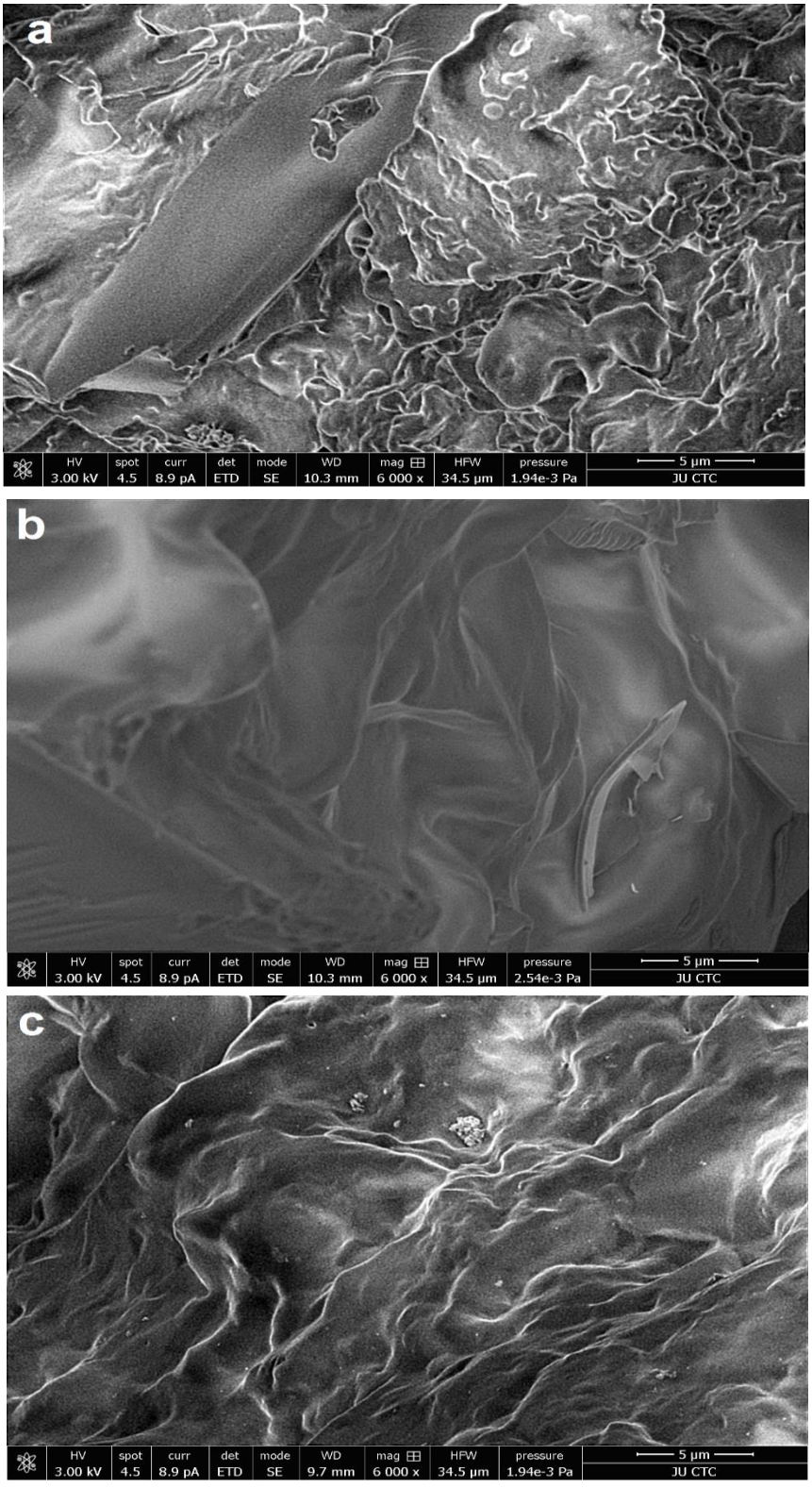

Figure 21: SEM micrograph (x6000) of a) polymer before adsorption, b) polymer adsorbed MO dye and c) polymer adsorbed RB dye

3.3.2 Effect of initial solution pH

The effect of pH on the adsorption of MO and RB by EET was investigated. 10 mg of EET was immersed in 10 ppm MO and RB individually at 298 K for 24 h. Different pH solutions were used (2 – 9) to achieve the highest adsorption amount of MO and RB. Figure 22 shows that; MO can be adsorbed by the cross-linked polymer at all pH; suggesting that both alkali and acidic solutions are suitable for the removal of methyl orange dye molecules, and the maximum adsorption occurred at pH 8 with 97% removal.

The pH_{pzc} of EET was obtained as 6.5, which means at pH values higher than the pH_{pzc}, the surface of the EET will be negatively charged and vice versa [120]. The adsorption of MO lower than 6.5 is attributed to electrostatic interaction between the positively charged EET surface and the negatively charged sulphonic group of the MO. Above 6.5, MO adsorption may due to hydrophobic interaction or noncovalent π–π interactions between aromatic rings of the dye and that of the trichlorophenol, which is reflected in the FTIR spectra (Figure 22). A similar observation has been reported elsewhere [121]. For RB, the highest removal at pH 3 with 70%; in the acidic medium, the adsorption of RB happened due to the interaction between the protonated amino group on the cross-linked polymer and the oxygen in carboxylic group on RB, π–π interactions or hydrophobic. EET cross-linked polymer exhibited a wide performance until pH 8, at pH 9, RB removal decreased sharply which is attributed to the electrostatic repulsion between the zwitterionic form of RB in solution and the negative charge on the surface of EET [61,122,123].

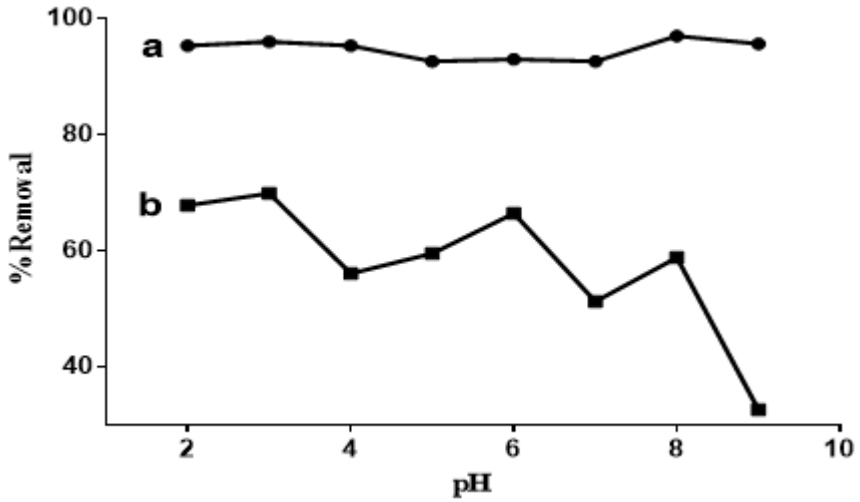

Figure 22: Effect of pH on a) MO and b) RB

3.3.3 Effect of adsorbent dosage

The effect of EET dosage is illustrated in Figure 23. % removal of RB increases from 65% to 80% and stabilize when the EET dosage increased from 10 to 20 mg. On the other hand, only slight increases in the percent removal (92.5 to 94%) of MO was noticed when the dosage increased from 10 to 20 mg. 10 and 15 mg EET dosage were chosen for further tests in this research with MO and RB dyes respectively.

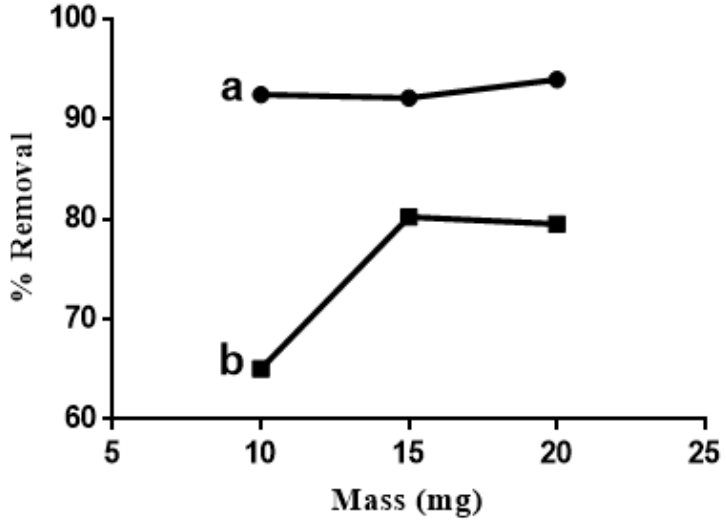

Figure 23: Effect of dosage vs % Removal of a) MO (20 ppm, pH 8.0 ± 0.1) and b) RB (10 ppm, pH 3.0 ± 0.1) at room temperature

3.3.4 Effect of initial concentration

Figure 24 illustrate the effect of initial dye concentration (10-100 ppm) on the removal of RB and MO dye solutions. When the concentration of RB increased from 10 to 100 ppm, the uptake capacity increased from 11.24 to 126.3 mg/g, while MO dye increased from 22.74 to 240.71 mg/g. The driving force of the concentration was the main reason for the increasing trend of the uptake capacity with increasing the initial dye concentration [61]. A similar observation was noticed by Ifebajo and Oladipo [120], they reported that a high concentration of rhodamine B dye facilitated a higher mass transfer driving flux. Hence more RB species were transported from the aqueous solution to the adsorbent surface, which resulted in a higher RB removal.

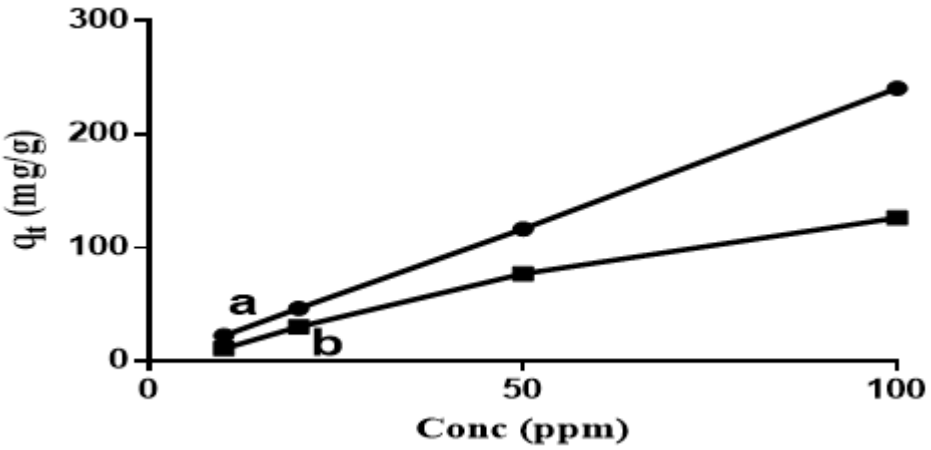

Figure 24: Effect of concentration of dye solutions, a) MO (pH 8.0 ± 0.1) and b) RB (pH 3.0 ± 0.1) vs intake capacity. Amount of polymer 10.0 mg, the volume of solutions was 25 mL and conducted at a room temperature

3.3.5 Adsorption isotherm

Langmuir, Temkin and Freundlich models were applied on the adsorption experimental results and tabulated in Table 3. Langmuir isotherm and Temkin model described the adsorption process of MO and RB dyes onto the cross-linked polymer respectively, where higher R^2 values were achieved. R^2 of MO is > 0.998 which reveals

that the cross-linked polymer possessed active functional groups that distributed on the surface with the same energy level and thus initiate a monolayer coverage of the dye molecules via chemisorption mechanism [124]. On the other hand, RB fitted with Temkin (R^2=0.9990). According to the Temkin model, the adsorption energy diminishes directly with the surface covering of EET polymer because of adsorbate-adsorbent interaction (chemisorption system) [116,120,125,126].

Table 3: Adsorption isotherms parameters of MO and RB onto EET cross-linked polymer.

Dye type	Langmuir $\frac{C_i}{q_e}=\frac{C_e}{q_{max}}+\frac{1}{k_L.q_{max}}$			Freundlich $Log(q_e)=Log(K_F)+\left(\frac{1}{n}\right)\log(C_e)$			Temkin $q_e=\left(\frac{RT}{b_T}\right)(\ln(C_e)+\ln(k_T))$		
	q_{max}	b_L	R^2	K_F	n	R^2	b_T	K_T	R^2
MO	144.9	0.56	0.9986	29.57	0.7	0.8687	110.1	4.1	0.9866
RB	149.3	0.24	0.9770	41.57	2.1	0.9911	43.7	1.0	0.9990

3.3.6 Effect of temperature and thermodynamic parameters

Three different temperatures (30, 40 and 50°C) were applied to examine the performance of EET, and the thermodynamic parameters including free Gibbs energy (ΔG^o), enthalpy change (ΔH^o) and entropy changes (ΔS^o) were calculated. The removal efficiencies of MO and RB decreased with increasing temperature which is consistent with the data listed in Table 4, where the adsorption of MO and RB is noted to be exothermic due to negative values of ΔH^o.

The negative value of ΔS^o for RB adsorption at pH 3 indicates a decrease in the degree of randomness of the RB dye molecule at the solid-liquid interface during the adsorption process. The positive ΔS^o value of MO denotes an increase in the degree of randomness since heat is not transferred from the environment to the system (ΔH^o is

negative) which is isolated, therefore the entropy is considered as the main driving force for adsorption. This value was expected since the MO molecule is anionic (has a negative charge) and the dye solution is basic (pH = 8) with a negative charge, leading to a significant repulsion between the negative charges of the solution and the dye molecules which results in rising of ΔS^o value (positive). Moreover, ΔG^o for MO is negative at all temperatures, and for RB is negative within the temperature range studied which revealed the spontaneity of the adsorption process [117,127].

Table 4: Thermodynamic parameters of the adsorption of MO and RB Dyes onto EET cross-linked polymer.

	ΔG^o (kJ/mol)			**ΔH^o**	**ΔS^o**
	303 K	313 K	323 K	**(kJ/mol)**	**(J/mol.K)**
(MO)	-9.849	-9.884	-9.918	-8.814	+3.417
% Removal	95.26	94.62	94.18		
(RB)	-7.870	-6.223	-4.576	-57.768	-164.68
% Removal	93.56	85.21	77.90		

3.3.7 Kinetics studies

Figure 25 shows the adsorption rate of MO and RB dyes when 10 and 15 mg of EET were used to remove 50 ppm of the MO and RB dye solutions respectively. The removal of the dyes was rapid where more than 50% was removed after 15 min for MO and 50 min for RB dye. Note that MO removal rate reached equilibrium after 4 h with more than 98% removal, while 91% of RB was removed after 12 h. The experimental results were fitted into the pseudo-first-order and pseudo-second-order kinetic models and obtained parameters are given in Table 5. Considering the correlation coefficient and calculated q_e, the pseudo-second-order model fits well with the experimental results. Specifically, the correlation coefficient of the pseudo-second-order model (R^2 of MO and RB $\geq$ 0.99) is higher than that of the pseudo-first-order

model (R^2 of MO ≥ 0.97 and RB ≥ 0.98). Also, the theoretical q_e values of pseudo-second order are nearer to the experimental values, suggesting chemisorption.

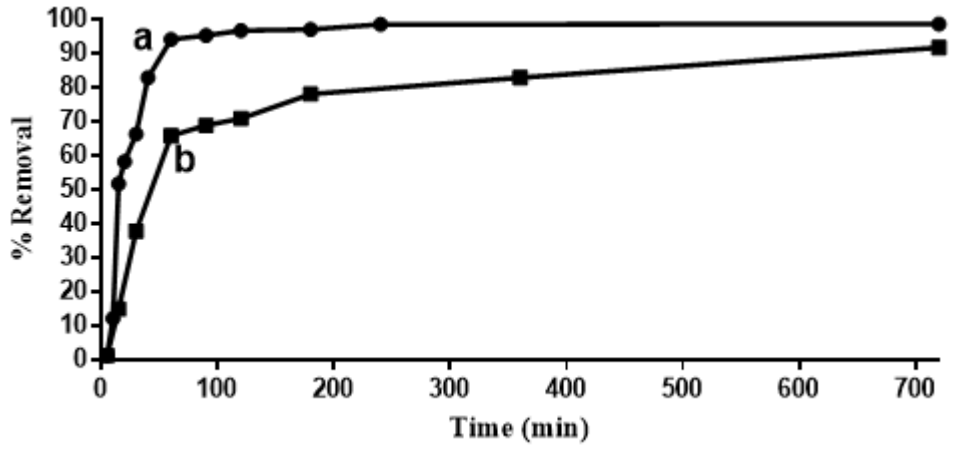

Figure 25: Effect of contact time on percent removal of a) MO dye solution (50 ppm, pH 8.0, 10.0 mg) and b) RB dye solution (50 ppm, pH 3.0, 15.0 mg) at room temperature

Table 5: Kinetic parameters of Methyl Orange and Rhodamine B Adsorption onto EET polymer

Type of dye	1st Order $\ln(q_e - q_t) = \ln(q_e) - k_1 \cdot t$				2nd Order $\left(\frac{t}{q_t}\right) = \left(\frac{1}{k_2 \cdot q_e^2}\right) - \left(\frac{t}{q_e}\right)$				q_e (Exp) (mg/g)
	q_e (mg/g)	k_1 (min^{-1})	R^2	$q_e - q_t$ (mg/g)	q_e (mg/g)	k_2 (g/mg.min)	R^2	$q_e - q_t$ (mg/g)	
RB	43.88	0.0064	0.97	-33.17	80	3.11×10^{-4}	0.9985	2.95	77.05
MO	129.31	0.0396	0.982	5.9	133.33	5.53×10^{-4}	0.9957	9.92	123.41

3.3.8 Desorption and regeneration of cross-linked polymer

The desorption of the adsorbed dyes from the polymer was investigated by using 0.1 M HCl and ethanol as eluents for MO and RB dyes, respectively. Clearly from Figure 26a, more than 50% of MO was desorbed after 5 min from the EET which extended to 98% after 45 min. Contrastingly, only 51% of RB dye was desorbed after 90 min as presented in Figure 26b. The reuse of the desorbed EET was evaluated after thermal

treatment at 40°C Table 6. EET maintained sufficiently high performance even after 5 recycle uses (98.72 – 98.65%) within 4 h.

In comparison, the removal efficiency for RB decreased from 92.45% to 47.39% after consecutive reuse within 24 h. It is worthy to note that EET efficiency decreased by 45.1% after reused twice for RB adsorption, suggesting it has higher affinity and remarkable adsorptive potential for MO, which may be due to its lower molecular weight (327.3 g/mol) compared to the larger (479.02 g/mol) RB dye. The performance of EET is compared with other reported polymeric adsorbents in the literature as presented in Table 7. As noted, EET performance is superior; for instance, Bahrudin et al. [128] reportedly applied polyaniline to remove MO dye and achieved 125 mg/g at pH 6.5, likewise, Allouche et al. [129] reported that chitosan only achieved 29 mg/g removal of MO from the aqueous solution at pH 3.0. EET efficiency is higher than the modified Moroccan clay containing cetyltrimethylammonium bromide, which removed 78.74 mg/g of RB dye at pH 7.

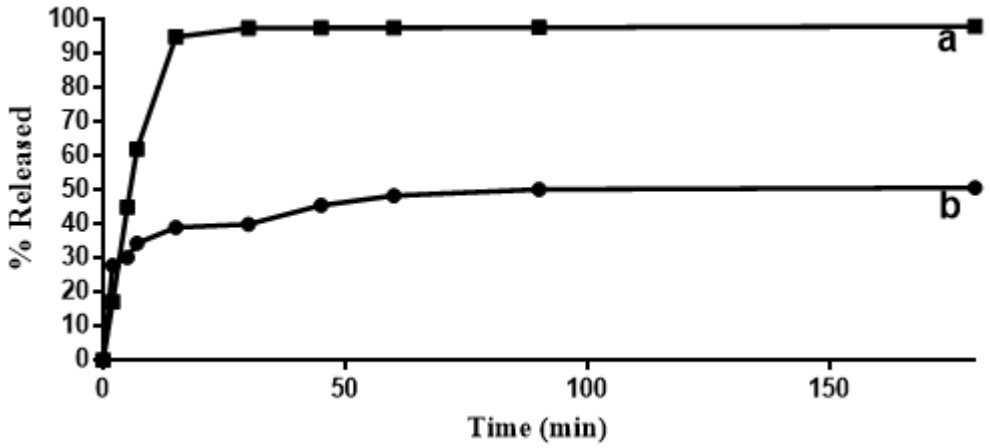

Figure 26: Releasing of a) MO from polymer by (0.1 M HCl) and b) RB from polymer by ethanol

Table 6: % Removal of MO and RB dye solutions by reuse the cross-linked polymer.

Number of Repetition	% Removal of MO dye solution	% Removal of RB dye solution
1st	**98.72**	**92.45**
2nd	**98.66**	**47.39**
3rd	**98.66**	**-**
4th	**98.65**	**-**
5th	**98.65**	**-**

Table 7: Comparison of the adsorption capacities of various adsorbents towards methyl orange and rhodamine b dyes.

	Adsorbent	Experimental conditions	q_{max} (mg/g)	Refs
MO	Activated carbons of corncob derived char wastes	pH 7, 298 K	11.57	[130]
	Graphene oxide	pH 3, 298 K	16.83	[131]
	Chitosan	pH 3, 298 K	29	[129]
	Chitosan intercalated montmorillonite	pH 2, 328.2 K	123.46	[121]
	Polyaniline	pH 6.5, 303	125	[128]
	EET cross-linked polymer	pH 8, 298 K	144.9	This work
RB	Paper industry waste sludge	pH 2.4, 308 K	6.711	[132]
	poly (ethylene terephthalate) fibers grafted by 4-vinyl pyridine and 2-methylpropenoic acid	pH 12, 298 K	45.28	[133]
	Poly(cyclotriphosphazene-co-4,4′-sulfonyldiphenol) Nanotubes	pH 1.2,298 K	46.06	[134]
	Modified Moroccan Clay with Cetyltrimethylammonium Bromide	pH 7, 298 K	78.74	[135]
	zinc oxide loaded activated carbon (ZnO-AC)	pH 7, 303 K	128.21	[136]
	EET cross-linked polymer	pH 3, 298 K	149.3	This work

3.3.9 Disc diffusion assay

Disc diffusion method was used to determine antimicrobial activity with *E. coli* and *S. aureus* bacteria by measuring the zones of the inhibition of EET cross-linked polymer. Figure 27 shows the result of this inhibition with 39 and 64 mm inhibition zone with *E. coli* and *S. aureus* bacteria. The antibacterial activities of EET are attributed to the presence of chlorine atoms (from trichlorophenol), hydroxyl and amine groups (in the backbone of the polymer). The protonated amino groups can interact electrostatically with the Gram-negative bacteria strain and inhibit its growth. The chlorine can interact with the bacterial lipids within the cell walls and destroys the enzymes, hence, making

the bacteria cells to be oxidized, and results in death. From these results, EET is a potential antimicrobial polymer with sufficient adsorption performance.

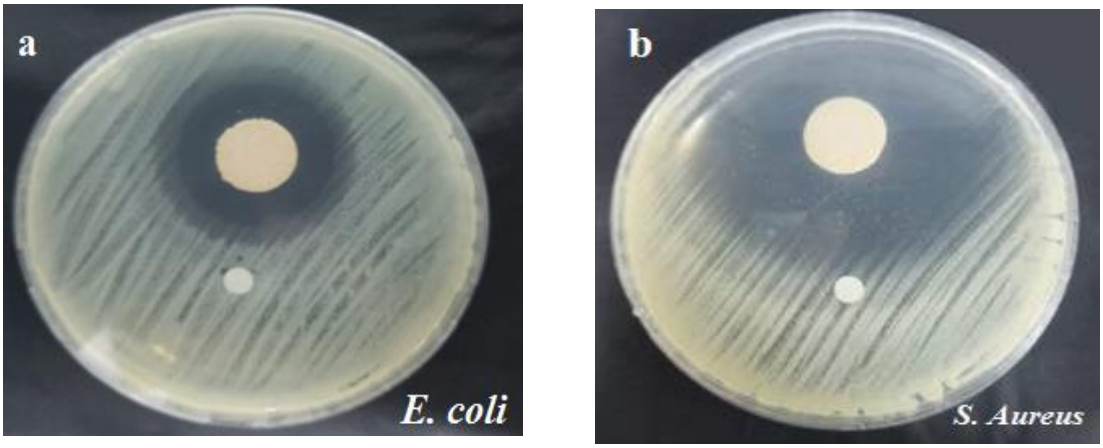

Figure 27: Disk diffusion assay for a) *E. coli* and b) *S. aureus* bacteria

3.4 Conclusion

Herein, an ethylenediamine-epichlorohydrin-trichlorophenol cross-linked polymer (EET) was synthesized and characterized. The performance of EET for the treatment of dye-containing synthetic solutions was investigated for the removal of both anionic dye (methyl orange) and cationic dye (rhodamine B).

98.72% and 92.45% of MO and RB dyes were adsorbed at pH 8 and 3 using 10 mg and 15 mg of EET, respectively. Notably, more than 50 % of MO was adsorbed during the first 15 min, which revealed that EET exhibited fast adsorption kinetically. According to the Langmuir isotherm, the maximum uptake of MO and RB is 145 mg/g and 149.3 mg/g under the optimum conditions. 98% of MO was desorbed by 0.1 M HCl from the spent EET after 45 min, while only 51% of RB was desorbed within 90 min by ethanol. The regenerated EET maintained high removal efficiency (~98.65%) after 5 recycling circles. Also, the toxicity of the prepared polymer was eliminated due

to its insoluble property, and EET exhibited excellent antimicrobial activities against *E. coli* and *S. aureus* with inhibition zones of 39 and 64 mm respectively via the disk diffusion assay. Results herein show that EET is an alternative polymeric adsorbent with antimicrobial functions for the treatment of dye contaminated industrial effluents.

Chapter 4

ANTIBACTERIAL NANOPARTICLES AND PHENOLIC DEGRADATION

4.1 Introduction

In agriculture, a lot of pesticides have been used to control pests and weeds. One of the strongest pesticide that was used before is 2,4,5-trichlorophenol compound. It has high killing and inhibitory effect on the growth of microorganisms [28]. However, it has limited application due to its cytotoxicity effect [28,30,34]. Although it has low solubility in water, it can spread easily into aquatic environment and accumulate in the lipid part of organisms [31].

To remove TCP from aqueous water, different techniques were applied. Among these techniques, adsorption method was used to remove it via montmorillonites material modified with an organic surfactant. This modified material demonstrated a maximum adsorption capacity of 368 mg/g at pH 4 [34]. Zheng et al. used chitosan to adsorb chlorophenol compound with an uptake capacity of 0.22 mmol/kg at pH 6.2 [78]. In addition, advanced oxidation processes like photocatalysis can degrade chlorophenol compounds to a permissible concentration [79]; TiO_2 was used to degrade TCP from 50 µM to 4 µM within five hours under UV-light [80].

Spinel ferrite magnetic nanoparticles are valuable nowadays due to their wide applications in nanoscience. Photocatalytic application is widely used to treat the

environment due to outstanding features such as super magnetic properties, photochemical stability, electrical properties, narrow bandgap, inexpensive and catalytic applications [20,21]. The structure of the spinel ferrite nanoparticles is MFe_2O_4, where M is a metal cation. Here, oxygen can form two different cubic shapes, tetrahedral and octahedral crystallographic sites with metal and iron ions, respectively [22]. These nanoparticles such as $ZnFe_2O_4$ was reported for photodegradation of acid orange II via photocatalytic process [88].

On the other hand, spinel ferrite nanoparticles were used as an adsorbent to remove pollutants. Among these nanoparticles, Fe_3O_4 modified with L-arginine was used to remove 66.66 mg/g of reactive blue 19 from wastewater suggested that the reactive blue 19 bound with the protonated amine groups of the coted surface of Fe_3O_4 [89]. $NiFe_2O_4$ was used to adsorb 138.5 mg/g of methylene blue and other heavy metals because of 3D interconnected porous structure [90]. Carbon nanotubes/$CoFe_2O_4$ developed by chitosan (hybrid material) was used to extract 42.48 mg/g of tetrabromobisphenol A and 140.1 mg/g of Pb(II) [137]. $AgCoFe_2O_4$-graphene oxide was used to remove 60.8 mg/g of lead from wastewater in which extraction depended on the surface area and zeta potential of the compound [138]. Nickel zinc ferrite is another type of ferrite nanomaterial with general formula $Ni_yZn_{1-y}Fe_2O_4$. It is soft magnetic material with high resistivity and saturation magnetization. It has been used in wide applications such as transformers and high-frequency inductance magnetic cores [139].

On contrast, reports reveled that nickel-zinc-ferrite nanoparticles ($Ni_{0.5}Zn_{0.5}Fe_2O_4$) have been used as antibacterial agent with 0.25 mg/L and 0.125 mg/L as MIC values against *E. coli* and *S. aureus* respectively [140].

In this study, Li doped $Ni_{0.5}Zn_{0.5}Fe_2O_4$ (Li/ZNF) photocatalyst was prepared by two-steps to degrade TCP under UV irradiations. The photocatalytic behaviour of Li/ZNF was investigated under different conditions and in the presence of different negative ions as an interference. Furthermore, the antibacterial studies of the Li/ZNF was evaluated against *S. aureus* and *E. coli* bacteria by time kill assay.

4.2 Methodology

4.2.1 Materials

Zinc (II) sulfate heptahydrate ($ZnSO_4.7H_2O$) was purchased from Analar Trada, nickel (II) sulfate hexahydrate ($NiSO_4.6H_2O$) was purchased from Alfa Aesar, lithium carbonate (Li_2CO_3), iron (III) chloride hexahydrate ($FeCl_3.6H_2O$), acetic acid, sodium hydroxide (NaOH) and 2,4,5-trichlorophenol (TCP) were purchased from Sigma Aldrich, hydrochloric acid (HCl, 35%), ethanol hydrogen peroxide (H_2O_2) and potassium persulfate ($K_2S_2O_8$) were purchased from Merch. *Staphylococcus aureus* (*S. aureus*, ATCC 2921) and *Escherichia coli* (*E. coli*, ATCC 25922), Muller Hinton Agar (MHA) and MacConkey agar (MCA), (Biomerieux, France)

4.2.2 Instruments

$Li/Zn_{0.5}Ni_{0.5}Fe_2O_4$ (Li/ZNF) was characterized by X-ray diffractometer (XRD) Bruker D8 (Bruker-AXS, Ettlingen, Germany) using a Cu Kα (λ =1.54187 Å) radiation at 40 kV and the crystalline phases were clarified using standard JCPDS files (Cyprus International University). Infrared absorption spectra (FTIR) (PerkinElmer, UK) (Eastern Mediterranean University). The pore size distribution and specific surface area were quantified at - 196°C on an Autosorb analyzer (QuantaChrome, USA) (Cyprus International University). The UV–vis diffuse reflectance spectra (DRS) were obtained using a UV–2450 spectrometer (Shimadzu, Japan) via the standard Kubelka-Munk method and from Tauc plots. The residual TCP concentration was determined

by a double beam UV-Vis spectrophotometer (T80+, PG Instruments Ltd, UK) (Cyprus International University).

4.2.3 Methods

4.2.3.1 Synthesis of $Ni_{0.5}Zn_{0.5}Fe_2O_4$ (ZNF)

The $Ni_{0.5}Zn_{0.5}Fe_2O_4$ (ZNF) nanoparticles were prepared by the co-precipitate method as follow: 5.5 g of $ZnSO_4.7H_2O$ was dissolved with 6 g of $NiSO_4.6H_2O$ and 5.7 g of $FeCl_3.6H_2O$ in 80 mL distilled water, the solution was stirred continuously at 250 rpm until became homogeneous then 20 mL of acetic acid (0.3 M) was added to prevent the aggregation. After that, the solution was transferred to an oil bath and heated at 80°C for 3 h with vigorously magnetically stirred (800 rpm). The solution was poured into a petri dish then heated and dried at 80°C overnight. The solid product was formed then transferred to a muffle furnace and calcined at 800°C for 2 h.

4.2.3.2 Synthesis of Li/ZNF composites

Li/ZNF composite was prepared by the hydrothermal route. This method was performed using 5 g of ZNF in 50 mL of 0.1 M Li_2CO_3. The solutions were stirred at 250 rpm for 45 min at R.T. After that the temperature was increased to 70°C and 30 mL of 75 mM NaOH was added dropwise into the suspension solution. After continuously stirred for 1 h at 70°C, the suspension solution was filtered and washed with water and 50% ethanol. Then, dried at 100°C for 24 h.

4.2.3.3 Photocatalytic activity evaluation

All photocatalytic degradation trials were performed at 200 rpm using a 100 mL beaker containing 25 mL of TCP solutions. The effect of photocatalytic degradation of TCP was tested by varying parameters such as pH (2 - 10), H_2O_2 and $K_2S_2O_4$ concentration (4 – 7 mM), amount of photocatalytic (10 – 50 mg), reaction time (0- 6 h) were carried out under UV fluorescent light with 353 nm wavelength except the first 30 min, the

solutions were agitated in dark to establish adsorption-desorption equilibrium on the surface of the composites. The pH of the solutions was adjusted by 0.1 M HCl/NaOH. Results notified in this work are the average of duplicate trials. After the photodegradation process, the nanoparticles were separated from the solution using an external magnet, then the solution was filtered by filter paper and the filtrate analyze for residual TCP concentration by UV-vis spectroscopy at the maximum wavelength 289 nm. The concentrations were resolved using a linear regression equation obtained by plotting a calibration curve of TCP absorption over a range of concentrations with $R^2 = 0.996$. To investigate the stability and reusability of the Li/ZNF catalyst, the photo-catalyst was separated from the solution by an external magnet at the end of the experiment, and eluted by water then dried at 40°C then reused repeatedly. Additionally, to emphasize the presence of reactive radical species (photo-generation holes (h^+), superoxide ($^{\bullet}O_2^-$) and hydroxyl radical ($^{\bullet}OH$)) during the photo-catalytic process, (5 mM) of the scavenger coefficients were added into the solutions, the process has been described elsewhere [141]. Furthermore, the interference of 50 ppm TCP individually with different anions (0.1 M of NaCl (Cl^-), KNO_3 (NO_3^-), and Na_2SO_4 (SO_4^{2-})) was studied respectively. The degradation efficiency (%D) was calculated elsewhere [142].

$$\%D = \left(\frac{(C_i - C}{C_i} \right) x100\% \quad (8)$$

Where C and C_i are the concentration at equilibrium and initial respectively.

4.2.3.4 Antimicrobial Time-Kill assay

The antimicrobial activities of Li/ZNF nanocomposite were evaluated quantitatively by time-kill assays. *S. aureus* and *E. coli* cultures were incubated overnight at 37°C in MHA, and MCA respectively. Then, bacterial stock solutions were prepared in MHB

and standardized by using the McFarland instrument (0.5 McFarland = 1 x 10^9 CFU/mL).

Furthermore, sterilized flasks were filled with 50 mL of sterile saline solution. Meanwhile, 50 µL from bacteria stock solutions were added individually to each solution to end up with 1 x 10^6 CFU/mL as the initial concentration of bacterial cells. Three different dosages (5, 15, and 25 mg) of nanocomposites were used to kill the bacteria. Afterwards, the flasks were agitated at 200 rpm under two different cases; under dark condition for 1 h and the UV fluorescent light (353 nm) for 6 h individually. At different interval times, 10 µL was withdrawn from all samples (including the control) and diluted three times in plates with 90 µL of MHB then plated on agar and incubated for 24 h at 37°C. After that, the colonies were counted and concentrations of bacteria (CFU/mL) were calculated then plotted vs Time (h).

(CFU/mL) = (number of colonies x dilution factor) / volume of culture plated (9)

4.3 Results and discussion

4.3.1 Characterization of $Li/Zn_{0.5}Ni_{0.5}Fe_2O_4$ (Li/ZNF)

4.3.1.1 Fourier-transform infrared spectroscopy (FT-IR)

Figure 28 shows the FTIR spectra of Li/ZNF before and after the photocatalytic process. The bands in the fingerprint 567 and 483 cm^{-1} referred to metal-oxygen octahedral (Fe-O) and tetrahedral (Ni-O and Zn-O) respectively [84]. Peaks at 3400 and 1120 were assigned to hydroxyl group stretching and bending respectively [143]. These peaks disappeared after the photocatalytic process because of the degradation of TCP. This result was supported by scavenger trapping experiment, hydroxyl group and holes have a major impact in the enhancement of photocatalytic activity which

leads to forming (•OH) that is required for the degradation mechanism of TCP. A similar observation was noted by Ali et. al. [144].

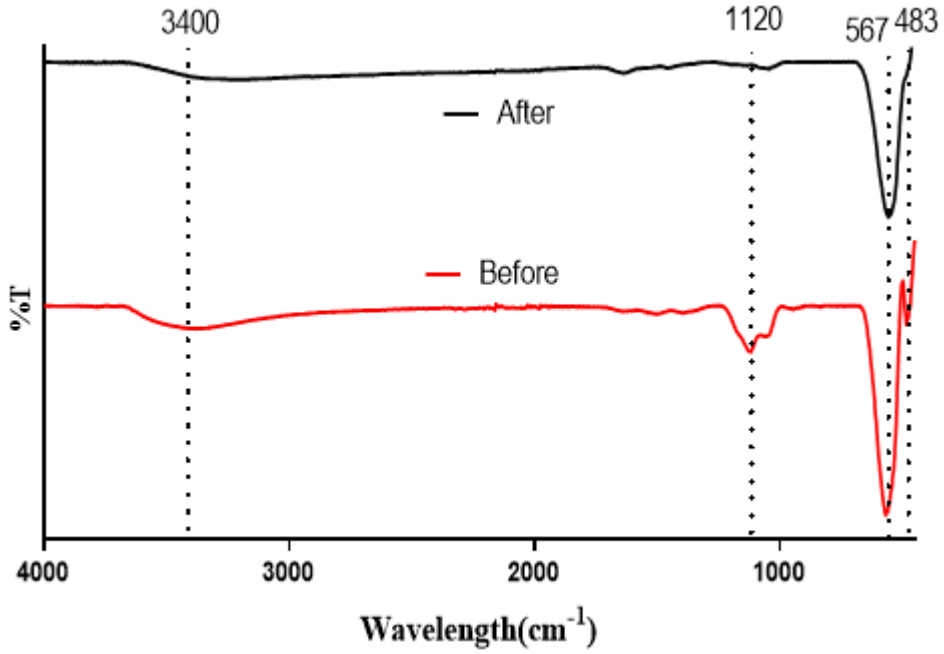

Figure 28: FTIR of $Li/Zn_{0.5}Ni_{0.5}Fe_2O_4$ before and after photo degradation process

4.3.1.2 Adsorption desorption isotherm of Li/ZNF by N_2 (BET) and X-ray diffraction (XRD) analysis

The adsorption-desorption of nitrogen and pore size distribution for Li/ZNF is illustrated in Figure 29. Nitrogen uptake was at $p/p^o \geq 0.99$, Li/ZNF possesses type I and IV isotherm with H3 hysteresis with micro and mesoporous. As listed in Table 8, Li/ZNF possesses 0.298 cm^3/g pore volumes and 56.8 m^2/g specific surface area.

The X-ray diffraction pattern of as-prepared ZNF and Li/ZNF are shown in Figure 29. The XRD results illustrated that $Zn_{0.5}Ni_{0.5}Fe_2O_4$ and $Li/Zn_{0.5}Ni_{0.5}Fe_2O_4$ possess a cubic spinel structure with diffraction peaks 2θ = 18.34°, 30.14°, 34.58°, 35.58°, 43.18°, 53.56°, 57.16°, 62.8°, and 71.42° and reflection planes (111), (311), (220), (222), (400), (422), (511), (440), (533) (JCPDS No. 08-0234) [145]. Notably, nickel

and zinc ions formed octahedral and tetrahedral sites respectively due to the difference in ionic radiuses; zinc ion possesses higher ionic radius (0.84 Å) with sp^3 hybridization orbital than nickel ion (0.74 Å) [146]. Also, weak diffraction peaks appeared at 49.4°, and 33.1° were consistent with (220) and (111) of Li_2O (JCPDS No. 12–0254), and the peaks at 40.9°, 37.38° and 24.12° were indexed to (101), (011) and (020) of Li_2CO_3 (JCPDS No. 83-1454) [147]. As calculated % crystallinity (Table 8), Li/ZNF has higher crystallinity of 76.8% than ZNF 66.8%.

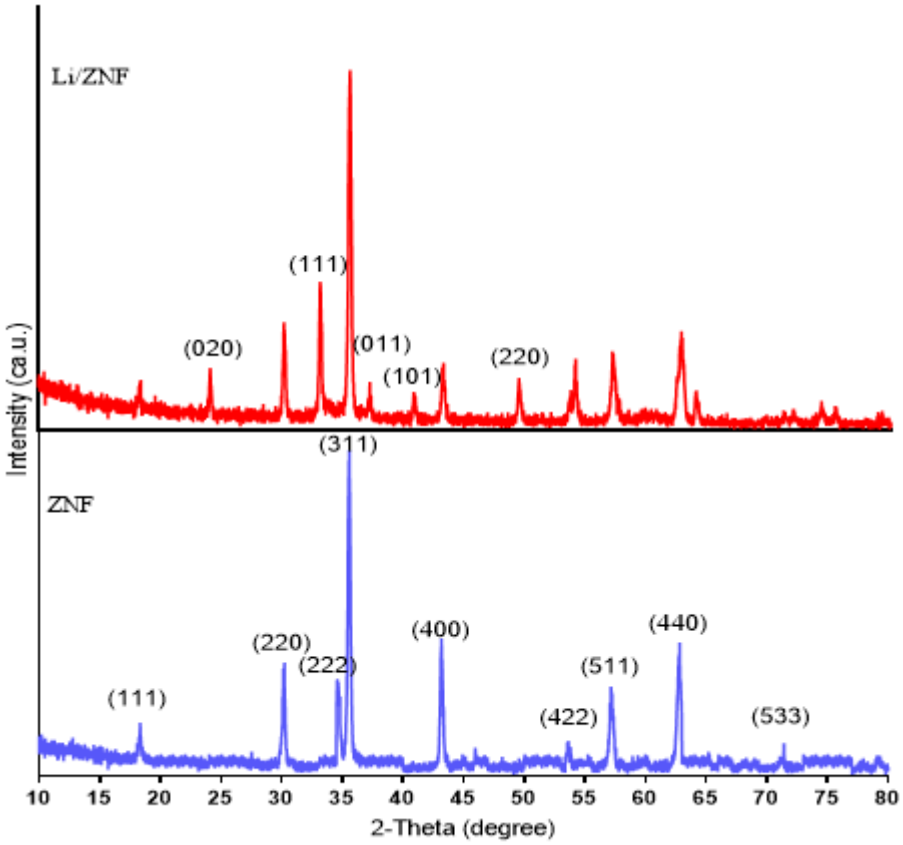

Figure 29: XRD pattern of ZNF and Li/ZNF nanoparticles

Table 8: Textural and XRD characteristics of NZF and Li/NZF.

	Surface area and pore volume				XRD structural parameters		
Sample	[a]S_{BET} (m^2/g)	[b]V_t (cm^3/g)	[c]V_{mic} (cm^3/g)	[d]V_{mes} (cm^3/g)	[e]D (nm)	[f]δ (nm^{-2})	[g]X (%)
NZF	73.5	0.287	0.158	0.129	19.9	2.52	66.8
Li/NZF	56.8	0.298	0.117	0.181	16.9	3.50	76.8

a: Brunauer-Emmett-Teller specific surface area obtained via nitrogen adsorption isotherm at $P/P_o = 0.05 – 0.35$, b: Total pore volume measured at $P/P_o \sim 0.99$, c and d: micro and mesopore volume, e: Average crystallite size calculated by Debye Scherer's formula, f: dislocation density calculated from $\delta \times 10^{-3}=1/D^2$, and g: is % crystallinity= $I_{crystalline\ peaks} / (I_{crystalline\ peaks}+ I_{amorphous\ peaks})$.

4.3.2 Effects of initial pH on the performance of Li/ZNF

Effect of pH on TCP removal under UV light with Li/ZNF alone and with oxidants (4 mM of H_2O_2 and $K_2S_2O_8$) were investigated. When 50 ppm TCP solution pH was varied within 2-10 in the presence of 25 mg of nanoparticle as shown in Figure 30. The pH drift method revealed the zero-point charge (pH_{zpc}) of Li/ZNF as 7.2 [148]. When $pH < pH_{zpc}$, degradation of TCP was low at pH 2 (~10%) with H_2O_2 because of the low amount of TCP as an ionic species [34].

Beyond pH 2, the percent degradation of TCP was increased gradually from 2 to 3 and stabilized (~32%) until pH 7. Notably, at pH 3; degradation of TCP was the highest with H_2O_2 (~55%), due to the presence of •OH which include in the mechanism of degradation, similar observation was reported by Azalok et al [149]. Furthermore, the nanocomposite has a positive charge on the surface when pH lower than 7.2, and TCP existed as unionized when the pH of the solution lower than pKa (6.8) of TCP, therefore, dispersion interaction occurred [150]. However, when $pH > pH_{zpc}$ (alkaline conditions) % removal of the pollutant was continued with ~32% until pH 10. Herein,

the reason referred to the electrostatic repulsion that occurred between the negative charge on the surface of nanocomposite and trichlorophenoxy ion [151].

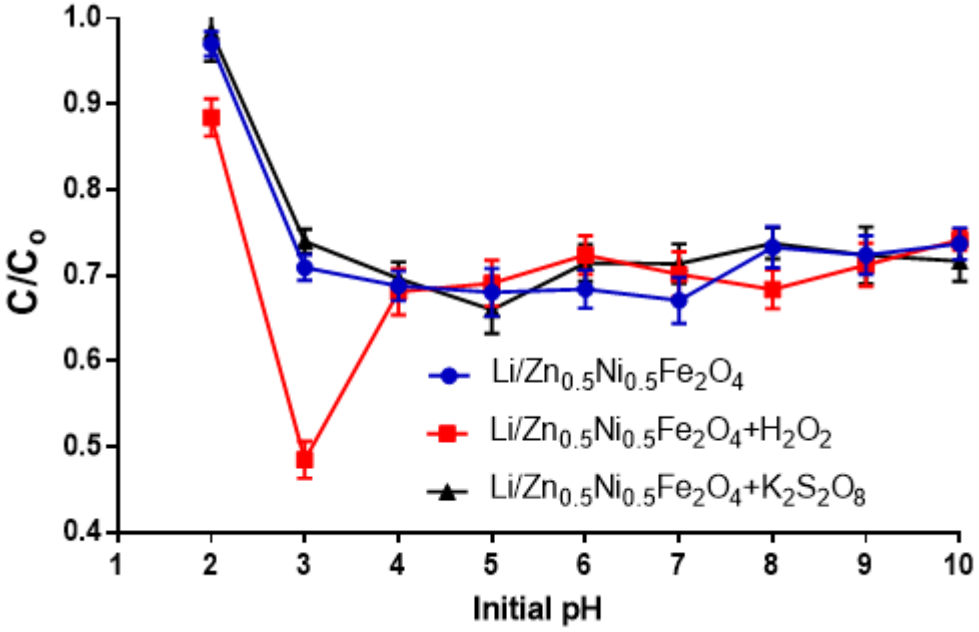

Figure 30: variation of solution pH on the performance of Li/ZNF to degradation TCP (Reaction conditions; TCP concentration: 50 ppm, concentration of oxidants: 4mM, sample dosage: 25 mg, volume of TCP: 25 mL, reaction time: 6 h under UV)

4.3.3 Influence of variation in oxidant concentration

Figure 31 illustrates the effect of varying concentrations of oxidants (H_2O_2 and $K_2S_2O_8$) on the degradation of TCP by the nanocomposite. When the concentration of H_2O_2 was 4 mM, the degradation of TCP reached 55%, beyond 4 mM, the degradation of TCP decreased to (33%) when the concentration increased to 7 mM due to the formation of less reactive hydroperoxyl radical ($^{\bullet}OOH$) that produced from the reaction of excess amount of hydrogen peroxide with hydroxyl radical ($^{\bullet}OH$) that generated before as shown in (equation 10) [152].

$$H_2O_{2(excess)} + {}^{\bullet}OH \rightarrow {}^{\bullet}OOH + H_2O \quad (10)$$

In contrast, at 4 mM $K_2S_2O_8$, the percent degradation of TCP reached 27%. However, when the concentration of potassium persulfate increased to 5 and 6 mM, % removal

of TCP was increased to 49%. Beyond 6 mM (7 mM $K_2S_2O_8$), self-quenched occurred between radicals ($^{\bullet}SO_4^-$) and/or with the excess $K_2S_2O_8$ (equation 11 and 12) that caused decreasing in the percent degradation of TCP (19 %). Similarly, in the degradation of tetracycline antibiotic (TC), authors reported that when the concentration of $K_2S_2O_8$ increased to 6 mmol/L, percent degradation of TC revealed 98% within 120 min while 8 mmol/L reached 70% because of self-reaction [148]. Considering the results, 4 mM of H_2O_2 was chosen as the appropriate concentration and selected for further tests in this research.

$$SO_4^{\bullet-} + SO_4^{\bullet-} \rightarrow SO_4^{2-} \quad (11)$$

$$S_2O_8^{2-} + SO_4^{\bullet-} \rightarrow SO_4^{2-} + S_2O_8^{\bullet-} \quad (12)$$

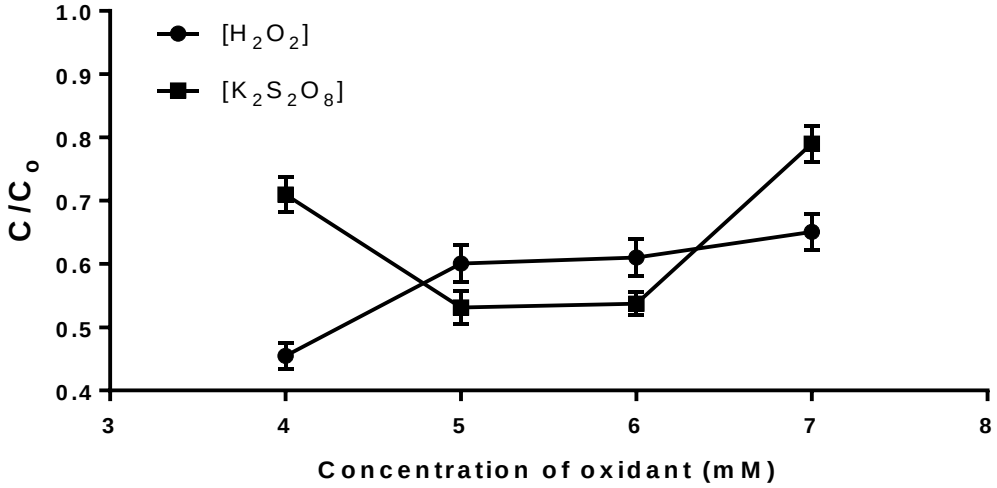

Figure 31: Variation of H_2O_2 and $K_2S_2O_8$ concentrations (4 - 7 mM) on the degradation of TCP (Reaction conditions; TCP concentration: 50 ppm, sample dosage: 25 mg, volume of TCP: 25 mL, reaction time: 6 h under UV)

4.3.4 Influence of variation in Li/ZNF dosage

Figure 32 shows the effectiveness of nanocomposite dosage on the degradation of TCP. The degradation efficiency of TCP decreased gradually with increasing Li/ZNF

dosage from 10 mg (80%) to 50 mg (53%), due to the presence of high solution turbidity and followed by light dispersion which affected the degradation efficiency [149]. 10 mg is the optimum dosage that has been chosen for further tests.

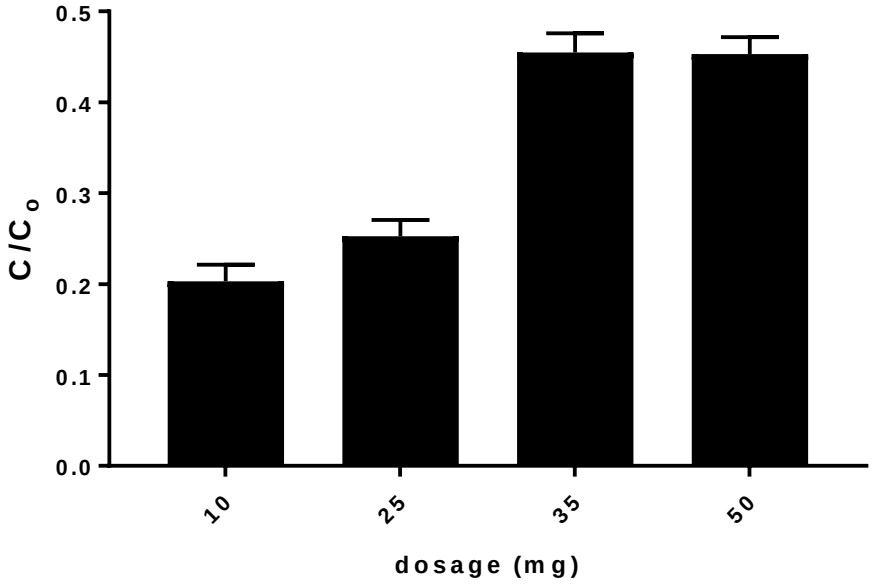

Figure 32: Effect of Li/ZNF dosage on degradation of TCP (Reaction conditions; TCP concentration: 50 ppm, volume of TCP: 25 mL, $[H_2O_2]$ = 4 mM, reaction time: 6 h under UV at pH 3)

4.3.5 Comparative performance of processes for degradation of TCP

Figure 33 illustrates the % adsorption and degradation of TCP under dark and UV light conditions for 6 h by $Zn_{0.5}Ni_{0.5}Fe_2O_4$ and $Zn_{0.5}Ni_{0.5}Fe_2O_4$ doped with lithium. The adsorption of TCP by ZNF was three times higher than Li/ZNF due to crystal size and surface area. ZNF without doping has a higher crystal size (19.9 nm) and surface area (73.5 m^2/g) than ZNF doped by lithium (16.9 nm, 56.8 m^2/g). A similar observation was noted by Tsvetkov et al [153]. The authors reported that the crystal size of ZNF (18.39 nm) was higher than ZNF doped by lanthanide ions (~14.8 nm). Jiang's et al. research [154] was based on the same property for adsorption of bovine serum albumin (33 mg/g) by ZNF. However, the percent degradation of TCP under UV- light reached

80% after 6 h with Li/ZNF which was almost twice the degradation with ZNF (45.5%). As expected, the photoactivity of ZNF was improved by Li doping, lithium nanoparticles deposited on ZNF acts as an electron reservoir, enhancing the electron-hole separation, therefore, enhancing the photocatalytic performance. The same result was reported by Albiter et al [155]. The authors reported that the degradation of Rhodamine B dye reached 80% removal by TiO_2 after 60 min. In contrast, the % degradation increased to 95% by Ag-TiO_2 that was prepared from silver acetylacetonate.

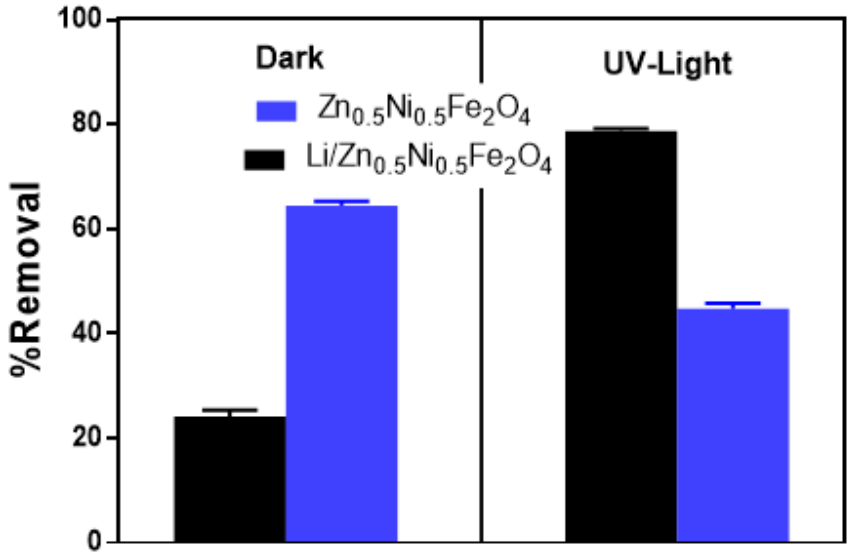

Figure 33: Adsorption and degradation of TCP under dark and UV-light conditions by Li/ZNF (Reaction conditions; TCP concentration: 50 ppm, volume of TCP: 25 mL, [H_2O_2] = 4 mM, reaction time: 6 h, at pH 3)

4.3.6 Degradation kinetics and radical trapping test

Figure 34 shows the degradation rate of TCP (No scavenger) with 10 mg nanocomposite to remove 50 ppm of TCP in the presence of 4 mM H_2O_2 at pH 3. In the dark mode, % removal of TCP reached 38%. However, this percentage increased to 80% under UV the light within 330 min. Furthermore, first and second orders were applied to determine the kinetic absorption and degradation of TCP with Li/ZNF and

summarized in Table 9. From the results, kinetic absorption of TCP in the dark mode was fitted with pseudo-second-order kinetic (R^2 = 0.9993) with fast absorption and absorption rate constant (K_2 = 0.0423 $L.mg^{-1}min^{-1}$). Also, the theoretical q_e is nearer to the experimental value. However, the kinetic behaviour changed under UV-light and fitted with pseudo-first-order kinetic (R^2 = 0.949) with slow degradation rate and degradation rate constant (K_1 = 0.0019).

Radical trapping test by scavenger coefficients (5 mM of t−BuOH, BQ, and Na–Ox) was studied for 330 min under UV- light. The degradation of TCP was remarkably prevented by sodium oxalate then followed by 1,4-benzoquinone and finally by t-butanol with 0.07, 35, and 50% TCP degradation in the presence of H_2O_2 respectively. Therefore, $^{\bullet}OH$, and $^{\bullet}O_2^-$ were not the dominant active species during the TCP photocatalytic process. However, after the addition of sodium oxalate (as an efficient hole scavenger, h^+), Surprisingly, no photodegradation of TCP is observed (0.07%) in 60 min, illustrated that the photocatalytic degradation process was majorly administered by photogenerated holes (h^+). Similar results were reported by An et al [156]. They used isopropanol ($^{\bullet}OH$), gas bubbling ($^{\bullet}O_2^-$), and ethylenediaminetetraacetic acid (EDTA) (h^+) as scavenger coefficients. Notably, scavenger holes had the majority to degradant TCP by Cu–TiO_2–Cu_2O triple junction.

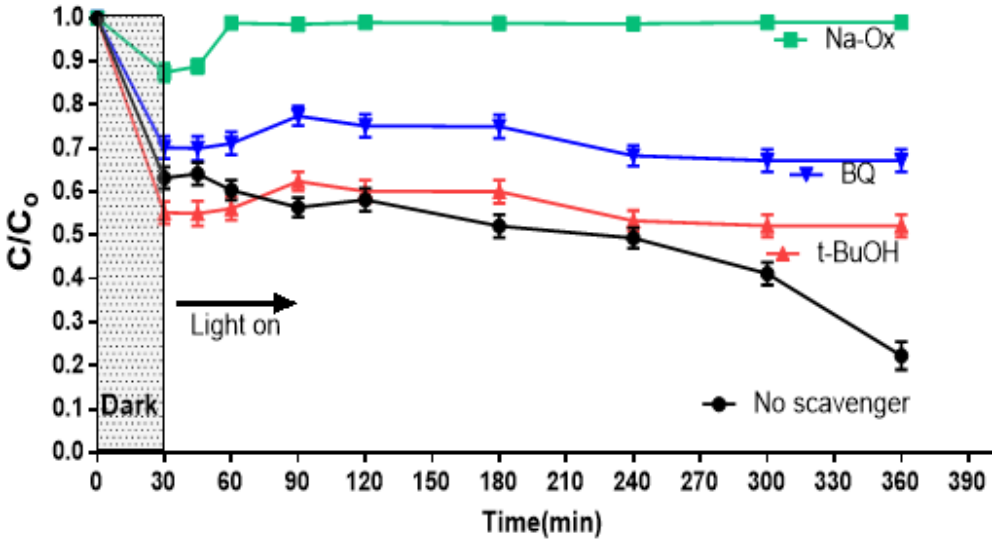

Figure 34: Effect of different scavengers 5 mM (sodium oxalate (Na-Ox), 1,4-benzoquinone (BQ), and tert-butanol (t-BuOH)) for reactive oxygen species (ROS) capture during TCP degradation (TCP concentration: 50 ppm, 10 mg dosage ZNF, 4 mM H_2O_2, pH 3, first 30 min

Table 9: Degradation kinetics of TCP and correlation coefficients (R^2) under different processes [157].

		Dark Absorption	UV-light Degradation
1st Order		$\ln(q_e - q_t) = \ln(q_e) - k_1.t$	$\ln(\frac{1}{1-X}) = Kt$
	K(min^{-1})	0.004	0.0019
	R^2	0.4844	0.949
	q_e(mg/L)	59.5	-
	$q_e - q_t$(mg/L)	36.19	-
2nd Order		$\left(\frac{t}{q_t}\right) = \left(\frac{1}{k_2 . q_e^2}\right) - \left(\frac{t}{q_e}\right)$	
	K(L/mg.min)	0.0423	
	R^2	0.9993	
	q_e(mg/L)	29.76	
	$q_e - q_t$(mg/L)	6.45	

4.3.7 Effect of interferences on the degradation of TCP and reusability of Li/ZNF

Degradation of TCP alone and TCP in presence of anions interferences (0.1 mol. L^{-1}) such as (Cl^-, SO_4^{2-}, and NO_3^-) were studied. Figure 35 illustrates the effect of anionic on the degradation of 50 ppm TCP; inorganic anions can inhabit the surface activity of the nanocomposites, reduce colloidal stability and surface contact between TCP and Li/ZNF [158]. Because of these influences, degradation of TCP had been decreased by 16% with chorine ion, followed by 30% with sulfate ion because these ions can inhibit the active species such as holes (h^+) and hydroxyl radical ($^{\bullet}OH$) (equations 13 and 14) as reported by Matthews and McEvoy [159].

$$Cl^- + {}^{\bullet}OH \rightarrow Cl^{\bullet} + {}^{-}OH \quad (13)$$

$$Cl^- + h^+ \rightarrow Cl^{\bullet} \quad (14)$$

The lowest degradation was recorded in the presence of NO_3^- due to its quenching effect (equations 15-18); nitrate ions can be activated by UV light to generate NO_2^- ions which reacted with $^{\bullet}OH$ radicals to produce less reactive nitrogen dioxide radicals ($NO_2^{\bullet}$) that eventually decreased TCP degradation according to the following equations:

$$NO_3^- + h\upsilon \rightarrow NO_2^- + \frac{1}{2}O_2 \quad (15)$$

$$NO_2^- + {}^{\bullet}OH \rightarrow NO_2^{\bullet} + {}^{-}OH \quad (16)$$

$$NO_2^- + {}^{\bullet}OH \rightarrow NO_3^- + H^+ \quad (17)$$

$$NO_2^- + h\upsilon + H^+ \rightarrow NO^{\bullet} + {}^{\bullet}OH \quad (18)$$

This is consistent with the study of Zaviska et al [160] who reported that the degradation rate of phenol (0.027 min^{-1}) decreased to 0.02 min^{-1} in the presence of NO_3^- ions.

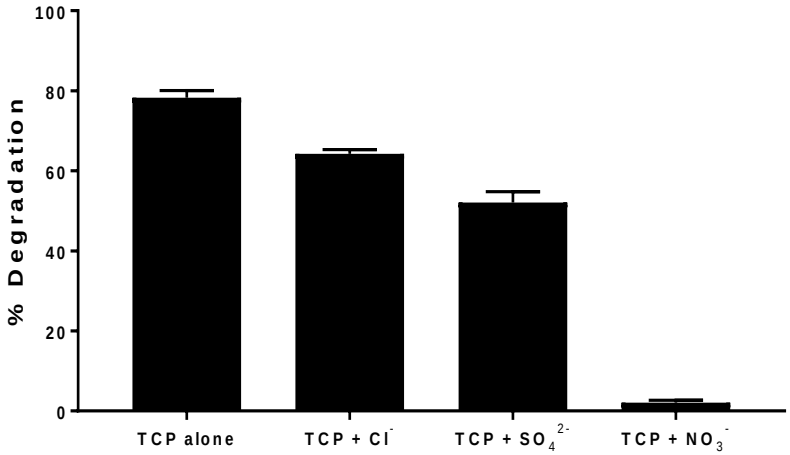

Figure 35: % degradation of TCP alone and with presence anionic species 0.1 M (Cl^-, SO_4^{2-} and NO^{3-}), (TCP concentration: 50 ppm, 10 mg dosage, 25 mL volume, 4 mM H_2O_2, pH 3, 6 h under UV light)

Reusability and stability of the Li/ZNF photocatalyst were conducted via five reusable cycles with 10 mg nanocomposite and 50 ppm TCP concentration (Figure 36). The degradation efficiency for TCP decreased from 80% to 66% after five consecutive reuse cycles within 6 h under UV- light, due to the decreasing of active sites of the Li/ZNF as shown by FTIR (OH) groups were disappeared after the first treatment. Similarly, the degradation efficiency of nitrobenzene by TiO_2/Pr/Y_2SiO_5 loaded on a glass fibre filter was decreased from 95% to 75.9% after 6 reusable cycles because of the decrease in the active sites on this material [161].

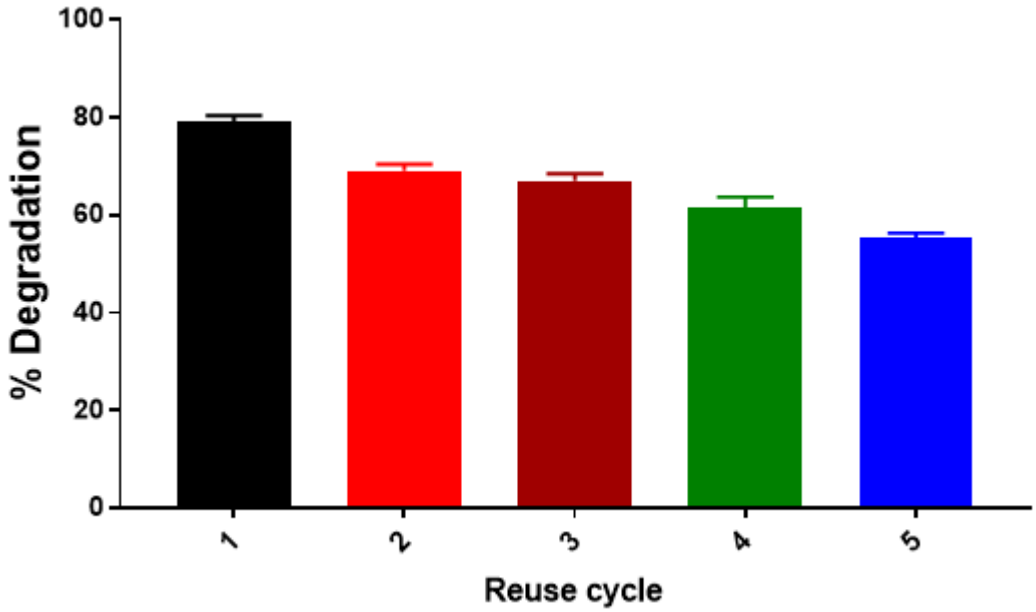

Figure 36: Recyclability and stability experiments for Li/ZNF (Reaction conditions: pH 3, 50 ppm TCP, 10 mg reusable dosage under UV for 6 h)

4.3.8 Probable photodegradation mechanism

Herein, the photodegradation mechanism of TCP with Photoresponse and physicochemical properties of Li/ZNF under optimized conditions is proposed. The bandgap energy of Li/ZNF is 2.89 eV meanwhile the potentials valence band (VB) and conduction band (CB) were found 2.22 and -0.67 eV respectively according to the following equations:

$$E_{CB} = \chi - E^{e} - \frac{E_g}{2} \quad (19)$$

$$E_{VB} = E_{CB} + E_g \quad (20)$$

The absolute electron negativity (χ) of Li/ZNF is 5.3 eV and the energy of free electron Vs hydrogen (E^e) is 4.5 eV. Herein, Li/ZNF is activated by UV-light (353 nm) and photoexcited electrons transferred from the E_{VB} to the E_{CB} with the formation of photo-generated electron−hole pairs (e^-/h^+) which is oxidized and/or reduced the adsorbed TCP and oxygen on the surface of Li/ZNF. Although the photo-generated holes (h^+) contributed dominantly during the degradation of TCP, $^{\bullet}OH$ and $^{\bullet}O_2^-$ also participated moderately in the photodegradation mechanism of TCP.

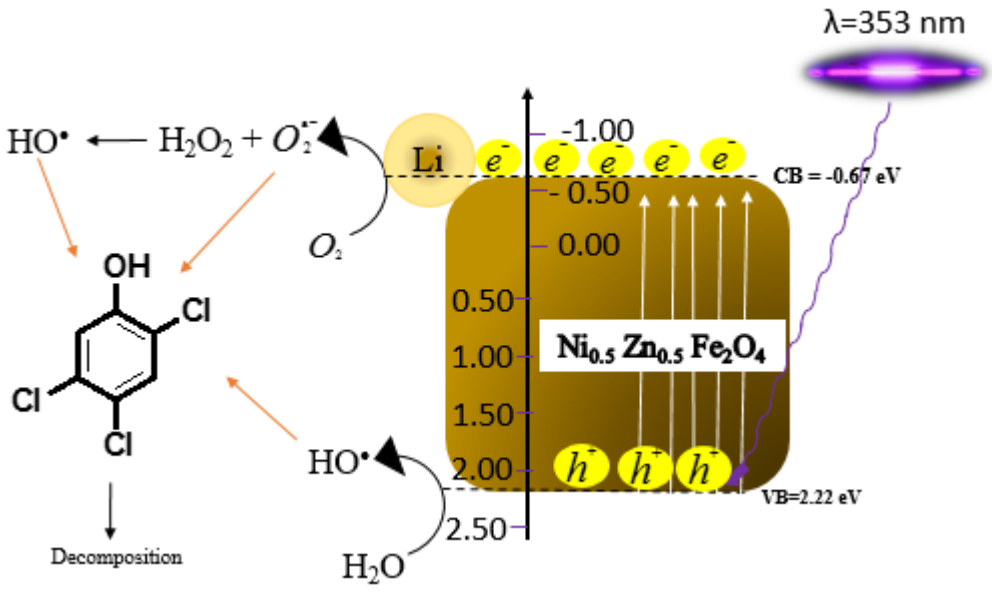

Figure 37: schematic illustration of the probable photocatalytic disinfection mechanism of Li/ZNF / oxidant and UV system

Notably, the reduction potential of ($O_2/^{\bullet}O_2^-$) is -0.33 eV Vs NHE is less than E_{CB} of Li/ZNF (-0.67 eV), hence the electron that photogenerated at E_{CB} immediately reduced adsorbed oxygen molecule to $^{\bullet}O_2^-$ which degraded the TCP molecules that adsorbed

on the surface of the composites. Moreover, E_{VB} of Li/ZNF (2.22 eV) is more positive than $H_2O/^{\bullet}OH$ (1.99 eV) and O_2/H_2O (1.23 eV) which induced the formation of $^{\bullet}OH$ radicals that can effectively degrade the TCP. The probable degradation pathway for TCP is shown in Figure 37, where TCP molecules are decomposed by the h^+, $^{\bullet}OH$, or $^{\bullet}O_2^-$ which is consistent with previous studies [162].

4.3.9 Antibacterial studies

Time kill assay was used to determine antibacterial activity with *S. aureus* (Gram-positive) and *E. coli* (Gram-negative) bacteria by counting the number of colonies after variable time under UV light condition and comparison with dark for 60 min. Various amount of Li/ZNF (5, 15, and 25 mg) was used with 1 x 10^6 CFU/mL bacteria, a control (without nanoparticle) was used to compare the results as shown in Figure 38.

Figure 38a illustrates 25 and 15 mg of the nanocomposite killed Gram-positive within 60 min. However, 5 mg needed 30 min more to eliminate the same amount of bacteria. Significantly, the control's bacteria solution was still observed until 180 min with 8.3 x 10^4 CFU/mL under UV light. On the other hand, surprisingly 5 and 15 mg nanocomposite were needed to kill *E. coli* bacteria within 2 h under UV-light, however, the same amount of bacteria was eliminated within 1 h by 25 mg of Li/ZNF Figure 38b.

Considering various similar studies reported in the literature and the radical quenching analysis of the Li/NZF; it can be assumed that the $^{\bullet}O_2^-$ and $^{\bullet}OH$ radicals formed in the system are capable of disrupting the bacteria cells then oxidized the protein and lipid in the cell membrane of the bacteria which eventually caused death [147,163]. Bacteria that were exposed to a different amount of nanoparticles without UV light (under dark conditions) for one hour (Figure 38c-d) revealed the performance of Li/NZF without

being activated by light. The blank concentration of *S. aureus* and *E. coli* decreased to 10.7 x 10^4 and 36 x 10^4 CFU/mL respectively. Herein, 25 mg nanocomposite killed both *S. aureus* and *E. coli* under dark conditions. However, when the number of composites decreased to 15 and 5 mg, the growth of *S. aureus* bacteria was inhibited to 10 x10^3 and 17 x10^3 CFU/mL. Moreover, the growth of *E. coli* bacteria under the same condition was decreased to 52 x10^3 and 55 x10^3 CFU/mL respectively, due to the sensitivity of these bacteria to the Li/NZF which might be implied with Li^+ releases during the bacteria inactivation process. The concentration of lithium can be harmful if it reaches 10 mg/L [164], therefore, releasing lithium-ion from nanocomposite into the solution with the maximum amount used to treat bacteria (25 mg) still in the safe range (theoretical, 0.35mg/L). This result is in line with the study of Tian et al [147] who reported that 700 µg/mL of 3mol% magnesium oxide doped with Li inhibit similar bacteria used in this work within 24 h. The performance of Li/ZNF is compared with other reported doped materials and presented in Table 10.

As tabulated Li/ZNF performance is superior compare to other reported similar materials. For instance, Alotaibi et al [75] used TiO_2 doped by Cu to increase the antibacterial effect of TiO_2, they successfully decreased *E. coli* bacteria from 4 x 10^6 CFU/mL to 1.5 x 10^5 CFU/mL and 1.3 x 10^3 CFU/mL within 4 h under dark and UV-light conditions respectively. Also, *S. aureus* bacterial was decreased from 4 x 10^6 CFU/mL to 1.5 x 10^5 CFU/mL and 1 x 10^2 CFU/mL within same time and conditions respectively. Likewise, X. Li et al [163] used Li/MgO under nitrogen calcination which inhibits *E. coli* (99.6%) within 24 under UV.

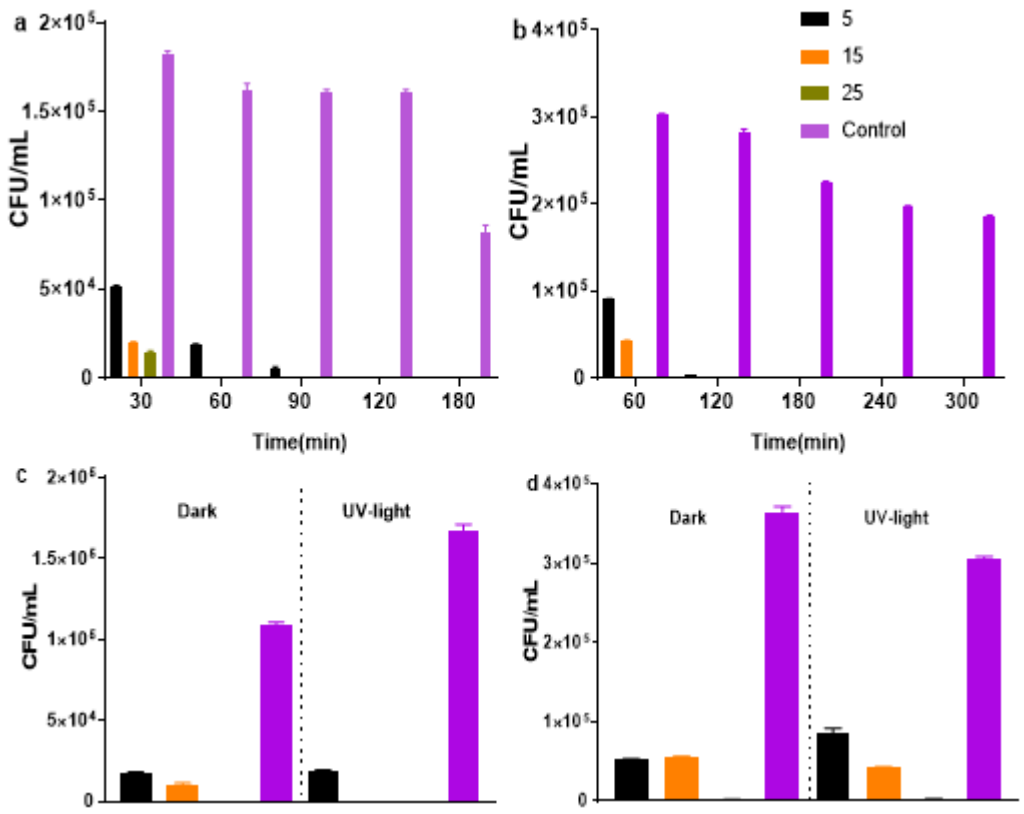

Figure 38: Time kill assay of (1 x 10^6 CFU/mL) *S. aureus* and *E. coli* with (5, 15, 25 mg) Li/$Zn_{0.5}Ni_{0.5}Fe_2O_4$ a) *S. aureus* under UV light for 180 min, b) *E. coli* under UV-light for 300 min, c) *S. aureus* comparison between dark and UV-light for 60 min, and d) *E. coli* comparison between dark and UV-light for 60 min

Table 10: Comparison of various metal doped antibacterial results.

Antibacterial material	Thin film Cu/TiO_2		S-GO-SnO_2	Li/MgO	1mol% (Li/MgO)	$Li/Zn_{0.5}Ni_{0.5}Fe_2O_4$
amount	1 cm^2		200µg/mL	100 µg/mL	600 µg/mL	500 µg /mL
E. coli CFU/mL initial	$4x10^6$		$2.9x10^8$	$1x10^8$	$1x10^5$	$1x10^6$
E. coli CFU/mL (Dark)	2h $1x10^6$	4h $1.5x10^5$	-	-	-	1h (%inhibition) 99.72%
E. coli CFU/mL (UV)	2h $1.5x10^5$	4h $1.3x10^3$	12h (visible) $1.7x10^6$	24h 99.6%	24h %inhibition 92.4%	1h (%inhibition) 99.34%
S. aureus CFU/mL initial	$4x10^6$		-	-	$1x10^5$	$1x10^6$
S. aureus CFU/mL (Dark)	2h $1x10^5$	4h $1.5x10^5$	-	-	-	1h 0
S. aureus CFU/mL (UV)	2h $1.7x10^4$	4h $1x10^2$	-	-	24h %inhibition 90.2%	1h 0
Reference	[75]		[165]	[163]	[147]	This work

4.4 Conclusion

Zinc nickel ferret nanoparticles were synthesized via co-precipitation reaction, then doped with lithium to form Li/$Ni_{0.5}Zn_{0.5}Fe_2O_4$ (Li/NZF) for photocatalytic 2,4,5-trichlorophenol (TCP) and antibacterial application. XRD characteristics revealed the doped nanoparticle possessed higher crystallinity (76.8%) than NZF (66.8%). In contrast, NZF had a higher surface area (73.5 m^2/g) than Li/NZF (56.8 m^2/g). Additionally, Li/NZF had bandgap energy 2.89 eV with conduction band (CB) -0.67 eV and valence band (VB) 2.22 eV.

Degradation of TCP under optimum conditions (pH 3, 4 mM H_2O_2 and 50 ppm TCP) with 10 mg of Li/NZF reached 80% within 360 min under UV light with rate constant 0.0019 min^{-1}, this percentage decreased to 66% after five successful reusable cycles and 64% with chlorine ion as an interference. Furthermore, Li/NZF showed nice results as antibacterial with *Staphylococcus aureus* (*S. aureus*) and *E. coli*. Notably, 15 and 25 mg of the composite were enough to inhibit 1 x 10^6 CFU/mL of *S. aureus* bacteria within 60 min under UV light and dark respectively. On contrast, 25 mg inhibited 99.72% (under dark) and 99.34% (under UV light) of 1 X 10^6 CFU/mL of *E. coli* within 60 min.

Chapter 5

CONCLUSION AND RECOMMENDATION

In conclusion, three different products were synthesized, characterized and used as antibacterial with different applications in this work. In chapter 1; {[1,3-bis(2,4,5-trichlorophenoxy) propan-2-yl] oxy}-3-(2,4,5-trichlorophenoxy) hexan-2-ol (TPTH) was synthesized and characterized. Around 98% of TPTH was decomposed at 370°C. Notably, less than 1% of TPTH was decomposed during the first 160°C which revealed that TPTH exhibited thermal stability. The performance of TPTH for the inhibition of different bacteria was investigated for the killing of both Gram-positive (*S. aureus* and MRSA) and Gram-negative (*E. coli*). 0.15, 0.08, and 0.02 µg/mL of TPTH were the minimum inhibition concentrations against *E. coli*, MRSA, and *S. aureus* respectively. Also, TPTH exhibited excellent antimicrobial activities against the bacteria mentioned before with inhibition zones of 18, 22, and 24 mm respectively via the well diffusion assay. Furthermore, MTT assay (toxicity test) showed 97% viability of stem cells until 10 µg/mL of TPTH concentration after 72 h, this range includes MIC values of three different bacteria. Results herein show that TPTH is an alternative antimicrobial material with low toxicity and thermal stability that can be used for humans, animals, and the environment without risks or concerns.

Chapter 2 of this work includes an ethylenediamine-epichlorohydrin-trichlorophenol cross-linked polymer (EET), this polymer was synthesized and characterized. The performance of EET for the treatment of dye-containing synthetic solutions was

investigated for the removal of both anionic dye (methyl orange) and cationic dye (rhodamine B). 98.72% and 92.45% of MO and RB dyes were adsorbed at pH 8 and 3 using 10 mg and 15 mg of EET, respectively. Notably, more than 50 % of MO was adsorbed during the first 15 min, which revealed that EET exhibited fast adsorption kinetically. According to the Langmuir isotherm, the maximum uptake of MO and RB is 145 mg/g and 149.3 mg/g under the optimum conditions. 98% of MO was desorbed by 0.1 M HCl from the spent EET after 45 min, while only 51% of RB was desorbed within 90 min by ethanol. The regenerated EET maintained high removal efficiency (~98.65%) after 5 recycling circles. Also, the toxicity of the prepared polymer was eliminated due to its insoluble property, and EET exhibited excellent antimicrobial activities against *E. coli* and *S. aureus* with inhibition zones of 39 and 64 mm respectively via the disk diffusion assay. Results herein show that EET is an alternative polymeric adsorbent with antimicrobial functions for the treatment of dye contaminated industrial effluents.

Finally, chapter 3 of this work exhibited antibacterial nanoparticles with phenolic compound degradation. Herein, Zinc nickel ferret nanoparticles were synthesized via co-precipitation reaction, then doped with lithium to form $Li/Ni_{0.5}Zn_{0.5}Fe_2O_4$ (Li/NZF) for photocatalytic 2,4,5-trichlorophenol (TCP) and antibacterial application. XRD characteristics revealed the doped nanoparticle possessed higher crystallinity (76.8%) than NZF (66.8%). In contrast, NZF had a higher surface area (73.5 m2/g) than Li/NZF (56.8 m2/g). Additionally, Li/NZF had bandgap energy 2.89 eV with conduction band (CB) -0.67 eV and valence band (VB) 2.22 eV.

Degradation of TCP under optimum conditions (pH 3, 4 mM H_2O_2 and 50 ppm TCP) with 10 mg of Li/NZF reached 80% within 360 min under UV light with rate constant

0.0019 min^{-1}, this percentage decreased to 66% after five successful reusable cycles and 64% with chlorine ion as an interference. Furthermore, Li/NZF showed nice results as antibacterial with *Staphylococcus aureus* (*S. aureus*) and *E. coli*. Notably, 15 and 25 mg of the composite were enough to inhibit 1 x 10^6 CFU/mL of *S. aureus* bacteria within 60 min under UV light and dark respectively. On contrast, 25 mg inhibited 99.72% (under dark) and 99.34% (under UV light) of 1 X 10^6 CFU/mL of *E. coli* within 60 min.

REFERENCES

[1] S. Mahira, A. Jain, W. Khan, and A. J. Domb, “Antimicrobial Materials—An Overview,” 2019.

[2] A. Jones, A. Mandal, and S. Sharma, “Protein- based bioplastics and their antibacterial potential,” *J. Appl. Polym. Sci.*, vol. 132, no. 18, 2015.

[3] N. Beyth, Y. Houri-Haddad, A. Domb, W. Khan, and R. Hazan, “Alternative antimicrobial approach: nano-antimicrobial materials,” *Evidence-based Complement. Altern. Med.*, vol. 2015, 2015.

[4] I. Chopra, L. Hesse, and A. J. O’Neill, “Exploiting current understanding of antibiotic action for discovery of new drugs,” *J. Appl. Microbiol.*, vol. 92, pp. 4S-15S, 2002.

[5] M. A. Kohanski, D. J. Dwyer, and J. J. Collins, “How antibiotics kill bacteria: from targets to networks,” *Nat. Rev. Microbiol.*, vol. 8, no. 6, pp. 423–435, 2010.

[6] H. Ullah and S. Ali, “Classification of anti-bacterial agents and their functions,” *Antibact. agents*, vol. 10, 2017.

[7] K. Drlica, M. Malik, R. J. Kerns, and X. Zhao, “Quinolone-mediated bacterial death,” *Antimicrob. Agents Chemother.*, vol. 52, no. 2, pp. 385–392, 2008.

[8] E. Santacesaria, R. Tesser, M. Di Serio, L. Casale, and D. Verde, “New process for producing epichlorohydrin via glycerol chlorination,” *Ind. Eng. Chem. Res.*, vol. 49, no. 3, pp. 964–970, 2009.

[9] K. Segawa, S. Mizuno, M. Sugiura, and S. Nakata, “Selective synthesis of ethylenediamine from ethanolamine over modified H-mordenite catalyst,” in *Studies in Surface Science and Catalysis*, vol. 101, Elsevier, 1996, pp. 267–276.

[10] N. Meng *et al.*, “A low-pressure GO nanofiltration membrane crosslinked via ethylenediamine,” *J. Memb. Sci.*, vol. 548, pp. 363–371, 2018.

[11] Y. Shimizu, S. Izumi, Y. Saito, and H. Yamaoka, “Ethylenediamine tetraacetic acid modification of crosslinked chitosan designed for a novel metal- ion adsorbent,” *J. Appl. Polym. Sci.*, vol. 92, no. 5, pp. 2758–2764, 2004.

[12] R. Molinari, P. Argurio, and T. Poerio, “Comparison of polyethylenimine, polyacrylic acid and poly(dimethylamine-co-epichlorohydrin-co-ethylenediamine) in Cu2+ removal from wastewaters by polymer-assisted ultrafiltration,” *Desalination*, vol. 162, no. 1–3, pp. 217–228, 2004.

[13] A. Piozzi and I. Francolini, “Editorial of the special issue antimicrobial polymers.” Multidisciplinary Digital Publishing Institute, 2013.

[14] N. R. Sudarshan, D. G. Hoover, and D. Knorr, “Antibacterial action of chitosan,” *Food Biotechnol.*, vol. 6, no. 3, pp. 257–272, 1992.

[15] Y.-C. Chung and C.-Y. Chen, “Antibacterial characteristics and activity of acid-soluble chitosan,” *Bioresour. Technol.*, vol. 99, no. 8, pp. 2806–2814, 2008.

[16] K. R. Kirker, S. T. Fisher, G. A. James, D. McGhee, and C. B. Shah, “Efficacy of polyhexamethylene biguanide-containing antimicrobial foam dressing against MRSA relative to standard foam dressing,” *Wounds*, vol. 21, no. 9, pp. 229–233, 2009.

[17] I. Erol, “Novel methacrylate copolymers with fluorine containing: synthesis, characterization, reactivity ratios, thermal properties and biological activity,” *J. Fluor. Chem.*, vol. 129, no. 7, pp. 613–620, 2008.

[18] P. Majumdar *et al.*, “Combinatorial materials research applied to the development of new surface coatings XV: an investigation of polysiloxane anti-fouling/fouling-release coatings containing tethered quaternary ammonium salt groups,” *ACS Comb. Sci.*, vol. 13, no. 3, pp. 298–309, 2011.

[19] Y. Jiao, L. Niu, S. Ma, J. Li, F. R. Tay, and J. Chen, “Quaternary ammonium-based biomedical materials: State-of-the-art, toxicological aspects and antimicrobial resistance,” *Prog. Polym. Sci.*, vol. 71, pp. 53–90, 2017.

[20] Y. Jia *et al.*, “One-pot solvothermal synthesis of magnetic SnFe 2 O 4 nanoparticles and their performance in the photocatalytic degradation of chlortetracycline with visible light radiation,” *RSC Adv.*, vol. 6, no. 80, pp. 76542–76550, 2016.

[21] D. S. Mathew and R.-S. Juang, “An overview of the structure and magnetism of spinel ferrite nanoparticles and their synthesis in microemulsions,” *Chem. Eng. J.*, vol. 129, no. 1–3, pp. 51–65, 2007.

[22] C. Lin, X. Xie, C. Li, and Q. Yan, “Co0. 5Zn0. 5Fe2O4/Ag3PO4: A magnetic, highly efficient visible-light photocatalyst and the Z-scheme mechanism for removal of anionic dye and tetracycline hydrochloride,” *Mater. Sci. Semicond. Process.*, vol. 82, pp. 46–53, 2018.

[23] W. Chen, C.-A. Cheng, and J. I. Zink, “Spatial, temporal, and dose control of drug delivery using noninvasive magnetic stimulation,” *ACS Nano,* vol. 13, no. 2, pp. 1292–1308, 2019.

[24] C. Lopez-Abarrategui *et al.*, “The intrinsic antimicrobial activity of citric acid-coated manganese ferrite nanoparticles is enhanced after conjugation with the antifungal peptide Cm-p5,” *Int. J. Nanomedicine,* vol. 11, p. 3849, 2016.

[25] S. S. Teske and C. S. Detweiler, “The biomechanisms of metal and metal-oxide nanoparticles’ interactions with cells,” *Int. J. Environ. Res. Public Health,* vol. 12, no. 2, pp. 1112–1134, 2015.

[26] N. Koprivanac and H. Kušić, *Hazardous organic pollutants in colored wastewaters*. Nova Science Publishers, Inc., 2009.

[27] M. Nendza and J. K. Seydel, “Application of bacterial growth kinetics to in vitro toxicity assessment of substituted phenols and anilines,” *Ecotoxicol. Environ.*

Saf., vol. 19, no. 2, pp. 228–241, 1990.

[28] T. A. B. Ogunniyi, P. O. Oni, A. Juba, S. O. Asaolu, and D. O. Kolawole, "Disinfectants/antiseptics in the management of guinea worm ulcers in the rural areas," *Acta Trop.*, vol. 74, no. 1, pp. 33–38, 2000.

[29] M. Czaplicka, "Sources and transformations of chlorophenols in the natural environment," *Sci. Total Environ.*, vol. 322, no. 1–3, pp. 21–39, 2004.

[30] J. Michałowicz and W. Duda, "Phenols--Sources and Toxicity.," *Polish J. Environ. Stud.*, vol. 16, no. 3, 2007.

[31] E. O. Igbinosa *et al.*, "Toxicological profile of chlorophenols and their derivatives in the environment: the public health perspective," *Sci. World J.*, vol. 2013, 2013.

[32] P. C. Abhilash and N. Singh, "Distribution of hexachlorocyclohexane isomers in soil samples from a small scale industrial area of Lucknow, North India, associated with lindane production," *Chemosphere*, vol. 73, no. 6, pp. 1011–1015, 2008.

[33] G. U. Balcke, S. Wegener, B. Kiesel, D. Benndorf, M. Schlömann, and C. Vogt, "Kinetics of chlorobenzene biodegradation under reduced oxygen levels," *Biodegradation*, vol. 19, no. 4, pp. 507–518, 2008.

[34] H. Zaghouane-Boudiaf and M. Boutahala, "Adsorption of 2, 4, 5-

trichlorophenol by organo-montmorillonites from aqueous solutions: Kinetics and equilibrium studies," *Chem. Eng. J.*, vol. 170, no. 1, pp. 120–126, 2011.

[35] R. Parette *et al.*, "Modeling the formation of 2, 3, 7, 8-tetrachlorodibenzo-p-dioxin in the historical manufacture of 2, 4, 5-trichlorophenol," *Environ. Forensics*, vol. 18, no. 4, pp. 307–317, 2017.

[36] J. D. Doedens, "Chlorophenols," in *Kirk-Othmer encyclopedia of chemical technology*, vol. 5, John Wiley & Sons New York, 1964, pp. 325–338.

[37] Y. Okamoto and M. Tomonari, "Formation pathways from 2, 4, 5-trichlorophenol (TCP) to polychlorinated dibenzo-p-dioxins (PCDDs): An ab initio study," *J. Phys. Chem. A*, vol. 103, no. 38, pp. 7686–7691, 1999.

[38] G. M. Ratnamala, K. V. Shetty, and G. Srinikethan, "Removal of remazol brilliant blue dye from dye-contaminated water by adsorption using red mud: equilibrium, kinetic, and thermodynamic studies," *Water, Air, Soil Pollut.*, vol. 223, no. 9, pp. 6187–6199, 2012.

[39] R. Gong, M. Li, C. Yang, Y. Sun, and J. Chen, "Removal of cationic dyes from aqueous solution by adsorption on peanut hull," *J. Hazard. Mater.*, vol. 121, no. 1–3, pp. 247–250, 2005.

[40] F. M. D. Chequer, G. A. R. de Oliveira, E. R. A. Ferraz, J. C. Cardoso, M. V. B. Zanoni, and D. P. de Oliveira, "Textile dyes: dyeing process and environmental impact," *Eco-friendly Text. Dye. Finish.*, vol. 6, pp. 151–176,

2013.

[41] R. Jain and S. Sikarwar, “Photocatalytic and adsorption studies on the removal of dye Congo red from wastewater,” *Int. J. Environ. Pollut.*, vol. 27, no. 1–3, pp. 158–178, 2006.

[42] G. Mishra and M. Tripathy, “A critical review of the treatment for decolorization of dye wastewater,” *Colourage*, vol. 40, pp. 35–38, 1993.

[43] H. Tahir, M. Sultan, N. Akhtar, U. Hameed, and T. Abid, “Application of natural and modified sugar cane bagasse for the removal of dye from aqueous solution,” *J. Saudi Chem. Soc.*, vol. 20, pp. S115–S121, 2016.

[44] C. A. Peters and B. C. Redmon, “Phenolphthalein and methyl orange,” *J. Chem. Educ.*, vol. 17, no. 11, p. 525, 1940.

[45] S. A. Hassanzadeh-Tabrizi, M. M. Motlagh, and S. Salahshour, “Synthesis of ZnO/CuO nanocomposite immobilized on γ-Al2O3 and application for removal of methyl orange,” *Appl. Surf. Sci.*, vol. 384, pp. 237–243, 2016.

[46] A. Moazami, M. Montazer, and M. K. Dolatabadi, “Rapid Discoloration of Methyl Orange in Water by Conductive Cu/Cu 2 O/rGO Modified Polyester Fabric,” *J. Polym. Environ.*, vol. 26, no. 6, pp. 2502–2513, 2018.

[47] Q. Xin *et al.*, “Polypyrrole nanofibers as a high-efficient adsorbent for the removal of methyl orange from aqueous solution,” *J. Environ. Chem. Eng.*, vol.

3, no. 3, pp. 1637–1647, 2015.

[48] R. W. Ramette and E. B. Sandell, “Rhodamine B equilibria,” *J. Am. Chem. Soc.*, vol. 78, no. 19, pp. 4872–4878, 1956.

[49] A. A. Oladipo, A. O. Ifebajo, N. Nisar, and O. A. Ajayi, “High-performance magnetic chicken bone-based biochar for efficient removal of rhodamine-B dye and tetracycline: competitive sorption analysis,” *Water Sci. Technol.*, vol. 76, no. 2, pp. 373–385, 2017.

[50] T.-M. Geng, D.-Y. Wu, W. Huang, R.-Y. Huang, and G.-H. Wu, “Fluorogenic detection of Hg 2+, Cd 2+, Fe 2+, Pb 2+ cations in aqueous media by means of an acrylamide-acrylic acid copolymer chemosensor with pendant rhodamine-based dyes,” *J. Polym. Res.*, vol. 21, no. 3, p. 354, 2014.

[51] B. S. Inbaraj, J. T. Chien, G. H. Ho, J. Yang, and B. H. Chen, “Equilibrium and kinetic studies on sorption of basic dyes by a natural biopolymer poly (γ-glutamic acid),” *Biochem. Eng. J.*, vol. 31, no. 3, pp. 204–215, 2006.

[52] K. Kadirvelu, C. Karthika, N. Vennilamani, and S. Pattabhi, “Activated carbon from industrial solid waste as an adsorbent for the removal of Rhodamine-B from aqueous solution: Kinetic and equilibrium studies,” *Chemosphere*, vol. 60, no. 8, pp. 1009–1017, 2005.

[53] P. K. Pandey, P. H. Kass, M. L. Soupir, S. Biswas, and V. P. Singh, “Contamination of water resources by pathogenic bacteria,” *Amb Express*, vol.

4, no. 1, p. 51, 2014.

[54] K. S. Gurusamy, R. Koti, C. D. Toon, P. Wilson, and B. R. Davidson, "Antibiotic therapy for the treatment of methicillin-resistant *Staphylococcus aureus* (MRSA) infections in surgical wounds," *Cochrane Database Syst. Rev.*, no. 8, 2013.

[55] P. E. Akpaka, S. Monecke, W. H. Swanston, A. V. C. Rao, R. Schulz, and P. N. Levett, "Methicillin sensitive *Staphylococcus aureus* producing Panton-Valentine leukocidin toxin in Trinidad & Tobago: a case report," *J. Med. Case Rep.*, vol. 5, no. 1, p. 157, 2011.

[56] P. C. Appelbaum, "Microbiology of antibiotic resistance in *Staphylococcus aureus*," *Clin. Infect. Dis.*, vol. 45, no. Supplement_3, pp. S165–S170, 2007.

[57] D. Transposable Elements, B. Charlesworth, and C. H. Langley, "the Population Genetics of." 1989.

[58] G. Crini, E. Lichtfouse, L. D. Wilson, and N. Morin-Crini, "Adsorption-oriented processes using conventional and non-conventional adsorbents for wastewater treatment," in *Green Adsorbents for Pollutant Removal*, Springer, 2018, pp. 23–71.

[59] A. Saberi, E. Alipour, and M. Sadeghi, "Superabsorbent magnetic Fe 3 O 4-based starch-poly (acrylic acid) nanocomposite hydrogel for efficient removal of dyes and heavy metal ions from water," *J. Polym. Res.*, vol. 26, no. 12, p.

271, 2019.

[60] V. S. Munagapati, V. Yarramuthi, and D.-S. Kim, “Methyl orange removal from aqueous solution using goethite, chitosan beads and goethite impregnated with chitosan beads,” *J. Mol. Liq.*, vol. 240, pp. 329–339, 2017.

[61] M. Kaushal and A. Tiwari, “Removal of Rhodamine-B from Aqueous Solution by Adsorption onto Crosslinked Alginate Beads,” *J. Dispers. Sci. Technol.*, vol. 31, no. 4, pp. 438–441, 2010.

[62] N. Biçaak and B. F. Şenkal, “Removal of nitrite ions from aqueous solutions by cross-linked polymer of ethylenediamine with epichlorohydrin,” *React. Funct. Polym.*, vol. 36, no. 1, pp. 71–77, 1998.

[63] C. Sun, X. Zhang, Z. Zhang, and Y. Zhang, “Color removal from dyeing wastewater by the polymer of epichlorohydrin- ethylenediamine,” vol. 752, pp. 1448–1451, 2013.

[64] S. W. Krasner *et al.*, “Occurrence of a new generation of disinfection byproducts,” *Environ. Sci. Technol.*, vol. 40, no. 23, pp. 7175–7185, 2006.

[65] S. Sivagnanam and D. Deleu, “Red man syndrome,” *Crit. care*, vol. 7, no. 2, pp. 1–3, 2002.

[66] Y. L. Chew, A. M. Mahadi, K. M. Wong, and J. K. Goh, “Anti-methicillin-resistance *Staphylococcus aureus* (MRSA) compounds from Bauhinia kockiana

Korth. And their mechanism of antibacterial activity," *BMC Complement. Altern. Med.*, vol. 18, no. 1, p. 70, 2018.

[67] A. L. Frank *et al.*, "Clindamycin treatment of methicillin-resistant *Staphylococcus aureus* infections in children," *Pediatr. Infect. Dis. J.*, vol. 21, no. 6, pp. 530–534, 2002.

[68] S. Bhambri and G. Kim, "Use of Oral Doxycycline for Community-acquired Methicillin-resistant *Staphylococcus aureus* (CA-MRSA) infections," *J. Clin. Aesthet. Dermatol.*, vol. 2, no. 4, p. 45, 2009.

[69] C. Rayner and W. J. Munckhof, "Antibiotics currently used in the treatment of infections caused by *Staphylococcus aureus*.," *Intern. Med. J.*, vol. 35, pp. S3-16, 2005.

[70] D. J. Tipper and J. L. Strominger, "Mechanism of action of penicillins: a proposal based on their structural similarity to acyl-D-alanyl-D-alanine.," *Proc. Natl. Acad. Sci. U. S. A.*, vol. 54, no. 4, p. 1133, 1965.

[71] P. Sahariah and M. Masson, "Antimicrobial chitosan and chitosan derivatives: a review of the structure–activity relationship," *Biomacromolecules*, vol. 18, no. 11, pp. 3846–3868, 2017.

[72] Z. Tan, Y. Shi, B. Xing, Y. Hou, J. Cui, and S. Jia, "The antimicrobial effects and mechanism of ε-poly-lysine against *Staphylococcus aureus*," *Bioresour. Bioprocess.*, vol. 6, no. 1, p. 11, 2019.

[73] A. Muñoz-Bonilla and M. Fernández-García, “Polymeric materials with antimicrobial activity,” *Prog. Polym. Sci.*, vol. 37, no. 2, pp. 281–339, 2012.

[74] X. Zhu *et al.*, “Highly effective antibacterial activity and synergistic effect of Ag-MgO nanocomposite against *Escherichia coli*,” *J. Alloys Compd.*, vol. 684, pp. 282–290, 2016.

[75] A. M. Alotaibi *et al.*, “Enhanced Photocatalytic and Antibacterial Ability of Cu-Doped Anatase TiO2 Thin Films: Theory and Experiment,” *ACS Appl. Mater. Interfaces*, vol. 12, no. 13, pp. 15348–15361, 2020.

[76] M. Laurenti and V. Cauda, “ZnO nanostructures for tissue engineering applications,” *Nanomaterials*, vol. 7, no. 11, p. 374, 2017.

[77] R. Sulaiman, I. Adeyemi, S. R. Abraham, S. W. Hasan, and I. M. AlNashef, “Liquid-liquid extraction of chlorophenols from wastewater using hydrophobic ionic liquids,” *J. Mol. Liq.*, vol. 294, p. 111680, 2019.

[78] S. Zheng, Z. Yang, and Y. H. Park, “Removal of chlorophenols from groundwater by chitosan sorption,” *Water Res.*, vol. 38, no. 9, pp. 2315–2322, 2004.

[79] M. Pera-Titus, V. García-Molina, M. A. Baños, J. Giménez, and S. Esplugas, “Degradation of chlorophenols by means of advanced oxidation processes: a general review,” *Appl. Catal. B Environ.*, vol. 47, no. 4, pp. 219–256, 2004.

[80] G. Li, S. Park, D.-W. Kang, R. Krajmalnik-Brown, and B. E. Rittmann, “2, 4, 5-Trichlorophenol degradation using a novel TiO2-coated biofilm carrier: roles of adsorption, photocatalysis, and biodegradation,” *Environ. Sci. Technol.*, vol. 45, no. 19, pp. 8359–8367, 2011.

[81] H. Zhu *et al.*, “Effective photocatalytic decolorization of methyl orange utilizing TiO2/ZnO/chitosan nanocomposite films under simulated solar irradiation,” *Desalination*, vol. 286, pp. 41–48, 2012.

[82] R. Afeesh, N. A. M. Barakat, S. S. Al-Deyab, A. Yousef, and H. Y. Kim, “Nematic shaped cadmium sulfide doped electrospun nanofiber mat: highly efficient, reusable, solar light photocatalyst,” *Colloids Surfaces A Physicochem. Eng. Asp.*, vol. 409, pp. 21–29, 2012.

[83] A. R. Unnithan, N. A. M. Barakat, M. F. Abadir, A. Yousef, and H. Y. Kim, “Novel CdPdS/PVAc core–shell nanofibers as an effective photocatalyst for organic pollutants degradation,” *J. Mol. Catal. A Chem.*, vol. 363, pp. 186–194, 2012.

[84] A. O. Ifebajo, A. A. Oladipo, and M. Gazi, “Sun-light driven enhanced azo dye decontamination from aqueous solution by CoO-CuFe2O4 derived from layered double hydroxide,” *Desalin. Water Treat.*, vol. 177, no. May 2019, pp. 423–430, 2020.

[85] S. Mandal and S. Natarajan, “Adsorption and catalytic degradation of organic dyes in water using ZnO/ZnxFe3− xO4 mixed oxides,” *J. Environ. Chem. Eng.*,

vol. 3, no. 2, pp. 1185–1193, 2015.

[86] A. Azimi, A. Azari, M. Rezakazemi, and M. Ansarpour, “Removal of heavy metals from industrial wastewaters: a review,” *ChemBioEng Rev.*, vol. 4, no. 1, pp. 37–59, 2017.

[87] S. M. A. El-Gamal, M. S. Amin, and M. A. Ahmed, “Removal of methyl orange and bromophenol blue dyes from aqueous solution using Sorel’s cement nanoparticles,” *J. Environ. Chem. Eng.*, vol. 3, no. 3, pp. 1702–1712, 2015.

[88] M. Su *et al.*, “Mesoporous zinc ferrite: synthesis, characterization, and photocatalytic activity with H2O2/visible light,” *J. Hazard. Mater.*, vol. 211, pp. 95–103, 2012.

[89] A. Dalvand, R. Nabizadeh, M. R. Ganjali, M. Khoobi, S. Nazmara, and A. H. Mahvi, “Modeling of Reactive Blue 19 azo dye removal from colored textile wastewater using L-arginine-functionalized Fe3O4 nanoparticles: Optimization, reusability, kinetic and equilibrium studies,” *J. Magn. Magn. Mater.*, vol. 404, pp. 179–189, 2016.

[90] X. Hou *et al.*, “Synthesis of 3D porous ferromagnetic NiFe2O4 and using as novel adsorbent to treat wastewater,” *J. Colloid Interface Sci.*, vol. 362, no. 2, pp. 477–485, 2011.

[91] S.-J. Park, F. L. Jin, J. R. Lee, and J. S. Shin, “Synthesis and cure behaviors of diglycidylether of bisphenol-S epoxy resins,” *Polym. KOREA*, vol. 26, no. 4,

pp. 501–507, 2002.

[92] C.-C. Wu and W.-J. Lee, “Curing and thermal properties of copolymer epoxy resins prepared by copolymerized bisphenol-A and epichlorohydrin with liquefied Dendrocalamus latiflorus,” *Polym. J.*, vol. 42, no. 9, p. 711, 2010.

[93] A. N. Hasanah, A. Muhtadi, I. Elyani, and I. Musfiroh, “Epichlorohydrin as crosslinking agent for synthesis of carboxymethyl cellulose sodium (Na-CMC) as pharmaceutical excipient from water hyacinth (Eichorrnia crassipes L.),” *Int. J. Chem. Sci*, vol. 13, no. 3, pp. 1227–1237, 2015.

[94] B. Hastuti, A. Masykur, and S. Hadi, “Modification of chitosan by swelling and crosslinking using epichlorohydrin as heavy metal Cr (VI) adsorbent in batik industry wastes,” in *IOP Conference Series: Materials Science and Engineering*, 2016, vol. 107, no. 1, p. 12020.

[95] W. Zhang, X. Ji, C. Sun, and X. Lu, “Fabrication and characterization of macroporous epichlorohydrin cross-linked alginate beads as protein adsorbent,” *Prep. Biochem. Biotechnol.*, vol. 43, no. 5, pp. 431–444, 2013.

[96] O. Stephenson, “The condensation of epichlorohydrin with monohydric phenols and with catechol,” *J. Chem. Soc.*, pp. 1571–1577, 1954.

[97] M. Balouiri, M. Sadiki, and S. K. Ibnsouda, “Methods for in vitro evaluating antimicrobial activity: A review,” *J. Pharm. Anal.*, vol. 6, no. 2, pp. 71–79, 2016.

[98] M. Siam *et al.*, “Evidence for heterodimers of 2,4,5-trichlorophenol on planar lipid layers. A FTIR-ATR investigation,” *Biochim. Biophys. Acta - Biomembr.*, vol. 1664, no. 1, pp. 88–99, 2004.

[99] R. N. Oliveira *et al.*, “FTIR analysis and quantification of phenols and flavonoids of five commercially available plants extracts used in wound healing,” *Matéria (Rio Janeiro)*, vol. 21, no. 3, pp. 767–779, 2016.

[100] M. Jiao, K. Yang, J. Cao, Q. Diao, W. Zhang, and M. Yu, “Influence of epichlorohydrin content on structure and properties of high-ortho phenolic epoxy fibers,” *J. Appl. Polym. Sci.*, vol. 133, no. 18, 2016.

[101] M. G. González, J. C. Cabanelas, and J. Baselga, “Applications of FTIR on epoxy resins-identification, monitoring the curing process, phase separation and water uptake,” *Infrared Spectrosc. Sci. Eng. Technol.*, vol. 2, pp. 261–284, 2012.

[102] M. V Kennedy, B. J. Stojanovic, and F. L. Shuman Jr, “Chemical and thermal aspects of pesticide disposal,” *J. Environ. Qual.*, vol. 1, no. 1, pp. 63–65, 1972.

[103] I. B. Johns, E. A. Mcelhill, and J. Smith, “of Some Organic Compounds,” vol. 7, no. 2, pp. 2–6, 1962.

[104] M. Mosharraf and C. Nyström, “The effect of particle size and shape on the surface specific dissolution rate of microsized practically insoluble drugs,” *Int. J. Pharm.*, vol. 122, no. 1–2, pp. 35–47, 1995.

[105] R. K. Mitchum, J. R. Althaus, W. A. Korfmacher, K. L. Rowland, K. Nam, and J. F. Young, “Atmospheric pressure ionization mass spectrometry: The routine determination of 2,4,5-trichlorophenoxyacetic acid and its metabolites,” *Biol. Mass Spectrom.*, vol. 8, no. 11, pp. 539–545, 1981.

[106] O. Assadian *et al.*, “Minimum inhibitory (MIC) and minimum microbicidal concentration (MMC) of polihexanide and triclosan against antibiotic sensitive and resistant *Staphylococcus aureus* and *Escherichia coli* strains,” *GMS Krankenhhyg. Interdiszip.*, vol. 6, no. 1, 2011.

[107] G. McDonnell and A. D. Russell, “Antiseptics and disinfectants: activity, action, and resistance,” *Clin. Microbiol. Rev.*, vol. 12, no. 1, pp. 147–179, 1999.

[108] L. K. Omosa *et al.*, “Antibacterial activities and structure–activity relationships of a panel of 48 compounds from Kenyan plants against multidrug resistant phenotypes,” *Springerplus*, vol. 5, no. 1, p. 901, 2016.

[109] M. J. Gray, W.-Y. Wholey, and U. Jakob, “Bacterial responses to reactive chlorine species,” *Annu. Rev. Microbiol.*, vol. 67, pp. 141–160, 2013.

[110] J. S. Karns, J. J. Kilbane, S. Duttagupta, and A. M. Chakrabarty, “Metabolism of Halophenols by 2, 4, 5-trichlorophenoxyacetic acid-degrading Pseudomonas cepacia.,” *Appl. Environ. Microbiol.*, vol. 46, no. 5, pp. 1176–1181, 1983.

[111] X. Zhang, X. Zhang, Z. Niu, Y. Qi, D. Huang, and Y. Zhang, “2, 4, 6-Trichlorophenol cytotoxicity involves oxidative stress, endoplasmic reticulum

stress, and apoptosis," *Int. J. Toxicol.*, vol. 33, no. 6, pp. 532–541, 2014.

[112] D. Kwon *et al.*, "Evaluation of pulmonary toxicity of benzalkonium chloride and triethylene glycol mixtures using in vitro and in vivo systems," *Environ. Toxicol.*, vol. 34, no. 5, pp. 561–572, 2019.

[113] S. S. Imam and H. F. Babamale, "A short review on the removal of rhodamine b dye using agricultural waste-based adsorbents," *AJOCS*, vol. 7, no. 1, pp. 25–37, 2020.

[114] A. A. Oladipo and M. Gazi, "Two-stage batch sorber design and optimization of biosorption conditions by Taguchi methodology for the removal of acid red 25 onto magnetic biomass," *Korean J. Chem. Eng.*, vol. 32, no. 9, pp. 1864–1878, 2015.

[115] M. Alkan and M. Doğan, "Adsorption of copper (II) onto perlite," *J. Colloid Interface Sci.*, vol. 243, no. 2, pp. 280–291, 2001.

[116] M. T. Nakhjiri, G. B. Marandi, and M. Kurdtabar, "Effect of bis [2-(methacryloyloxy) ethyl] phosphate as a crosslinker on poly (AAm-co-AMPS)/Na-MMT hydrogel nanocomposite as potential adsorbent for dyes: kinetic, isotherm and thermodynamic study," *J. Polym. Res.*, vol. 25, no. 11, p. 244, 2018.

[117] M. Alokour and E. Yilmaz, "Photoinitiated synthesis of poly (poly (ethylene glycol) methacrylate-co-diethyl amino ethyl methacrylate) superabsorbent

hydrogels for dye adsorption," *J. Appl. Polym. Sci.*, vol. 136, no. 26, p. 47707, 2019.

[118] L. Segal and F. V Eggerton, "Infrared spectra of ethylenediamine and the dimethylethylenediamines," *Appl. Spectrosc.*, vol. 15, no. 4, pp. 116–117, 1961.

[119] C. Zhan, F. Chen, H. Dai, J. Yang, and M. Zhong, "Photocatalytic activity of sulfated Mo-doped TiO2@ fumed SiO2 composite: A mesoporous structure for methyl orange degradation," *Chem. Eng. J.*, vol. 225, pp. 695–703, 2013.

[120] A. A. Oladipo and A. O. Ifebajo, "Highly efficient magnetic chicken bone biochar for removal of tetracycline and fluorescent dye from wastewater: two-stage adsorber analysis," *J. Environ. Manage.*, vol. 209, pp. 9–16, 2018.

[121] C. Umpuch and S. Sakaew, "Removal of methyl orange from aqueous solutions by adsorption using chitosan intercalated montmorillonite.," *Songklanakarin J. Sci. Technol.*, vol. 35, no. 4, 2013.

[122] Q. Li *et al.*, "Removal of Rhodamine B from wastewater by modified Volvariella volvacea: batch and column study," *RSC Adv.*, vol. 5, no. 32, pp. 25337–25347, 2015.

[123] B. R. Venkatraman, U. Gayathri, S. Elavarasi, and S. Arivoli, "Removal of Rhodamine B dye from aqueous solution using the acid activated Cynodon dactylon carbon.," *Der Chem. Sin.*, vol. 3, no. 1, pp. 99–113, 2012.

[124] A. A. Babaei, A. Khataee, E. Ahmadpour, M. Sheydaei, B. Kakavandi, and Z. Alaee, “Optimization of cationic dye adsorption on activated spent tea: equilibrium, kinetics, thermodynamic and artificial neural network modeling,” *Korean J. Chem. Eng.*, vol. 33, no. 4, pp. 1352–1361, 2016.

[125] C. Türkcan, D. A. Uygun, S. Akgöl, and A. Denizli, “Reactive red 120 and NI (II) derived poly (2-hydroxyethyl methacrylate) nanoparticles for urease adsorption,” *J. Appl. Polym. Sci.*, vol. 131, no. 2, 2014.

[126] M. A. Al-Ghouti and D. A. Da’ana, “Guidelines for the use and interpretation of adsorption isotherm models: A review,” *J. Hazard. Mater.*, p. 122383, 2020.

[127] P. Li, X. Dai, Q. Yan, Z. Wang, S. Zhang, and M. Cao, “A novel modification method for polystyrene microspheres with dithizone and the adsorption properties for Pb 2+,” *J. Polym. Res.*, vol. 27, no. 7, pp. 1–10, 2020.

[128] N. N. Bahrudin, M. A. Nawi, and W. I. N. W. Ismail, “Physical and adsorptive characterizations of immobilized polyaniline for the removal of methyl orange dye,” *Korean J. Chem. Eng.*, vol. 35, no. 7, pp. 1450–1461, 2018.

[129] F.-N. Allouche, N. Yassaa, and H. Lounici, “Sorption of methyl orange from aqueous solution on chitosan biomass,” *Procedia Earth Planet. Sci.*, vol. 15, pp. 596–601, 2015.

[130] X.-X. Hou, Q.-F. Deng, T.-Z. Ren, and Z.-Y. Yuan, “Adsorption of Cu 2+ and methyl orange from aqueous solutions by activated carbons of corncob-derived

char wastes," *Environ. Sci. Pollut. Res.*, vol. 20, no. 12, pp. 8521–8534, 2013.

[131] D. Robati *et al.*, "Removal of hazardous dyes-BR 12 and methyl orange using graphene oxide as an adsorbent from aqueous phase," *Chem. Eng. J.*, vol. 284, pp. 687–697, 2016.

[132] A. Thakur and H. Kaur, "Response surface optimization of Rhodamine B dye removal using paper industry waste as adsorbent," *Int. J. Ind. Chem.*, vol. 8, no. 2, pp. 175–186, 2017.

[133] M. Arslan and K. Günay, "Synthesis and use of PET fibers grafted with 4-vinyl pyridine and 2-methylpropenoic acid for removal of rhodamine B and methylene blue from aqueous solutions," *J Polym Sci Appl 2*, vol. 1, p. 2, 2018.

[134] M. Wang *et al.*, "Removal of rhodamine B, a cationic dye from aqueous solution using poly (cyclotriphosphazene-co-4, 4′-sulfonyldiphenol) nanotubes," *J. Macromol. Sci. Part A*, vol. 52, no. 2, pp. 105–113, 2015.

[135] B. Damiyine, A. Guenbour, and R. Boussen, "Rhodamine B adsorption on natural and modified moroccan clay with cetyltrimethylammonium bromide: Kinetics, equilibrium and thermodynamics," *J. Mater. Environ. Sci*, vol. 8, no. 3, pp. 860–871, 2017.

[136] J. Saini, V. K. Garg, R. K. Gupta, and N. Kataria, "Removal of Orange G and Rhodamine B dyes from aqueous system using hydrothermally synthesized zinc oxide loaded activated carbon (ZnO-AC)," *J. Environ. Chem. Eng.*, vol. 5, no.

1, pp. 884–892, 2017.

[137] L. Zhou *et al.*, “Development of carbon nanotubes/CoFe2O4 magnetic hybrid material for removal of tetrabromobisphenol A and Pb (II),” *J. Hazard. Mater.*, vol. 265, pp. 104–114, 2014.

[138] S. Ma, S. Zhan, Y. Jia, and Q. Zhou, “Highly Efficient Antibacterial and Pb(II) Removal Effects of Ag-CoFe2O4-GO Nanocomposite,” *ACS Appl. Mater. Interfaces*, vol. 7, no. 19, pp. 10576–10586, May 2015.

[139] M. M. Kothawale, R. B. Tangsali, G. K. Naik, and J. S. Budkuley, “Effect of sintering on magnetic properties of Ni0.55Zn 0.45Fe2O4,” *J. Supercond. Nov. Magn.*, vol. 26, no. 11, pp. 3293–3298, 2013.

[140] H. Aali *et al.*, “High antibacterial and photocatalytic activity of solution combustion synthesized Ni0. 5Zn0. 5Fe2O4 nanoparticles: Effect of fuel to oxidizer ratio and complex fuels,” *Ceram. Int.*, vol. 45, no. 15, pp. 19127–19140, 2019.

[141] A. A. Oladipo, “MIL-53 (Fe)-based photo-sensitive composite for degradation of organochlorinated herbicide and enhanced reduction of Cr (VI),” *Process Saf. Environ. Prot.*, vol. 116, pp. 413–423, 2018.

[142] J. Shah, M. R. Jan, and F. Khitab, “Sonophotocatalytic degradation of textile dyes over Cu impregnated ZnO catalyst in aqueous solution,” *Process Saf. Environ. Prot.*, vol. 116, pp. 149–158, 2018.

[143] R. Maulia, R. A. Putra, and E. Suharyadi, “Effect of Synthesis Parameter on Crystal Structures and Magnetic Properties of Magnesium Nickel Ferrite (Mg 0.5 Ni 0.5 Fe 2 O 4) Nanoparticles,” in *IOP Conference Series. Materials Science and Engineering (Online)*, 2017, vol. 202, no. 1.

[144] T. Ali, A. Ahmed, U. Alam, I. Uddin, P. Tripathi, and M. Muneer, “Enhanced photocatalytic and antibacterial activities of Ag-doped TiO2 nanoparticles under visible light,” *Mater. Chem. Phys.*, vol. 212, pp. 325–335, 2018.

[145] C. Jiang, R. Liu, X. Shen, L. Zhu, and F. Song, “Ni0. 5Zn0. 5Fe2O4 nanoparticles and their magnetic properties and adsorption of bovine serum albumin,” *Powder Technol.*, vol. 211, no. 1, pp. 90–94, 2011.

[146] A. M. El-Sayed, “Influence of zinc content on some properties of Ni–Zn ferrites,” *Ceram. Int.*, vol. 28, no. 4, pp. 363–367, 2002.

[147] Q. Tian *et al.*, “Highly effective antibacterial activity of lithium-doped magnesium oxide particles synthesized by the microwave-assisted hydrothermal route,” *Powder Technol.*, vol. 371, pp. 130–141, 2020.

[148] K. A. Azalok, A. A. Oladipo, and M. Gazi, “Journal of Photochemistry & Photobiology , A : Chemistry UV-light-induced photocatalytic performance of reusable MnFe-LDO – biochar for tetracycline removal in water,” *J. Photochem. Photobiol. A Chem.*, vol. 405, no. August 2020, p. 112976, 2021.

[149] K. A. Azalok, A. A. Oladipo, and M. Gazi, “Chemosphere Hybrid MnFe-LDO

e biochar nanopowders for degradation of metronidazole via UV-light-driven photocatalysis : Characterization and mechanism studies," *Chemosphere*, no. xxxx, p. 128844, 2020.

[150] A. A. Oladipo, E. O. Ahaka, and M. Gazi, "Pyrochar/AgBr-derived from discarded chewing gum for decontamination of trichlorophenol via fixed-bed adsorption system," *Chem. Eng. Commun.*, pp. 1–13, 2020.

[151] H. N. Catherine, M.-H. Ou, B. Manu, and Y. Shih, "Adsorption mechanism of emerging and conventional phenolic compounds on graphene oxide nanoflakes in water," *Sci. Total Environ.*, vol. 635, pp. 629–638, 2018.

[152] M. Gazi, A. A. Oladipo, Z. E. Ojoro, and H. O. Gulcan, "High-performance nanocatalyst for adsorptive and photo-assisted Fenton-like degradation of phenol: modeling using artificial neural networks," *Chem. Eng. Commun.*, vol. 204, no. 7, pp. 729–738, 2017.

[153] M. Tsvetkov *et al.*, "Magnetic properties of binary and ternary mixed metal oxides NiFe2O4 and Zn0.5Ni0.5Fe2O4 doped with rare earths by sol-gel synthesis," *Chem. Pap.*, vol. 70, no. 12, pp. 1600–1610, 2016.

[154] C. Jiang, R. Liu, X. Shen, L. Zhu, and F. Song, "Ni0.5Zn0.5Fe2O4 nanoparticles and their magnetic properties and adsorption of bovine serum albumin," *Powder Technol.*, vol. 211, no. 1, pp. 90–94, 2011.

[155] E. Albiter, M. A. Valenzuela, S. Alfaro, G. Valverde-Aguilar, and F. M.

Martínez-Pallares, “Photocatalytic deposition of Ag nanoparticles on TiO2: Metal precursor effect on the structural and photoactivity properties,” *J. Saudi Chem. Soc.*, vol. 19, no. 5, pp. 563–573, 2015.

[156] X. An, H. Liu, J. Qu, S. J. A. Moniz, and J. Tang, “Photocatalytic mineralisation of herbicide 2,4,5-trichlorophenoxyacetic acid: Enhanced performance by triple junction Cu-TiO2-Cu2O and the underlying reaction mechanism,” *New J. Chem.*, vol. 39, no. 1, pp. 314–320, 2015.

[157] Y. Qingshan, L. Yongjin, and M. A. O. Lingling, “Kinetics of photocatalytic degradation of gaseous organic compounds on modified TiO2/AC composite photocatalyst,” *Chinese J. Chem. Eng.*, vol. 20, no. 3, pp. 572–576, 2012.

[158] A. Kumar and G. Pandey, “A review on the factors affecting the photocatalytic degradation of hazardous materials,” *Mater. Sci. Eng. Int. J*, vol. 1, no. 3, pp. 1–10, 2017.

[159] R. W. Matthews and S. R. McEvoy, “A comparison of 254 nm and 350 nm excitation of TiO2 in simple photocatalytic reactors,” *J. Photochem. Photobiol. A Chem.*, vol. 66, no. 3, pp. 355–366, 1992.

[160] F. Zaviska, P. Drogui, E. M. El Hachemi, and E. Naffrechoux, “Effect of nitrate ions on the efficiency of sonophotochemical phenol degradation,” *Ultrason. Sonochem.*, vol. 21, no. 1, pp. 69–75, 2014.

[161] Y. Jiao, Y. Wang, M. Li, Y. Liu, P. Mao, and Y. Yang, “Visible Light Excited

Catalysis and Reusability Performances of TiO2@ Pr: Y2SiO5 Upconversion Materials," *J. Nanomater.*, vol. 2017, 2017.

[162] N. Y. Fairooz and S. M. Aliwi, "Kinetic Study of 2, 4, 5-Trichlorophenol Photodegredation in the Presence of TiO2," *Iraqi Natl. J. Chem.*, no. 32, pp. 716–731, 2008.

[163] X. Li *et al.*, "Antibacterial property improvement of nano-MgO prepared by lithium doping under nitrogen calcination," *Ceram. Int.*, no. December, 2020.

[164] H. Aral and A. Vecchio-Sadus, "Toxicity of lithium to humans and the environment—a literature review," *Ecotoxicol. Environ. Saf.*, vol. 70, no. 3, pp. 349–356, 2008.

[165] R. Pandiyan, S. Mahalingam, and Y.-H. Ahn, "Antibacterial and photocatalytic activity of hydrothermally synthesized SnO2 doped GO and CNT under visible light irradiation," *J. Photochem. Photobiol. B Biol.*, vol. 191, pp. 18–25, 2019.

APPENDIX

List of Publication

(2021) F.S. Mustafa, A.A. Oladipo. Photocatalytic degradation of metronidazole and bacterial disinfection activity of Ag-doped $Ni_{0.5}Zn_{0.5}Fe_2O_4$. Journal of Water Process Engineering. 42, 1-11. Impact Factor: 3.465

(2021) F.S. Mustafa, G. Şanlıtürk, M. Güran, & M. Gazi, Novel "Virkon S" releasing alginate beads for water disinfection: Synthesis, characterization and antimicrobial activity analysis". Environmental Earth Sciences, 80:32, 1-8. Impact Factor: 2.18

(2020) F.S. Mustafa, et al. "Fabrication of a novel nontoxic trichlorophenolepichlorohydrin- based compound with high antimicrobial activity and thermal stability." Journal of Environmental Science and Health, Part A, 55:13, 1469-1474. doi.org/10.1080/10934529.2020.1806633. Impact Factor: 1.724

(2020) F.S. Mustafa, M. Güran & M. Gazi, "Effective removal of dyes from aqueous solutions using a novel antibacterial polymeric adsorbent". Journal of Polymer Research 27, 247. Impact Factor: 2.426